Dissertation

submitted to the

Combined Faculties for the Natural Sciences and for Mathematics

of the Ruperto-Carola University of Heidelberg, Germany

for the degree of

Doctor of Natural Sciences

Put forward by

Diplom-Physiker Christian Vinzenz Guthier

born in Heppenheim, Germany

Oral examination: 11.11.2015

Development of a real-time inverse planning system for radiation therapy based on compressed sensing

Referees: Prof. Dr. Jürgen Hesser

Prof. Dr. Peter Bachert

Entwicklung eines echtzeitfähigen Planungssystems für die Strahlentherapie basierend auf Compressed Sensing

Ziel dieser Arbeit ist die Entwicklung eines auf Compressed Sensing (CS) basierenden inversen Planungssystems für die Strahlentherapie. Dieses wird am Beispiel der Brachytherapie getestet, bei der eine schnelle Optimierung für eine intraoperative Planung essenziell ist.
Im Rahmen dieser Arbeit wird ein neuer Ansatz vorgestellt, der zum ersten Mal eine intraoperative Echtzeitplanung ermöglicht. Hierfür wurde das inverse Problem in ein CS äquivalentes Optimierungsproblem überführt. Dafür wurden spezifische Löser entwickelt und in ein neues Planungssystem integriert. Durch die Verwendung biologischer Modelle und klinisch relevanter dosimetrischer Kriterien können so realistischere Zielfunktionen eingeführt werden.
Der CS basierte Ansatz ist etwa zwei Größenordnungen schneller als alle bisherigen Methoden bei garantierter gleicher oder besserer Planqualität. Der mit dem CS einhergehende Spärlichkeitsansatz erlaubt eine Reduzierung der verwendeten Nadeln um bis zu 25%. Dies reduziert die Behandlungsdauer und das Risiko für Nebenwirkungen. Zudem erleichtern die neuen Zielfunktionen den Planungsprozess.
Der neue CS basierende Ansatz und die entwickelten Löser können auf verschiedene Modalitäten in der Strahlentherapie, z.B. Intensitätsmodulierte Strahlentherapie, angewandt werden. Der Ansatz einer spärlichen Lösung ist ein neues und vielversprechendes Paradigma für Planoptimierung in der Medizinischen Physik.

Development of a real-time inverse planning system for radiation therapy based on compressed sensing

The aim of this work is to develop a compressed sensing (CS) based optimization for inverse treatment planning in radiation therapy. This approach is applied to the example of brachytherapy where fast optimization is essential during intra-operative treatment planning.
In this thesis, a novel approach is presented that allows real-time intra-operative planning for the first time. The standard inverse treatment problem is reformulated to resemble a CS problem. Highly specific solvers are developed and incorporated into a novel treatment planning system. By incorporating biological models and clinically important dosimetric criteria, the objective functions become more realistic.
Being approximately two orders of magnitude faster than state-of-the-art methods, the CS based approach is proven to return the same or better quality in plans. The inherit sparsity approach in CS allows to decrease the amount of needles by up to 25% reducing the intervention time and the probability of side effects. In addition, the new objective functions further simplify the treatment planning.
The novel CS based strategy and solvers can also be applied to other modalities in radiation therapy, e.g. intensity-modulated radiation therapy. The incorporation of sparse solution is a novel and promising paradigm for optimization in medical physics.

In memory of my grandmother

Contents

List of Figures

List of Tables

List of Abbreviations

AAPM American Association of Physicists in Medicine

APP applied plan

BBOF biological model based objective function

BED biological effective dose

BFGS Broyden-Fletcher-Goldfarb–Shanno algorithm

BILP binary linear programming

BP basis pursuit

CBOF criteria based objective function

COIN conformal index

CoSaMP compressive sampling matching pursuit

CS Compressed Sensing

DBOF dose based objective function

DNA Deoxyribonucleic acid

DVH dose-volume histogram

ESTRO European Society for Radiotherapy & Oncology

EUD equivalent uniform dose

FM figure of merit

GA genetic algorithm

GEC Groupe Européen de Curiethérapie

GrO graphical optimization

HBio HDR biological model based optimization

HCB HDR criteria based optimization

HDR high-dose-rate

HIPO hybrid inverse planning and optimization

HSIS HDR splitting iterative subspace pursuit algorithm

HTA HDR thresholding algorithm

ILP integer linear programming

IPSA inverse planning by simulated annealing

ITP inverse treatment planning

LBio LDR biological model based optimization

LCB LDR criteria based optimization

L-BFGS Limited-memory Broyden–Fletcher–Goldfarb–Shanno algorithm

LDR low-dose-rate

LOMA LDR orthogonal matching pursuit

LP linear programming

LST LDR split thresholding algorithm

LSPA LDR splitting inspired subspace pursuit algorithm

LSUP LDR subspace pursuit

LTA LDR thresholding algorithm

MILP mixed integer linear programming

MP matching pursuit

NTCP normal tissue complication probability

OARs organs at risk

OMP orthogonal matching pursuit

PTV planning target volume

SA simulated annealing

SISA split iterative shrinkage algorithm

SP subspace pursuit

SSE Streaming SIMD Extensions

TCP tumor control probability

TG-43 American Association of Physicists in Medicine Task Group No. 43

TPS treatment planning system

VOI volume of interest

wMP weak matching pursuit

List of Nomenclature

	Symbol	Description
General parameters	i, k, l	indices
Mathematical model	o	total number of organs
	n	total number of needles
	s	total number of dwell-positions
	p_i	total number of dwell-position per needle
	$\boldsymbol{\rho} \in \mathbb{R}^3$	dose-point
	$\boldsymbol{\xi} \in \mathbb{R}^3$	dwell-position
	$\boldsymbol{\chi} \in \mathbb{R}^3$	intersection needle with organ
	$\boldsymbol{x}$	dwell-time vector
	$\boldsymbol{x}^{(acc)}$	accumulated dwell-time vector per needle
	$\boldsymbol{n}$	needle configuration vector
	$\boldsymbol{D}$	dose-rate dictionary
	$\boldsymbol{d}$	dose vector
	ι	set of parameters
	ν	set of all organs
	$\boldsymbol{P}$	set of all dose-points
	$\boldsymbol{S}$	set of all dwell-positions
	$\boldsymbol{\Lambda}_\nu$	set of all available dose points per organ ν
	$\boldsymbol{\Pi}$	set of all needles
	$\boldsymbol{\Gamma}_i$	set of dwell-points per needle i
	$\boldsymbol{\Upsilon}_i$	set of indices of all dwell-position per needle
Dose calculation	r	radius
	θ	polar angle
	$\dot{D}(r, \theta)$	dose-rate
	$\mathcal{S}_k$	air kerma strength
	Λ	dose-rate constant
	$G_L(r, \theta)$	geometric function
	$F(r, \theta)$	form factor
	$g_L(r)$	radial dose function
	Ψ	photon flux

	μ_{tot}	linear attenuation coefficient
Objective function	$\mathcal{Q}(\boldsymbol{x})$	objective function
	$\mathcal{N}(\boldsymbol{x})$	function revaluating the number of needles
	$\mathcal{C}(\boldsymbol{x})$	function evaluating dosimetric criteria
	$\mathcal{P}(\boldsymbol{x})$	function evaluating biological probabilities
	$p(\cdot)$, $f(\cdot)$	penalty functions
	$\theta(\cdot)$	Heaviside step function
	ς	steepness
	q	objective function value
	$\lambda_{N/Q}$	Lagrange parameter
	t_C	threshold for dosimetric criteria
	t_P	threshold for biological probabilities
	$t_{L/U}$	dose thresholds for upper and lower bounds
	$\boldsymbol{t}$	vector of thresholds
	w	weighting factor
	$\boldsymbol{w}$	vector of weighting factors
Biological parameters	S	cell survival curve
	α, β	parameter linear-quadratic model
	T_{eff}	effective treatment time
	T_P	doubling time of tumor cells
	λ	decay constant
	μ	sub-lethal damage repair
	γ_t	elapsed unit of treatment time
	N_0	total number of tumor cells
	d_2	$2\,Gy$ fraction size
	ζ, δ	parameters for the NTCP of urethra
	$DU20$	dose that covers at least 20% of the organ
	k_ν, s_ν	parameters to describe seriality of an organ
	$D50$	dose leading to late injuries in 50% of the cases
Compressed Sensing	$\boldsymbol{f}$	measured signal
	$\boldsymbol{A}$	basis
	$\boldsymbol{g}$	signal
	$\boldsymbol{p}$	projection
	$\boldsymbol{r}$	residual
	$\boldsymbol{v}$	support vector
	$H(\cdot)$, $\Psi(\cdot)$	convex functionals
	λ_L	Lagrange parameter
Algorithms	η	maximally allowed needles

σ	maximally allowed seeds
κ	sparsity threshold
Q_0	quality tolerance
γ	threshold shrinkage operator
$\mathcal{S}$	dwell-positions support
$\mathcal{N}$	needles support
$\mathbf{0}$	null matrix
$\mathbf{1}$	all-ones matrix
$\boldsymbol{G}$	accumulated dwell-time matrix
$\boldsymbol{I}$	unit matrix
$\boldsymbol{N}$	dwell-position-needle matrix
$\boldsymbol{W}$	weighting matrix
$\boldsymbol{e}$	unit vector
$\boldsymbol{s}$	slack variable vector
$\boldsymbol{u}$	temporary support vector
$\boldsymbol{z}$	amplitude vector

1 Introduction

Physics plays a major role in medicine. Starting in late 1890th, the discovery of X-rays by Wilhelm Conrad Röntgen, radioactivity by Henry Becquerel [1], and radium by Pierre and Marie Curie [2] laid the foundation of modern X-ray diagnostic and radiation therapy.
At the beginning of the 20th century, Becquerel observed skin reactions while carrying a tube with decigrams of radium chloride in his pocket which lead to the first studies and medical experience shortly after [1]. Already one decade later, a book on radium therapy was published by Wickham and Degrais [1].
Brachytherapy, an internal radiation therapy, was established in 1904 by the "electrotherapist" Sinclar Tousey who placed a X-ray tube inside the rectum of a patient to treat tuberculosis of the prostate [3]. Brachytherapy treatment of the prostate carcinoma was first described in 1909, when two french urologists positioned catheters containing radium inside the urethra. With the discovery of artificial radioactivity in 1934 and the development of the first afterloader in 1962 [4], a remotely controlled unit which places radioactive sources inside the body, the technological prerequisites of modern brachytherapy were laid.
Today, brachytherapy is well-established in the clinical routine as an interstitial and intracavitary radiation therapy. The most common treatment sites are the cervix, prostate and breast [5]. Depending on the dose rate, a distinction is drawn between permanent low-dose-rate (LDR) and temporarily high-dose-rate (HDR) brachytherapy.

Despite declining mortality rates [6], prostate carcinoma still accounts for more than 258,000 deaths worldwide and is the second most common cancer in males [7]. The majority of the prostate patient cases are diagnosed with a localized disease that allow a local therapy [8]. From a total of 253,000 cases in the United States in the year 2014 almost 30 % received brachytherapy [9, 10].
Other than brachytherapy, curative treatment options include the surgical removal of the prostate gland or external beam radiation therapy [11]. A randomized comparison in clinical trials comparing the different treatment options has not been completed yet. There is an ongoing German study (PREFERE) which addresses this issue but it is not expected to be completed before 2030 [12]. Comparative analyses indicate that modern brachytherapy is favorable in terms of both prostate-specific antigen free survival and therapeutic side effects when compared to surgery and external beam radiation therapy [13]. Side effects for brachyther-

apy include rectal bleeding, urinary toxicity, and sexual dysfunction [14, 15]. Computer-based inverse treatment planning (ITP) tries to diminish side effects while at the same time trying to cover the tumor-region with at least the prescribed dose.

Over the last two decades different approaches for ITP have been proposed. The first were gradient-based and allowed local optimization [16, 17]. These simple approaches have been replaced by global stochastic optimization strategies like simulated annealing (SA) [18, 19, 20] or genetic algorithm (GA) [21]. SA and GA are general-purpose heuristics that are not tailored to the underlying structure of the optimization problem and can be used for multiple applications without modification of the programs code. However, it is often observed that problem-specific heuristics outperform general purpose strategies [22].
Very recently, the ITP was reformulated as linear programming (LP) or mixed integer linear programming (MILP) depending on the modality and optimization goal [23, 24, 25, 26]. LP problems can efficiently be solved for example by using the interior point or simplex methods in a few seconds [24].
Although for MILP the branch-and-bound method belong to the most efficient strategies in finding the global optimum [27], it is considered to be inappropriate for intra-operative ITP due to its long runtime. In 2014 Guthier and Hesser showed that for small problem sizes the global solutions can be found in reasonable time [28]. However, the solutions were found at much higher costs than traditional SA or GA.
Commercially available ITP is based on two different strategies, inverse planning by simulated annealing (IPSA) and hybrid inverse planning and optimization (HIPO) [29]. While the first can be used for LDR and HDR treatment planning, the latter was specially designed for needle optimization in HDR ITP. The optimization times range from a few seconds (IPSA) to several minutes (HIPO). These optimization techniques are therefore not suitable for real-time intra-operative planning.
In order to optimize a plan, the clinical criteria, i.e. the criteria that are used for rating whether a plan is clinically acceptable or not, are mathematically formulated as an objective function. The most commonly used is the so-called dose based objective function (DBOF), a linear objective function that penalizes dose values above and below dose thresholds [30]. The weightings to calculate the penalty term according to the dose thresholds are summarized in a set of parameters which have to be tailored to the patient's anatomy. The fine-tuning of the parameters is considered to be a non straightforward and time-consuming trial-and-error approach [31, 29].
A general observation is that due to the "large" run-times and the need for steering of the plan quality via abstract parameters most users prefer manual forward-planning. Forward-planning is a drag-and-drop approach where the user receives

a direct feedback of the changes. It is known that these plans deliver higher doses to the OARs, the dose to the tumor region is less homogeneous [32], and planning takes several minutes to hours.

The goal of this thesis is to develop new methods that are capable of real-time planning to provide an intermediate feedback in the form of an optimized plan to the user. In addition, the new strategy should be able to handle different and more realistic objective functions. Together this has the potential to change the treatment planning process and increases the quality of the intervention.

The novelty of this thesis is the reformulation of the ITP problem into a mathematical structure that is of Compressed Sensing (CS) type. CS is a method in the field of image processing, which has recently received a lot of attention in signal recovery and sampling problems. Especially greedy based optimizers are considered to be among the fastest optimization strategies for CS problems [33]. A reformulation of the ITP problem into a problem which is structural similar to the CS problem allows the use of these highly efficient solvers in ITP. The research question is whether the same performance gains can also be observed for ITP in brachytherapy as well. This would allow real-time adjustments of the treatment plan during intervention.
A gain in performance would allow to integrate more complex models into new objective functions which should be tested as well. The research question is whether more realistic objective functions can be introduced that are of the same mathematical structure as those of CS. Especially, the use of biological models for describing the tumor control probability (TCP) and normal tissue complication probability (NTCP)s of organs at risk (OARs) is of interest [34] . Due to its complexity, biological modelling is considered to be infeasible for ITP in brachytherapy.

The thesis is structured as follows. The theory section explains the underlying physical and biolgical mechanisms of radiation therapy and focuses on the principles of brachytherapy and the used mathematical models. In addition, the theory of CS and the used algorithms in this field are described briefly. Afterwards, the state-of-the-art of inverse treatment planning in brachytherapy and recent developments are summarized.
In materials and methods, the reformulation of the ITP problem in brachytherapy into a CS inspired problem is presented. The derivation is divided into LDR and HDR ITP with and without needle optimization. This is necessary since each modality and problem has its own mathematical structure. Afterwards, the novel CS inspired solvers are introduced. The introduction of the novel objective functions follows. An explanation of the developed ITP system as well as the parameters and settings used for the comparative tests are discussed in detail.

The results chapter presents these different comparative tests. Here, the CS inspired solvers are compared to the state-of-the-art methods with respect to calculation time, returned objective function value, and the clinical performance taking dosimetric criteria into account.
A discussion with respect to the benchmarking, limitations, and potential of the novel CS inspired approach follows. The focus is directed to the applicability regarding the different radiation therapy modalities, for example external beam radiation therapy, intra-operative radiation therapy, and stereotactic surgery with the gamma knife. A summary and outlook conclude this thesis.

Publications

In the course of this thesis two peer-reviewed journal article about the introduction of the CS inspired solvers to LDR ITP and about the feasibility of biological models for ITP were published [35, 34]. A paper with the title "Combined stereotactic biopsy and stepping-source interstitial irradiation of unresectable glioblastoma multiforme", will be submitted shortly after handing in this thesis.
In addition, there are two conference posters comparing two different MILP optimizer for LDR ITP and addressing the use of CS inspired solvers in dosimetric criteria based planning [28, 36]. Furthermore, I was an invited speaker at the "9th ZEISS INTRABEAM System User Meeting 2015" were I presented the use of the CS inspired solvers in the context of stereotactic intra-operative radiation therapy.
An journal article about the introduction of the novel strategy for HDR treatment planning is currently prepared.

2 Theory

In this chapter, the basics of radiation therapy and the used techniques are presented. Starting with the physical interactions and the biological effects that occur during treatment. A brief introduction to brachytherapy, its different modalities, and potential treatment sites follows. The theory of CS and the underlying principles finishes this chapter.

2.1 Basics of radiation therapy

In radiation therapy, the biological effects of radiation are used to treat cancer. The aim is to apply a prescribed dose to the tumor while sparing healthy tissue to reduce side effects. In brachytherapy, photon emitting sources are inserted into the patients body. The electromagnetic spectrum of the sources range from low energies of around 21 keV for Pd-103 to intermediate energies of 0.4 MeV of Ir-192 [37, 38]. During each passage through matter, photons and electrons undergo different physical interactions causing a biological response, that is discussed in the following.

2.1.1 Interactions with matter

Due to the energy of the emitted photons in brachytherapy a substantial amount is capable to pass thick layers of tissue. During this passage they interact with the electron shell of atoms and some quanta can be absorbed or scattered. These interactions can be divided into elastic and inelastic interactions.
The inelastic processes are the Photoelectric effect (PE), the Compton scattering (CE), and Pair production (PP). The process of elastic scatter is hereby called Thomson scattering (TH) and deflects only the photons. The inelastic processes, in contrast, release secondary electrons which undergo multiple interactions and ionize the tissue. However, due their low energy range and the related mean-free-path-length, they are reabsorbed within a few millimeters in soft tissue [39].
The energy loss of the photon flux $\Psi(r)$, either by scattering or absorption, is described by the Beer-Lambert law:

$$\Psi(r) = \Psi_0 \exp(-\mu_{tot} r) \tag{2.1}$$

Here, Ψ_0 is the initial photon flux of the incoming X-rays, r the thickness of the passed layer and μ_{tot} the total linear attenuation coefficient of the absorbing material. The total linear attenuation coefficients is the sum of the linear attenuation coefficients of the relevant processes:

$$\mu_{tot} = \mu_{PE} + \mu_{CE} + \mu_{PP} + \mu_{TH} \tag{2.2}$$

The total inear attenuation coefficient is proportional to the total cross section σ. For the Thomson scattering, the total cross section shows the following relation of the atomic number Z and the energy E_γ of incoming photons: $\sigma_{TH} \propto \frac{Z^2}{E_\gamma^2}$. Due to the dependence on the energy, this effect can be neglected for energies above $100\,keV$.
In the Photoelectric effect, an incoming photon is completely absorbed. An electron in the inner atomic shell leaves the atom with a kinetic energy of $E_{kin} = E_\gamma - E_B$. In this case, E_γ is the energy of the initial photon and E_B is the binding-energy of the electron. Energy and momentum can only be conserved if the atom compensates the momentum of the emitted electron. Thus, a Photoelectric effect with free electrons cannot be observed. The total cross section shows the following relation: $\sigma_{PE} \propto \frac{Z^3}{E_\gamma^5}$ [40]. This effect dominates the interactions for photon energies below $30\,keV$ in tissue [41].
The Compton scattering describes inelastic scatter from an initial photon to an outer electron of the atomic shell. The electron leaves the atom with a kinetic energy E_{kin}, the photon is scattered and its remaining energy is $E_\gamma - E_{kin} - E_B$. The total cross-section per unit solid angle and per electron is described by the Klein-Nishina formula [42]. In contrast to the photoelectric effect, the Compton effect is almost independent from the atomic number of the interacting material. Especially for intermediate energies above $100\,keV$ to high energies between $(2-3)\,MeV$, this is the predominant process [43].
Pair production describes the generation of an electron-positron pair by the interaction of high-energetic photons with the electromagnetic field of an atomic nucleus [44]. Due to energy conservation, this process can only occur for photon energies of $E_\gamma > 1.022\,MeV$. Due the low energies of the sources used in brachytherapy pair production can be neglected.
Using Lambert-Beers law and assuming that the absorbed dose is proportional to both, the change of photon flux $\Psi(r)$ and to the mass energy absorption coefficient $\frac{\mu_{ab}}{\rho}$, the absorbed dose can be approximated according to [45]:

$$D(r) = \Psi(r)\frac{\mu_{ab}}{\rho}E_\gamma \tag{2.3}$$

This estimation is valid for photon energies less than $5\,MeV$.

2.1.2 Biological aspects

The aim of radiation therapy is to introduce biological effects that damage the Deoxyribonucleic acid (DNA) and lead to mitotic or apoptotic death of the tumorcells [46]. The interactions of ionizing radiation with the biological target can be divided into direct and indirect actions. The direct actions are interactions that directly lead to ionization or excitation of the target molecules [46]. This is in contrast to indirect actions, where radiation interacts with water molecules inside the cell and produces free radicals in the vicinity of the DNA. The generated radicals can interact with the DNA and lead to chemical changes and the breaking of bonds. It was estimated that over two thirds of the DNA damage induced by X-ray radiation is caused by free radicals [46].
Both, indirect and direct actions yield a breaking of bonds in the double-stranded DNA. It is differentiated between single-strand breaks and double-strand breaks. Single-strand breaks are of little biological consequence since they can easily be repaired by different mechanisms of the cell. Double strand-beaks, which are only separated by a few base pairs, can break the DNA helix. They often undergo no repair and in frequent cases double strand-beaks result in cell killing.
Cell survival is directly linked to the delivered dose. Therefore, the goal is to deliver as much dose to the tumor as necessary to cause inactivation of the metabolism (cell arrest) or the death (apoptosis) of the tumor-cells. At the same time, the OARs should not be exposed to too much dose to ensure that the different repair mechanisms allow a recovery of the irradiated healthy tissue.
The effect of radiation is quantified using cell survival models. The most used is the linear-quadratic model, where the survival fraction as a function of the received dose D is given by

$$S = \exp\left(-\alpha \cdot D - \beta \cdot D^2\right), \tag{2.4}$$

where α and β are model parameters for the single-track lethality and inter-track quadratic interactions, respectively. These parameters are usually estimated using in-vitro studies or retrospective studies based on clinical experience [47]. Due to the simplicity of the linear-quadratic model it is commonly used to predict the biological consequences of radiation therapy.

2.2 Brachytherapy

Starting 1904, brachytherapy ($\beta\rho\alpha\chi\upsilon\sigma$ brachys, meaning "short-distance") has evolved to one of the major treatment modalities in radiation therapy with various applications [1]. In contrast to external radiation beam therapy, one or multiple photon emitting sources are either placed next to or inside a clinical target. This is commonly achieved using image-guided minimally invasive surgery where special

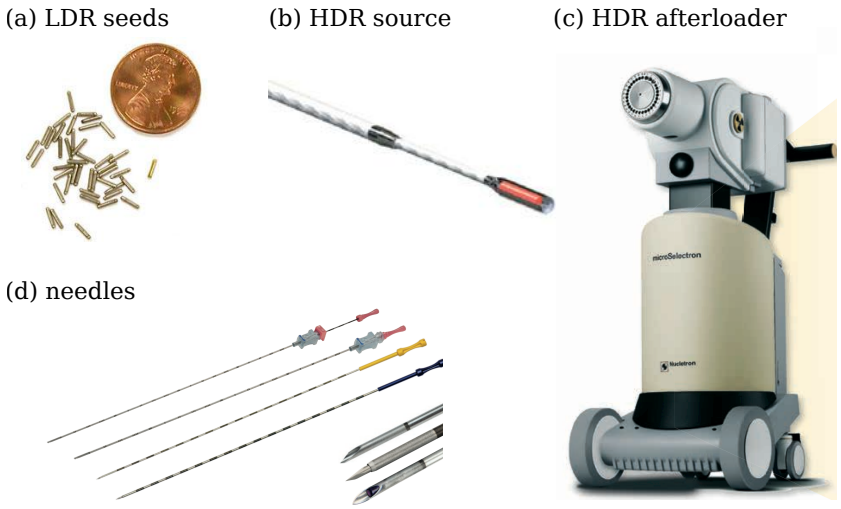

Figure 2.1: An overview of the used sources (a,b) [49, 50] the afterloader (c) [51] and the needles used for insertion of the sources (d) [52].

applicators (hollow needles (fig. 2.1 d)) are used to position the sources.
Depending on the dose rate, different types of radioactive sources with a variety of radionuclides are used. A table summarizing them can be found in appendix tab. A.1.
While for continuous LDR brachytherapy, the radionuclide is encapsulated in so-called seeds which remain in the tumor and allow a continuous irradiation (fig. 2.1 (a)).
The sources used for HDR brachytherapy are attached to wires (fig. 2.1 (b)). So-called afterloaders (fig. 2.1 (c)) are used to push the sources into the implanted needles to allow fractionated treatment similar to the fractionation schemes in external beam therapy. Between different fractions, the needles are either removed or remain inside the patient [48].

Although brachytherapy can be used for many treatment sites, this thesis concentrates on prostate brachytherapy. However, all concepts that will be discussed in the following are transferable to other sites such as cervix, breast, skin and many others [5].

2.2.1 Brachytherapy for treatment for prostate cancer

For early stage prostate cancer, brachytherapy is favorable with respect to prostate-specific antigen free survival and therapeutic side-effects when compared to external beam radiation therapy or radical prostatectomy [53]. The latter is a surgical removal of the prostate gland. Brachytherapy options are the one-day procedure of LDR, the fractionated HDR brachytherapy as a monotherapy, or the

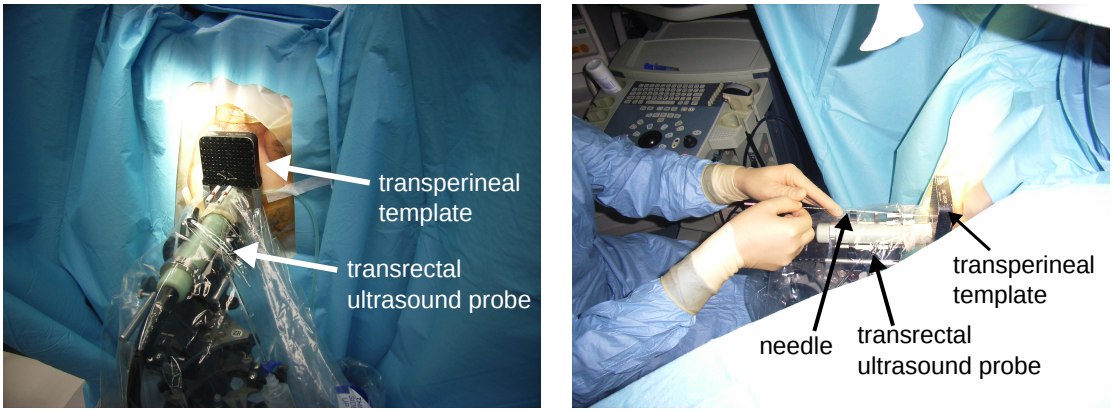

(a) (b)

Figure 2.2: Images of the intervention showing the setup before (a) and during needle insertion (b). The patient is placed in a lithotomy position.

combination with external beam radiation therapy as a so-called boost [54]. The brachytherapy interventions, independent of the used dose-rate, are described in the following.
During intervention the patient is placed in a lithotomy position (fig. 2.2). In order to view the prostate gland and the surrounding tissue, a transrectal ultrasound is used. This is a 3D ultrasound device that is inserted into the rectum. Potential source positions are defined using a template. The template has a rectangular grid-array of holes with a $5\,mm$ distance attached to the transrectal ultrasound. It defines the needle trajectories and can be used as a guidance for needles.
The workflow of the brachytherapy intervention is as follows (fig. 2.3):

1. The patient enters the surgery room and undergoes (local) anesthesia.
2. The ultrasound device is inserted into the rectum and the OARs as well as the planning target volume (PTV) are contoured.
3. Intra-operative treatment planning is performed.
4. The needles are inserted through the perineum using the transperineal template and the transrectal ultrasound for guidance.
5. If a deviation between planned and actual trajectory is detected, the plan is updated.
6. The source are inserted into the needle to deliver the treatment.

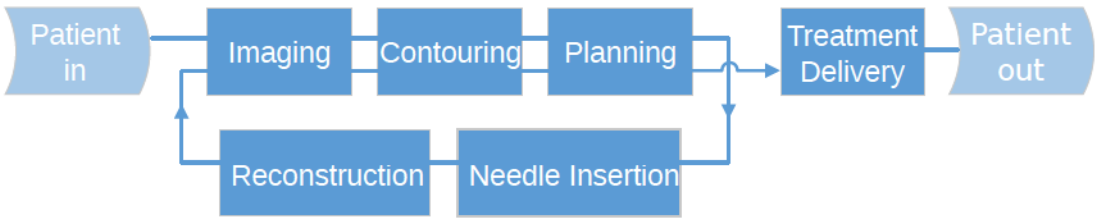

Figure 2.3: The wokflow of brachytherapy independent from the used modality.

The injection of the radioactive sources is usually performed automatically by a robotic systems for source placement such as the commercial devices MicroSelectron (HDR) or the SeedSelectron (LDR), Elekta AB, Sweden.

2.2.2 Treatment planning

The goal in ITP is to cover the PTV with a prescribed dose and to spare the OARs as well as possible. The approach is to reformulate the clinical requirements into a mathematical model using a so-called objective functions $\mathcal{Q}(\boldsymbol{x})$, which are able to score a plan. The optimization problem is to determine the number of needles, dwell-positions, and connected dwell-times. The term dwell-position describes the possible position where the source can be placed. In addition, dwell-time is the period of time the source remains at a certain dwell-position.
The goal of ITP is to minimize the objective function which can be written as an inverse problem. For the ITP in brachytherapy the problem is given by:

$$\boldsymbol{x}^* = \arg\min_{\boldsymbol{x}} \mathcal{Q}(\boldsymbol{x}) \tag{2.5}$$

This inverse problem can be solved with a wide variety of different optimizers as it will be discussed in detail in sec. 3.2.
To understand the underlying concepts in detail, a strict mathematical formulation is explained in the following. All introduced variables and notations used for ITP for the remainder of this thesis are introduced here.

The following treatment planning example show the complexity of the problem:
A typical setup contains a total of 40 possible needle trajectories and approximately five different dwell-positions per needle. The final plan should consist of 15 needles and 40 seeds. This leads to $\binom{40}{15} = 4 \cdot 10^{10}$ possible needle configurations and $\binom{5 \cdot 15}{40} = 3 \cdot 10^{21}$ possible arrangements of the seeds. In total this results in approximately $1.2 \cdot 10^{32}$ different possibilities. From these, the configuration with the best quality has to be chosen.

Mathematical model

In order to optimize a treatment plan, different organs and structures have to be represented by dose points. Dose points can be generated by two different approaches. Firstly, the points are randomly sampled within the volume of both, the organs and structures given by certain sampling densities. Secondly, the points can be generated using a regular grid with a certain sampling resolution inside the volume and equidistant points at each of the contours of the organs and structures in every 2D slice of the transrectal ultrasound image. For each of the organs or structures $\nu \in \{1, \ldots, o\}$, where o represents their total number, the calculated dose-points $\boldsymbol{\rho}_i^{(\nu)} \in \mathbb{R}^3$ can be summarized in the set $\boldsymbol{\Lambda}_\nu = \left\{\boldsymbol{\rho}_1^{(\nu)}, \ldots, \boldsymbol{\rho}_p^{(\nu)}\right\}$. The set of all dose points P can be written as the union:

$$\boldsymbol{P} = \bigcup_{i \in \nu} \boldsymbol{\Lambda}_i \tag{2.6}$$

Exemplary, the dose points of the volume and the surface for the PTV of a representative patient are shown in fig. 2.4.
The dwell-positions are a set of locations where the sources can be placed in the body. Those positions are located inside the needles and are placed equidistantly along the trajectory of the needle. Only the needles that hit the PTV and, at the same time, do not penetrate the surrounding OARs are considered for planning. They form the set of all available needles $\boldsymbol{\Pi} = \{1, \cdots, n\}$. Each needle trajectory intersects with the surface of the PTV (including all margins) such that the dwell-positions $\boldsymbol{\xi} \in \mathbb{R}^3$ are within the interval $[\boldsymbol{\chi}_i^s, \boldsymbol{\chi}_i^e]$. Finally the set of all potential positions $\boldsymbol{\Gamma}_i$ per needle i is given by:

$$\boldsymbol{\Gamma}_i = \left\{ \boldsymbol{\xi} \,|\, \boldsymbol{\xi} = \iota \boldsymbol{\chi}_i^s + (1-\iota)\boldsymbol{\chi}_i^e : \iota = \left\{ 0, \frac{1}{p_i - 1}, \ldots, \frac{p_i - 1}{p_i - 1} \right\} \right\}, \tag{2.7}$$

where p_i is the total number of potential dwell-positions on the corresponding needle. Thus, the set of all available dwell-positions is:

$$\boldsymbol{S} = \bigcup_{i \in \Pi} \boldsymbol{\Gamma}_i \tag{2.8}$$

When introducing oblique or bended needles, the line equation eq. (2.7) has to be replaced by an appropriate 3D parametrization of each of the needle paths.
For the later developed CS inspired optimization strategies, it is important to know which dwell-position j belongs to a needle i. The index set containing this information is given by:

$$\boldsymbol{\Upsilon}_i = \left\{ j \,|\, j = \iota \cdot \left(1 + \sum_{l=1}^{n} p_i \right) : \iota = \{0, \ldots, p_i - 1\} \right\} \tag{2.9}$$

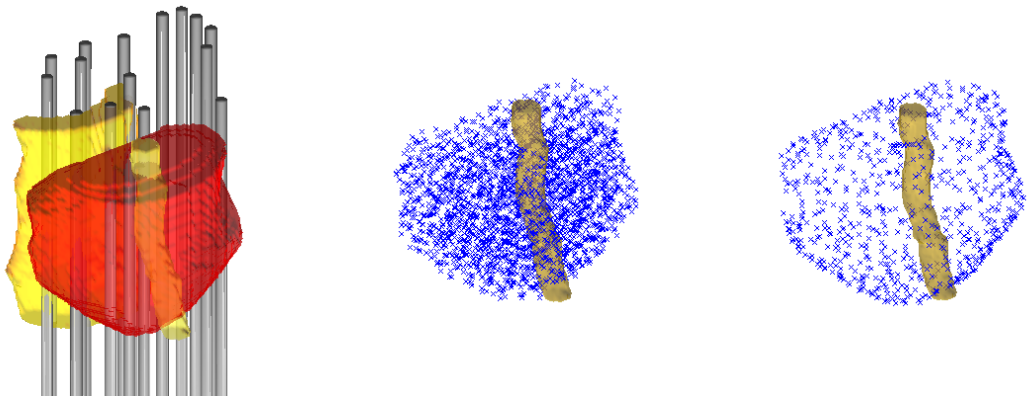

(a) overview (b) volume dose-points (c) surface dose-points

Figure 2.4: Overview of the 3D setup of PTV, OARs and all available needles (a). The prostate is shown in red urethra and rectum in yellow and needles are visualized in gray. In addition, the randomly generated dose-points of volume (b) and surface (c) of the PTV are shown.

Dose calculation

The dose calculation in brachytherapy is based on the recommendations of the American Association of Physicists in Medicine Task Group No. 43 (TG-43) and its updates [55, 56, 57]. This is a widely accepted protocol and currently the worldwide standard for brachytherapy dosimetry. The protocol was developed for LDR brachytherapy. But it is used as a virtual source model for almost all interstitial and intravascular sources [58]. Schematic drawings for LDR and HDR sources are shown in fig. 2.5 (a) and fig. 2.5 (b), respectively.
The TG-43 protocol is a look-up-table based approach, where the entries of the tables are determined using Monte Carlo simulations or measurements in water phantoms [58]. The dose-rate $\dot{D}(r,\theta)$ for a cylindrical (2D) distribution around a source can be calculated according to [57]:

$$\dot{D}(r,\theta) = \mathcal{S}_k \cdot \Lambda \cdot \frac{G_L(r,\theta)}{G_L(r_0,\theta_0)} \cdot g_L(r) \cdot F(r,\theta) \tag{2.10}$$

Where r is the distance between the source center and the point of interest. In addition, θ is the polar angle between this point and the source long axis z (fig. 2.5 (c)). The radius r_0 denotes a reference distance of $1\,cm$ and θ_0 a reference angle of $\frac{\pi}{2}$. The source strength $\mathcal{S}_k$ has the unit of $U := \mu\, Gy\, h^{-1}\, m^2$ and is usually measured in free air using lithium fluoride thermoluminescent dosimeters [55]. Λ defines the dose-rate constant in water in units of $cGy\, h^{-1}\, U^{-1}$. It depends on the used radionuclide and the source model. The geometric functions G_L are used to improve the accuracy of the dose calculation. From a physical point of view,

(a) LDR: I-125

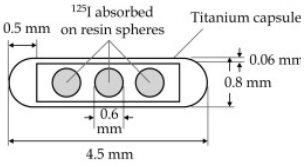

(b) HDR: Ir-192

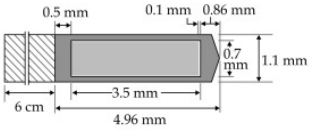

(c) TG-43

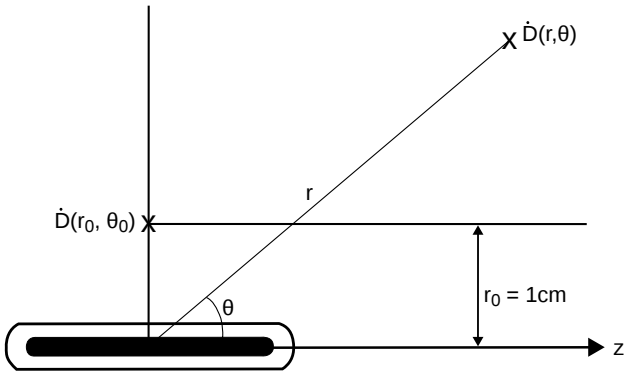

Figure 2.5: A schematic drawing of a I-125 seed for LDR (a) and a Ir-192 source for HDR (b)[57, 59]. The coordinate system used for brachytherapy dose-calculations used in the TG-43 protocol.

it corrects the obtained values by taking into account the spatial distribution of radionuclides inside the capsule based on an approximate model of the source. The radial dose function $g_L(r)$ considers the photon attenuation and scattering in tissue. $F(r,\theta)$ is a form factor that corrects the computed according to measured dose-distribution around the source. Causes of anisotropy are the distribution of the radionuclides, self-absorption, and filtering [55, 56, 57].
Considering the introduced mathematical model presented in the previous section, the dose contribution at a given dose-point $\boldsymbol{\rho_i}$ from a dwell-position $\boldsymbol{\xi_j}$ can be calculated according to:

$$\boldsymbol{D}_{ij} = d(\boldsymbol{\rho_i}, \boldsymbol{\xi_j}) = \left(\int_0^{t_{treat}} \dot{D}\left(r(\boldsymbol{\rho_i}, \boldsymbol{\xi_i}), \theta(\boldsymbol{\rho_i}, \boldsymbol{\xi_i})\right) dt \right), \tag{2.11}$$

where t_{treat} is the treatment time, $r = r(\boldsymbol{\rho_i}, \boldsymbol{\xi_i})$ is the Euclidean distance between dose-point $\boldsymbol{\rho_i}$ and dwell-position $\boldsymbol{\xi}_i$ and $\theta = \theta(\boldsymbol{\rho_i}, \boldsymbol{\xi_i})$ is the angle between the vector $(\boldsymbol{\xi_i} - \boldsymbol{\rho_i})$ and the source long axis z (fig. 2.5). Furthermore, $\boldsymbol{D}$ is the so-called dose-rate dictionary. Eq. (2.11) is valid for LDR dose-caclulation. For HDR, in good approximation, the air-kerma strength of the source dose not change, because the half-live of the source is much larger than the treatment time. Thus, the integral can be approximated by the mean of the dose-rate times the dwell-time t_i at dwell-position i. A visualization of the dose dictionary for a LDR source is shown in fig. 2.6.
Defining $\boldsymbol{x}_{LDR/HDR}$ to be an amplitude vector that labels if a certain dwell-position is occupied or not and $\boldsymbol{d}_\nu$ to be a dose vector for all available dose points of the set $\boldsymbol{\Lambda_\nu}$, the dose can be written as a matrix vector product:

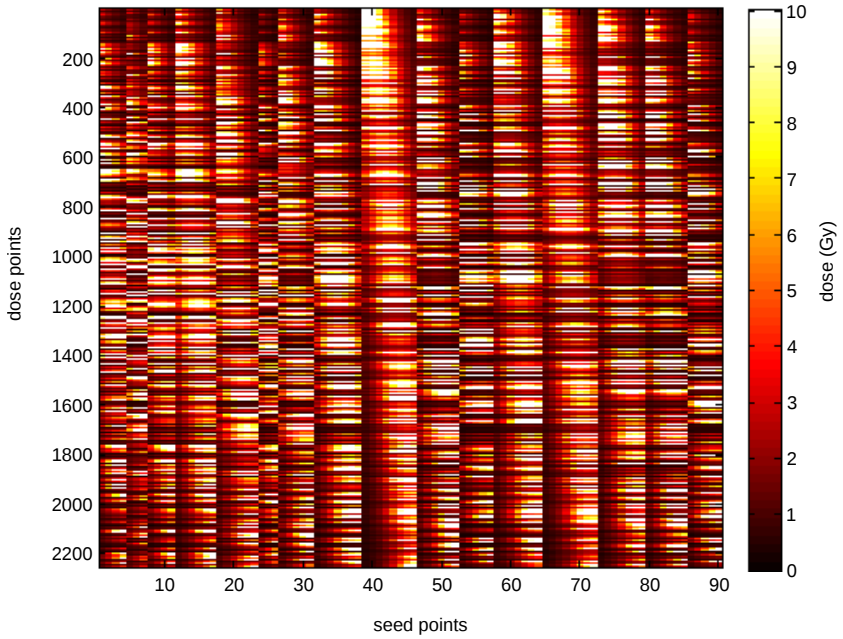

Figure 2.6: A visualization of the dose dictionary for a LDR source.

$$\boldsymbol{d}_\nu = \boldsymbol{D}_\nu \cdot \boldsymbol{x} \tag{2.12}$$

For LDR, $\boldsymbol{x}_{LDR} = \{0,1\}^s$ is a binary vector where an occupied dwell position is labeled with one and an unused is labeled with zero. In contrast to LDR, in HDR $\boldsymbol{x}_{HDR}$ is continuous and hence $\boldsymbol{x}_{HDR} = \{\mathbb{R}^+\}^s$.

2.2.3 Objective Function for ITP

A perfect plan would be able to deliver the prescribed dose to the target volume and to spare the surrounding OARs as good as possible. Ideally, the dose to the OARs would be zero, however, this is physically not achievable. Hence, a compromise between dose to the tumor and to the OARs has to be found, using an appropriate objective function. A sub-class of the objective functions is the DBOF that penalizes dose values below or above certain threshold [30].
A natural measure to quantify the deviation between the prescribed dose and the achievable dose is the Euclidean distance. This concept is also addressed by the DBOF that penalizes values above and below given dose bounds defined by the user. The functions in vector notation are [30]:

$$f_L^\nu(\boldsymbol{x}) = \theta\left(\boldsymbol{t}_L^\nu - \boldsymbol{D}^\nu \cdot \boldsymbol{x}\right)^T \cdot \left(\boldsymbol{t}_L^\nu - \boldsymbol{D}^\nu \cdot \boldsymbol{x}\right), \tag{2.13}$$

$$f_U^\nu(\boldsymbol{x}) = \theta\left(\boldsymbol{D}^\nu \cdot \boldsymbol{x} - \boldsymbol{t}_U^\nu\right)^T \cdot \left(\boldsymbol{D}^\nu \cdot \boldsymbol{x} - \boldsymbol{t}_U^\nu\right), \tag{2.14}$$

where $\theta(\cdot)$ is the Heaviside step function, $\boldsymbol{t}_L^\nu$ is the lower and $\boldsymbol{t}_U^\nu$ is the upper dose bound of the organ ν. Usually, upper and lower bound are only prescribed to the PTV since it should be covered at least with the prescribed dose but at the same time a certain dose should not be exceeded to avoid hot-spots. For OARs, solely an upper bound is assigned, which is the maximally acceptable dose. A list with prescribed doses for the different modalities and used radionuclides is summarized in appendix tab. A.4.
The final objective function value $\mathcal{Q}(\boldsymbol{x})$ is defined as a weighted sum of the different functions over all organs ν:

$$\mathcal{Q}(\boldsymbol{x}) = \sum_\nu \frac{1}{|\Lambda_\nu|} \cdot (w_L^\nu \cdot f_L^\nu + w_U^\nu \cdot f_U^\nu) \tag{2.15}$$

$|\Lambda_\nu|$ is the total number of dose-points at organ ν and w_L and w_U are weighting factor for penalizing under and over-dosage, respectively.
For needle optimization, the state of the art approaches is to penalize the number of used needles using a weighting factor, usually referred as cost per needle [30]:

$$\tilde{\mathcal{Q}}(\boldsymbol{x}) = \mathcal{Q}(\boldsymbol{x}) + \lambda_N \cdot \mathcal{N}(\boldsymbol{x}) \tag{2.16}$$

where $\mathcal{N}(\boldsymbol{x})$ is a function that returns the used number of needles for a given amplitude vector $\boldsymbol{x}$ and λ_N is the cost per needle, i.e. a Lagrange multiplier.

2.2.4 Plan evaluation

After optimization, each plan is rated according to different criteria and parameters. In general, users are encouraged to follow the definitions proposed by the PROBATE group of the Groupe Européen de Curiethérapie (GEC) European Society for Radiotherapy & Oncology (ESTRO) and the AAPMs Task Group No. 137 [60, 10]. In additional to those, parameters such as conformal index (COIN), equivalent uniform dose (EUD), TCP and NTCP based on biological models are used [10, 61].

Dosimetric criteria

Dosimetric criteria for each of the organs can be extracted from the dose-volume histogram (DVH) to rate a plan according to its clinical applicability. These empirically found values which correspond with good dose conformity for the PTV while, for the OARs, they correlate with an acceptable level of toxicity [60, 62, 10].
For example the used parameters for LDR are: For the prostate $V100 \geq 95\%$ and $V150 \leq 50\%$, for urehta $D30 \leq 120\%$ and $D10 \leq 150\%$, and for the rectum $D0.1cc \leq 150\%$ and $D2.0cc \leq 150\%$.

The $V100$ criterion of the prostate measures the coverage of the target volume with at least 100 % of the prescribed dose while D30 defines the dose received by at least 30 % of the urethral volume. The dosimetric criteria for the rectum are defined in absolute volumes in cc ($1\,cc = 1\,cm^3$).
If all given criteria are fulfilled, the plan is considered as clinically acceptable. A summary of the criteria for the different modalities can be found in appendix tab.A.3.

Conformal index

COIN is based on the combination of DVH parameters in order to include anatomical position relationships. It takes into account the coverage of PTV with the prescribed dose as well as the irradiation of the surrounding normal tissue (T) in the proximity of the PTV and is defined as [63]:

$$COIN = V100_{PTV} \cdot \frac{V100_{PTV} \cdot V_{PTV}}{V100_T \cdot V_T}, \tag{2.17}$$

where $V100_{PTV}$ and $V100_T$ are the relative sub-volumes of irradiated tissue that receive at least the prescribed dose with respective absolute volumes V_{PTV} and V_T. The irradiated tissue includes the PTV and all OARs. In an ideal situation, COIN equals one meaning that the PTV is covered with the prescribed dose and that the surrounding tissue does not receive any dose.

Biological models

The biological consequences can be described by dose-repsonse curves. The more dose the tumor receives, the higher is the probability of tumor control. A TCP of 100% means relapse free survival. However, due to the dose escalation, normal tissue complications arise as side-effects. Therefore, to find the ideal prescribed dose to target the treatment plan should also be rated according to its biological consequence.
In order to estimate TCP and NTCP, the biological effective dose (BED) for an inhomogeneous dose distribution has to be calculated. The conversion from dose to BED at a given dose point i from the set $\mathbf{\Lambda}_\nu$ is [64]:

$$BED_i = D(T_{eff}) \cdot RE(T_{eff}) - \ln 2 \cdot \frac{T_{eff}}{\alpha \cdot T_P}, \tag{2.18}$$

where T_{eff} is the efficient treatment time, T_P the potential doubling time of the tumor cells, α the model-parameter from the linear-quadratic model (eq. 2.4), and $RE(T_{eff})$ the relative effectiveness given by:

$$RE(T_{eff}) = 1 + \left(\frac{\beta}{\alpha}\right) \frac{\dot{D}_0}{(\mu - \lambda)} \cdot \frac{1}{1 - \exp(-\lambda \cdot T_{eff})} \cdot \left\{1 - \exp(-2 \cdot \lambda \cdot T_{eff}) - \frac{2\lambda}{\mu + \lambda}\left(1 - \exp(-(\mu + \lambda)T_{eff})\right)\right\} \quad (2.19)$$

Here, $\dot{D}_0$ defines the initial dose-rate, λ the decay constant of the radionuclide and μ the time for sub-lethal damage repair [10]. The parameter β is the quadratic parameter of the linear-quadratic model. The BED for an inhomogeneous dose-distribution is defined as:

$$BED = -\frac{1}{\alpha} \ln\left(\sum_i \frac{1}{|\mathbf{\Lambda}_\nu|} \exp(-\alpha \cdot BED_i)\right) \quad (2.20)$$

This yields the final TCP for a total number of tumor cells N_0:

$$TCP = \exp\left(-N_0 \cdot \exp(-\alpha \cdot BED)\right) \quad (2.21)$$

An additional parameter which can be used for rating of plans is the EUD. This is the dose leading to the same amount of cell killing as an external beam radiation therapy with a fraction size of $d_2 = 2\,Gy$ [10]. Using γ_t as the elapsed unit of treatment time, EUD can be calculated as [10]:

$$EUD = \frac{BED - \ln 2 \cdot \frac{\gamma_t}{\alpha \cdot T_P}}{1 + \frac{\beta}{\alpha} \cdot D - \gamma_t \frac{\ln 2}{\alpha \cdot d_2 \cdot T_p}} \quad (2.22)$$

In order to determine the biological reaction of the normal tissue, the equivalent dose $D_{eq,i}$ has to be calculated for every single dose point i of the OAR. The equivalent dose can be calculated using eq. (2.22) and replacing the BED with eq. (2.18) instead of using eq. (2.20). The terms addressing the proliferation are neglected.

For the urethra, the main complication is an unresolved grade-2 (or higher) toxicity. This NTCP was empirically found to be linked to the dose that at least covers 20% urethral volume ($DU20$). Using a logistic function, the probability is calculated according to [65]:

$$NTCPU = \frac{1}{1 + exp(-[\zeta + \delta \cdot DU20])}, \quad (2.23)$$

where $\zeta = -2.60 \pm 0.50$ and $\delta = (6.6 \pm 1.6) \cdot 10^{-3}\,Gy^{-1}$ are model parameters, which are determined empirically [65].

In order to calculate the NTCP of the rectum, the following logistic function describing severe late reactions is used [61]:

$$NTCPR = \left\{ 1 - \prod_i \left[1 - \left(1 + \left(\frac{D50}{D_{eq,i}} \right)^{k_\nu} \right)^{-s_\nu} \right]^{\frac{1}{|\mathbf{\Lambda}_\nu|}} \right\}^{-s_\nu}, \tag{2.24}$$

where $D50$ is the dose that leads to late injuries in 50% of the cases. In addition, k_ν und s_ν are parameters to describe the seriality of an organ [66]. Again, all parameters have to be empirically determined [67]. A table with the used parameters can be found in appendix tab. A.6.

2.3 Compressed Sensing

CS is a method in the field of image processing, which recently received a lot of interest in signal recovery and sampling problems [68].
In general, the conventional recovery and sampling approaches used in modern communication and medical image devices are based on the Shannon theorem. It states that in order to be able to sample or reconstruct a signal, the sampling rate must at least twice the maximum frequency of the signal [68].

$$f_{Sampling} \geq 2 \cdot \max(f_{Signal}) \tag{2.25}$$

In contrast, the theory of CS asserts that, when expressed in a proper basis, exact reconstruction can be achieved from far fewer samples or measurements. Surprisingly, almost all natural signals can be described by a sparse representation of base elements [68]. In CS, the basis elements are sometimes referred to as atoms. A sparse signal $\boldsymbol{g}$ is characterized by a sparse linear combination of k elements given by: $\boldsymbol{g} = \sum_{k \in K} \boldsymbol{f}_k \boldsymbol{a}_k$ where K is a subset of $N = \{1, \cdot, n\}$, n as the dimension of the problem, $\boldsymbol{f}_k$ is the amplitude, and $|K| \ll n$.
The choice of the basis depends on the problem. One prominent example is JPEG and JPEG2000 compression [69, 70]. JPEG uses a cosine dictionary and JPEG2000 relies on a discrete wavelet dictionary. When both have the sane factor of compression, JPEG2000 suffers from less artifacts compared to JPEG as depicted in fig. 2.7. It can be often observed that compression factors of up to 100 can be used without a perceptual loss in quality.
Next to image reconstruction and denoising, CS has its well-established niche in the field of medical physics, e.g. in magnetic resonance imaging reconstruction and compressed sensing in computed-tomography reconstruction techniques [71, 72, 73, 74].

(a) original (b) JPEG (c) JPEG 2000

Figure 2.7: Comparison of the orginal image against the compressed images using JPEG (b) and JPEG2000 (c)

2.3.1 The compressed sensing problem

Many of the CS problems are linear and have the following mathematical structure:

$$\boldsymbol{f}^* = \arg\min \|\boldsymbol{f}\|_0 \qquad s.t. \qquad \boldsymbol{A}\boldsymbol{f} = \boldsymbol{g}, \tag{2.26}$$

where $\boldsymbol{A}$ is a proper basis that allows a sparse representation $\boldsymbol{f}$ of a given measured signal $\boldsymbol{g}$. In addition [75],

$$\|\boldsymbol{f}\|_0 = \lim_{p\to 0} \|\boldsymbol{f}\|_p^p = \lim_{p\to 0} \sum_{k=1}^{m} |\boldsymbol{f}_k|^0 = \{i \in \{0,\ldots,n-1\} : \boldsymbol{f}_i \neq 0\} \tag{2.27}$$

is the l_0-norm, that counts the number of nonzero elements in a vector $\boldsymbol{f}$. This semi-norm does not fulfill all axiomatic requirements of a norm. However, it directly measures the sparsity of the solution.
Eq. (2.27) is a classical problem of combinational optimization and it is generally hard to solve. For example, assuming a matrix $\boldsymbol{A}$ with $m = 300$ basis vectors and a desired sparse solution with $k = 40$ elements, one way to find the global optimum is to test all possible non-zero subsets of $\boldsymbol{f}$. This leads to $\binom{300}{40} = 9.8 \cdot 10^{49}$ different configurations. Each of the configurations form small linear sub-problems, which have to be solved independently. Obviously, to calculate almost 10^{50} solutions takes too long. The complexity of this strategy is exponential in m and it was proven that the problem stated in eq. (2.26) is NP-hard [76, 77]. NP-hard means that there is no algorithm of polynomial complexity known that solves this class of problems.
The research question in the field of CS is whether the problem (eq. (2.26)) can be efficiently approximated by some greedy methods and which approximations lead to acceptable solutions [75].

2.3.2 Algorithms

Instead of finding the global optimum, the aim of the optimizers is to find an approximate solution near the global optimum. The requirements for such algorithms are that they have to be fast and return solutions near the global optimum [78]. At present, there are two major approaches, greedy pursuit algorithms such as matching pursuit (MP) with its variants [77] and basis pursuit (BP) algorithms [79]. The first are methods that iteratively optimize the problem using local updates and the latter use a convex relaxation method for solving the problem.

Matching Pursuit

One of the simplest algorithms to solve the CS problem is MP [80]. MP is a purely greedy algorithm with a straightforward approach to include the element from the dictionary which correlates most with the residual during each iteration.
The algorithm starts with an initial residual $\boldsymbol{r}^{(0)}$ that is equal to the signal $\boldsymbol{g}$ and an initial solution $\boldsymbol{f}^{(0)} = \boldsymbol{0}$. During each iteration step j, the following sub-problem is solved:

$$i_k^* = \underset{i=1,\dots,m}{\arg\max} \left| \left\langle \boldsymbol{r}^{(j-1)}, \boldsymbol{a}_i \right\rangle \right|, \tag{2.28}$$

where $\boldsymbol{a}_i$ is one element of $\boldsymbol{A}$. The index i_k^* defines the new residual $\boldsymbol{r}^{(j)}$ and an approximation of the solution $\boldsymbol{f}^{(j)}$ that is given by [78]:

$$\boldsymbol{f}^{(j)} = \boldsymbol{f}^{(j-1)} + \left\langle \boldsymbol{r}^{(j-1)}, \boldsymbol{a}_{i_k^*} \right\rangle \cdot \boldsymbol{a}_{i_k^*}, \tag{2.29}$$

and

$$\boldsymbol{r}^{(j)} = \boldsymbol{r}^{(j-1)} - \left\langle \boldsymbol{r}^{(j-1)}, \boldsymbol{a}_{i_k^*} \right\rangle \cdot \boldsymbol{a}_{i_k^*}. \tag{2.30}$$

A step where an element is added to form a new solution is later referred to as expansion step. The iterations continue as long as a k-sparse solution is not reached and/or the norm of the residual is above a certain error tolerance $\epsilon > \|\boldsymbol{r}^{(j)}\|_2^2$. For an orthonormal basis, the approximate solution leads to an optimal k-term approximation [78]. For general dictionaries it was proven that the norm of the residual converges towards zero [81].

Orthorgonal Matching Pursuit

An extension of the MP approach is orthogonal matching pursuit (OMP), which adds a least-square minimization to each of the iteration steps [82]. This leads to a significantly improved performance and robustness of the heuristic [75].
The initialization and the selection step during the iteration remain the same. Introducing the so-called support vector $\boldsymbol{v}^{(j)}$ of iteration j that is an index-vector

containing the indices of the selected elements of the dictionary $\boldsymbol{v}^{(j)} = \{v_1, \ldots, v_j\}$, the following least-square sub-problem can be defined:

$$\boldsymbol{f}^* = \arg\min_{\boldsymbol{f}} \|\boldsymbol{g} - \boldsymbol{A}^*\boldsymbol{f}\|_2^2 \qquad s.t. \qquad \boldsymbol{A}^* = \{\boldsymbol{a}_{v_1}, \ldots, \boldsymbol{a}_{v_j}\} \tag{2.31}$$

During each iteration, eq. (2.29) and eq. (2.30) are replaced with the following equations:

$$\boldsymbol{f}^{(j)} = \boldsymbol{f}^*, \tag{2.32}$$

$$\boldsymbol{r}^{(j)} = \boldsymbol{g} - \boldsymbol{A}^*\boldsymbol{f}^{(j)}, \tag{2.33}$$

where $\boldsymbol{f}^*$ is the solution of eq. (2.31). The stopping criteria are the same for MP. In contrast to MP, OMP has the advantage that an element of the dictionary cannot be included twice because the residual is orthonormal to these elements [78].
A simplification of OMP is the hard thresholding algorithm, which is one of the simplest greedy algorithms in literature [75]. After an initial so-called back-projection $\boldsymbol{p} = \boldsymbol{A}^T\boldsymbol{g}$, the set of k largest elements is taken to form the support vector $\boldsymbol{v}$. Afterwards, the least-square sub-problem subject to the found support is solved and the final solution is formed.

Basis Pursuit

BP follows the idea to replace the l_0-norm by the l_1-norm. This is a convex relaxation of the problem where the number of terms is approximated by the absolute sum of all coefficients. The relaxed optimization problem is hence given by [79]:

$$\boldsymbol{x}^* = \arg\min_{\boldsymbol{f}} \|\boldsymbol{f}\|_1 \qquad s.t. \qquad \boldsymbol{A}\boldsymbol{f} = \boldsymbol{g} \tag{2.34}$$

This problem can be solved by LP such as interior-point or simplex methods.

Advanced Greedy Algorithms

The aforementioned algorithms are the most basic and simple techniques used in CS. The greedy algorithms are among the fastest optimization algorithms in the field of CS [33]. However, a general observation is that the quality of BP cannot be achieved with MP or OMP.
Recent developments improve the existing greedy algorithms in oder to increase their quality. Approaches that are able to guarantee reconstruction accuracies in the same range as BP are subspace pursuit (SP) or compressive sampling matching pursuit (CoSaMP) [83, 84].
SP and CoSaMP are based on the principles of the original OMP algorithm. The

main idea is to add multiple elements, a so-called candidate set, to the solution at each iteration step. Afterwards, the least-square optimization is performed. As an additional step, a test is conducted to identify low-performing elements. Those elements are defined in terms of the order statistics of the inner product. Finally, the low-performing elements are discarded and their contribution to the solution is removed. After this reduction, the iterations continue until the stopping criterion is reached.
The only difference between CoSaMP and SP is the number of elements that are added to form the candidate set. While SP adds $u > 0$ elements, CoSaMP adds $2u > 0$ elements to the solution.

Further Approaches

With the introduction of BP, the class of l_1-optimization problems has received much of attention. Inspired by the greedy algorithms, several new algorithms have been introduced to tackle the unconstrained formulation of the BP problem:

$$\boldsymbol{f}^* = \|\boldsymbol{f}\|_1 + \lambda_L \cdot \frac{1}{2} \|\boldsymbol{g} - \boldsymbol{A}\boldsymbol{f}\|_2^2 \tag{2.35}$$

where λ_L is the so-called Lagrange multiplier. The problem can be solved efficiently using iterative shrinkage algorithms. The optimization principles among the different algorithms are similar and are explained on the example of stage-wise orthogonal matching pursuit introduced by Donoho et al. [85]. In this case, the expansion step is replaced by a back-projection of the residual $\boldsymbol{r}^{(j-1)}$ at the iteration j onto the matrix $\boldsymbol{A}$:

$$\boldsymbol{p} = \boldsymbol{A}^T \boldsymbol{r}^{(j-1)} \tag{2.36}$$

From $\boldsymbol{p}$, k dominant entries are chosen and added to the support $\boldsymbol{\upsilon}^{(j)} = \{\upsilon_1, \ldots, \upsilon_k\}$. Afterwards, the least-square problem:

$$\boldsymbol{f}^* = \arg\min_{\boldsymbol{f}} \|\boldsymbol{g} - \boldsymbol{A}^* \boldsymbol{f}\|_2^2 \qquad s.t. \qquad \boldsymbol{A}^* = \{\boldsymbol{a}_{\upsilon_1}, \ldots, \boldsymbol{a}_{\upsilon_j}\} \tag{2.37}$$

can be optimized using for example the conjugate gradient technique. With the obtained solution, the residual is updated and the iterations continue until the stopping criterion is fulfilled.
Another technique that can solve a broad class of l_1-regularization problems is the iterative Split Bregman method. It can be used to optimize the unconstrained problems with the form of:

$$\arg\min_{\boldsymbol{d},\boldsymbol{g}} \|\boldsymbol{d}\|_1 + H(\boldsymbol{g}) + \frac{\lambda_L}{2} \|\boldsymbol{g} - \Phi(\boldsymbol{f})\|_2^2, \tag{2.38}$$

where $H(\cdot)$ and $\Phi(\cdot)$ are convex functionals [74]. Usually, $H(\cdot)$ is assumed to be the l_2-norm. This problem can be solved using a Split Bregman iteration where during each iteration the following two steps are performed:

$$(\boldsymbol{f}^{(j)}, \boldsymbol{g}^{(j)}) = \arg\min_{\boldsymbol{d},\boldsymbol{g}} \|\boldsymbol{d}\|_1 + H(\boldsymbol{g}) + \frac{\lambda_L}{2}\|\boldsymbol{g} - \Phi(\boldsymbol{f}) - \boldsymbol{b}^{j-1}\|_2^2 \tag{2.39}$$

$$\boldsymbol{b}^{(j)} = \boldsymbol{b}^{(j-1)} + \left(\Phi(\boldsymbol{f}^{(j)}) - \boldsymbol{d}^{(j)}\right) \tag{2.40}$$

This reduces the regularization problem to a sequence of Bregman updates [72]. However, for eq. (2.39), i.e. a combination of an l_1 and l_2-optimization problem, there are no efficient solvers available. One approach is to decouple the l_1-optimization from the l_2-optimization problem. This de-coupling leads to two independent problems:

$$\boldsymbol{f}^{(j)} = \arg\min_{\boldsymbol{f}} H(\boldsymbol{f}) + \frac{\lambda_L}{2}\|\boldsymbol{g}^{(j-1)} - \Phi(\boldsymbol{f}) - \boldsymbol{b}^{(j-1)}\|_2^2 \tag{2.41}$$

$$\boldsymbol{d}^{(j)} = \arg\min_{\boldsymbol{d}} |\boldsymbol{d}| + \frac{\lambda_L}{2}\|\boldsymbol{g} - \Phi(\boldsymbol{f}^{(j-1)}) - \boldsymbol{b}^{(j-1)}\|_2^2 \tag{2.42}$$

Both problems can be solved independently using efficient techniques, like conjugate gradient methods and thresholding for the l_2 and l_1 optimization problem, respectively. These iteration steps continue until the stopping criterion is reached. The Split Bregman approach is an efficient algorithm which can be used for image denoising and CS inspired problems in medical-physics [71, 72, 73, 74].

3 State of the Art

Accurate treatment planning is essential for the success of brachytherapy treatments. A variety of algorithms which accomplish this for the modalities LDR and HDR brachytherapy have been developed. Some of them are used in clinical routine. Furthermore, recent developments towards the usage of user-friendly objective functions are presented.

3.1 Treatment planning problem

The objective of brachytherapy and radiation therapy in general is to deliver a sufficiently high dose to the tumor and, at the same time, spare the surrounding healthy tissue as well as possible.
Assuming a given set of all potential dwell-positions, the goal is to determine the number of needles and their position as well as the used dwell-positions and connected dwell-times in order to form a plan which meets all clinical constraints.
In order to rate a plan, a measure that quantifies the quality of a given dose distribution with respect to the clinical criteria is used. Almost all recent publications consider the DBOF [26, 20, 86, 24, 86, 87, 88, 31].
The inverse optimization algorithms used in brachytherapy ITP depend on the selected objective function and the modality. Some of them are general and can be used for both LDR and HDR treatment planning while some are specific for one of these modalities. The following section provides an overview of the state-of-the-art algorithms and objective functions.

3.2 Algorithms

The used algorithms for ITP in brachytherapy are presented in the following. Additionally, one method which is not an inverse planning algorithm is graphical optimization (GrO). It is a "forward-planning" method, which is widely used in clinical routine as a stand-alone strategy or to manually update plans after ITP.

Graphical optimization

GrO is an interactive manual forward-planning method based on drag and drop actions to generate the desired isodose lines within a single slice of the 3D transrec-

tal ultrasound volume [89, 32]. This is achieved by either adjusting the dwell-times manually or by "inverse planning" where the dwell-times are either decreased or increased using a pre-defined fixed increment.
Changing the dose distribution in one slice changes the distribution in another slice, which has to be adjusted as well. This leads to a sometimes time-consuming trial-and-error method. Even for experienced users this can approach take up to one hour [29]. No objective function or anatomical information is used. Benefits are that the result of a drag-and-drop action is directly visible to the user and that it can be applied for both, LDR and HDR treatment planning.

3.2.1 LDR

In LDR brachytherapy ITP, the optimizers have to identify the binary dwell-time vector that optimizes the given objective function the most. This binary combinational problem is well-known to be intrinsically NP-hard [90]. The problem can be tackled either with deterministic approaches [91] or stochastic approaches that approximate the solution of the problem [90]. The different approaches used for LDR ITP are presented in the order they were developed.

Gradient based optimization

The earliest optimizers for LDR ITP were based on gradient descent methods [16, 17], which require a starting point and then follow the gradients iteratively until a local minimum is reached. The user has to provide an initial starting point and, thus, these methods are called semi-automatic approaches.

Genetic algorithm

The GA is a stochastic optimization strategy that is used in LDR ITP since 1996 [21]. In contrast to the gradient approaches, GA can be used to optimize the needle configuration as well.
The algorithm is a heuristic model that mimics the process of evolution. Based on the survival-of-the-fittest-principle, starting from an initial population (different solutions), the strongest individuals (best rated according to the used objective function) are selected to parent offspring. Different genetic operations, such as crossover and inversion [90] contribute forming the new generation, which repopulates again. Due to this heuristic, the probability that the solution is trapped in a local minimum is significantly reduced [90].

Simulated annealing

Another stochastic approach that mimics processes found in nature is SA [92]. The concept of SA annealing is based on the prinicples of statistical mechanics in

condensed matter physics [92].
To find the ground state of a material, i.e. the state with the lowest internal energy, experiments showed that cooling a liquid down to low temperatures is not sufficient. The ground state can only be reached when letting the system cool down slowly (annealing). Following this analogy, the SA is used to find a minimal objective function value. The algorithm starts with an initial configuration and iteratively changes this state according to a transition mechanism. This mechanism changes the present configuration to a new one which is rated with respect to its objective function value. Depending on the energy of the system, determined by a so-called cooling schedule, the transition is either accepted or rejected. If an appropriate cooling schedule is used, the algorithm is able to converge towards the global optimum [93].
The principle of SA was introduced in for radiation therapy plan optimization [93] and was adapted for LDR brachytherapy in 1996 by Pouliot et al. [18] and is usually referred as IPSA. It allows for an efficient and rapid optimization of dose distributions. One drawback of SA is that it requires a priori information such as an estimation of the used amount of seeds and needles. This restricts the domain of all potential seed positions which may yield sub-optimal solutions. The latest development in LDR ITP was the implementation of an inference system which allows the user to steer the SA search [94].

Mixed integer linear programming

Instead of using stochastic approaches such as SA and GA, another strategy is a reformulation of the objectives into an integer linear programming (ILP) or MILP problem.
To solve these problems, the branch-and-bound strategy is most widely used [95]. It starts with a relaxation of the problem without integer restriction that can be solved using the simplex method or interior point methods. During branching, one of the variables is picked and bound to form two constrained sub-problems. All sub-problems have to be solved independently and hence a tree like structure builds up. The branches are pruned when the sub-problem becomes infeasible or its objective function value is greater than the best integer or mixed-integer solution so far [95].
For LDR brachytherapy, different mixed integer programming problems were formulated starting from simple impositions of dose constraints for the different organs to the reformulation of the DBOF as MILP problem including needle optimization [96, 87, 27, 97, 28]. An important aspect is that, if the MILP is solvable, the branch-and-bound method is able to find the global optimum [91].

Greedy heuristics

Other heuristics that are not related to the optimization of the DBOF are greedy heuristics which optimize the ITP with a so-called adjoint function of the different organs and structures. The used adjoint function is a ratio that ranks each dwell-position according to its ability to irradiate the target while sparing OARs [23]. The ratio can be computed in advance and the optimization is performed using a greedy heuristic that is based on the same strategy as MP algorithms used in CS. While the discussed algorithm is not able to address needle optimization, a more recent approach suggests a methodology which can be used to rate possible combinations of needles and, thus, allows needle optimization [25].

3.2.2 HDR

In contrast to LDR, the HDR solution vector is continuous and non-negative. This problem can be tackled with a wide variety of optimization strategies, of which the most commonly used ones are presented in the following.

Gradient based optimization

Deterministic gradient-based methods for quadratic objective functions for HDR ITP were introduced by Milickovic et al. in 2002 [98]. They use a constraint free gradient-based reformulation which provides the local optimum for convex objective functions [99]. However, due to the Heaviside stepping function the used objective function is not convex and local optima may occur. A global convergence analysis with respect to the quadratic objective function used in HDR showed that the obtained solutions are near the global optimum [100].
By comparing different optimizers, the Limited-memory Broyden–Fletcher–Goldfarb–Shanno algorithm (L-BFGS) algorithm was found to be better than Broyden-Fletcher-Goldfarb–Shanno algorithm (BFGS) with respect to optimization time and quality [100]. The L-BFGS is today the standard optimizer for conjugate gradient based methods in HDR ITP.

Simulated annealing

Based on their previous work for LDR brachytherapy ITP, Lessard and Pouliot introduced a SA based optimization strategy for the HDR problem in 2001 [101, 102].
The principle is very similar to SA used in LDR brachytherapy. The difference is the transition step from the previous to the new configuration. Rather than activating or deactivating dwell-positions, the time is increased or decreased randomly by a given time resolution.

SA obtains an optimized dose distribution in a couple of seconds and allows an automatic needle optimization.

Hybrid inverse treatment planning and optimization

The HIPO algorithm is an optimization strategy especially designed for HDR treatment planning that was introduced by Karabis et al. in 2009 [20]. It supports inverse optimization of dwell-times including needle optimization [103].
HIPO unites the gradient-based dwell-time optimization with SA for needle optimization [20]. The algorithm starts with an initial needle-configuration and tests new configurations according to the objective function value of the dwell-time optimized sub-problem during the iteration. The sub-problem is optimized using L-BFGS.
The convergence to the global optimum cannot be guaranteed, but comparative tests showed that the retrieved solutions are near the global optimum [20].

Linear programming

LP problems can be solved with simplex or interior-point algorithms. The simplex algorithm is a global deterministic optimization method. It solves the problem by considering the $(n + 1)$-dimensional polytype, n is the number of free variables, and moving along the edges towards new feasible solutions with better objective function values. It stops when the global optimum is reached [104].
In 1989, Renner et al. introduced LP for HDR treatment planning. The idea was to minimize the total treatment time while the generated plans should fulfill predefined dose constraints on the target [105]. Almost two decades later, Alterovitz et al. presented a reformulation of the DBOF into an LP problem [24]. It solves the HDR ITP problem within several seconds.

3.2.3 Bottom-line algorithms

There is a variety of different algorithms available for brachytherapy treatment planning. However, only IPSA and HIPO are the main available and are implemented in commercially available treatment planning system (TPS)s, e.g. Oncentra Prostate, Elekta AB, Sweden [29]. While IPSA is mainly used for optimizing LDR treatment plans, HIPO is the method of choice for HDR treatment planning including fast needle optimization. The optimization times vary from a few seconds (ISPA) to several minutes (HIPO).
Although LP ITP can be performed within several seconds, it is not implemented in a commercially available TPS. In contrast, the optimization times for MILP vary between several hours and days and MILP is, thus, inappropriate for intraoperative treatment planning. However, it was shown that clinically acceptable

plans can be generated within few minutes if the optimizer is stopped manually [26, 28]. The returned solution is the best possible solution found by the branch-and-bound method at the time when the iteration is terminated.
All algorithms mentioned in this sections are commonly used to compare the solution of newly developed algorithms against returned objective function value as it is done in this thesis [20, 26].
Due to the runtime of IPSA and HIPO, a general observation is that interactive planning strategies like GrO are preferred by the user. Considering the large number of possible solutions GrO plans are most likely to be far away from the global optimum. Comparative studies showed that plans generated using IPSA or HIPO provide target coverage similar to those obtained using GrO but with lower dose to normal structures and better dose homogeneity [32].

3.3 Objective functions

Despite algorithmic developments, recent approaches try to improve the plan quality by introducing more realistic objective functions or to adapt existing methods by slightly modifying the underlying heuristics. A summary of the developments within the last four years is presented in the following.

3.3.1 Recent optimization strategies

The DBOF uses weights and thresholds to quantify the quality of a plan. If a plan does not meet the dosimetric criteria, manual fine-tuning of the parameters is necessary. Adapting weights and thresholds is not very intuitive and therefore often avoided by the users. Siauw et al. introduced an MILP problem formulation that is able to optimize the dosimetric criteria [31]. To accelerate calculation time, Siauw et al. relaxed the initial problem to an LP problem and applied a threshold to approximate the MILP solution afterwards. This strategy is called IPIP and it is able to generate clinically acceptable plans in several seconds.
An extension of the model that includes skew needle optimization was published in 2012 [106]. The idea was to perform needle optimization independent from dwell-time optimization. The needle optimization was subject to the constraint that all the dose-points should be within a certain range δ from the next adjacent dwell-position. This forms a binary problem that has to be solved to determine the needle configuration and which takes approximately four minutes [106]. Afterwards, the dwell-times are optimized using IPIP. With this concept, they proved that it is possible to independently optimize needles from dwell-positions and that the retrieved plans meet all dosimetric criteria.

It was observed that the ITP plans generated using the DBOF have a ten-

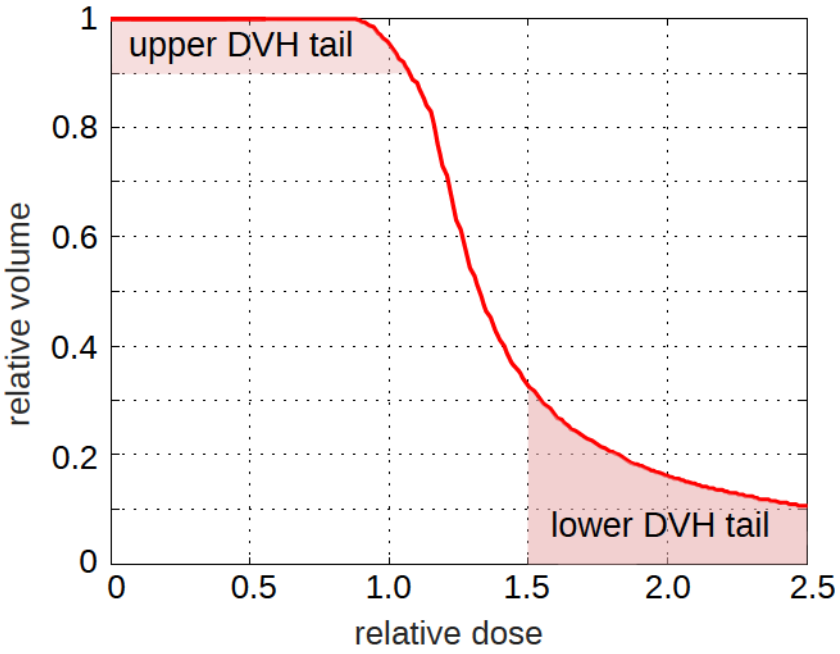

Figure 3.1: Illustration of the upper and lower DVH tail of the prostate.

dency towards less dwell-positions and longer dwell-times compared to manually generated plans. Concerns regarding those hot-spots raised [107, 108]. Solutions are to introduce virtual normal tissue around the catheter [107] or to introduce restrictions on the dwell-time in terms of upper bounds for the dwell-times [108]. Recently, Holm et al. proposed a method of a piecewise linear objective function that is able to significantly reduce the appearance of long dwell-times [109].

Another method trying to incorporate dosimetric criteria is based on a surrogate function utilizing the mean value of the upper and lower DVH tails (fig. 3.1) [86]. They can be mathematically modeled as linear functions by assigning upper thresholds. This leads to an LP problem which can be efficiently solved. Holm et al. reported that this strategy is able to generate plans that are equivalent to the competing strategies based on DBOF minimization. Nevertheless, when defining the bounds, the problem may be infeasible resulting in a tedious trial-and-error process. The time to generate a plan using this technique is approximately one minute.

Towards more realistic models, Giantsoudi et al. proposed a method based on the generalized EUD optimization [110]. The objective function was optimized using the gradient-based methods used in HDR ITP. When comparing the DBOF with the general EUD-based optimized plans, the latter show a slight decrease in COIN but a better sparing of the OARs.

Recently, enhanced geometrical optimization (EGO) and interactive inverse planning was published by Dinkla et al. [111]. EGO is a slightly modified version of GrO and is applied to create a dose distribution as homogeneously as possible. The interactive inverse planning can be used to tailor the dose distribution to the anatomy of the patient. This can be done by interactively changing the dose thresholds on a complete ROI. The algorithm iteratively increases or decreases the dwell-times in the vicinity until the new constraints are fulfilled. With this strategy clinically acceptable plans are generated in approximately five minutes.

3.3.2 Bottom-line developments

There are only three research groups working in the field of brachytherapy ITP worldwide and, thus, treatment planning in brachytherapy evolves slowly. Almost all developments are exclusively designed for the HDR ITP problem. Since the LDR ITP problem is more complex due to the binary dwell-times it is often neglected for the sake of simplicity. The same accounts for the needle optimization problem. Only the methodolgy proposed by Siauw et al. is able to optimize the ITP problem including needle optimization with a runtime similar to HIPO and IPSA [106].
All new developments are build on already used strategies and try to slightly modify or combine those [20, 31, 111]. Most of the used strategies are general heuristics and not tailored to the underlying structure of the ITP problem.
There is a tendency to develop more realistic models and objective functions to directly optimize dosimetric criteria. NPIP and the DVH tail-based optimization strategies are the only two methods which are able to address dosimetric criteria directly. However, due to fairly simple heuristic and the constraints, the solution might be suboptimal or infeasible compared to MILP solutions. NPIP and the DVH tail-based approach can be reformulated into a LDR ITP optimization problem. Due to the long runtime compared with standard optimizers this has not been investigated yet. Most likely this is due to the complexity of the problem. Even with modern computers the optimization time exceeds several days.
With respect to more realistic objective functions, there is no biological optimization method up to now. In brachytherapy, biological models are only used to retrospectively evaluate plans with respect to TCP and NTCP [112, 10, 61].

4 Materials and Methods

In the previous chapter, different state of the art optimizers for the ITP with advantages and disadvantages were discussed in detail. The goal of ITP is to cover the PTV with the prescribed dose and to spare the OARs as much as possible by minimizing the dose objective function. The state-of-the-art optimizers are general class solutions and not tailored to the underlying structure of the ITP and are hence inefficient. However, the obtained solutions are close to the global optimum.
Another optimization strategy which has not yet been considered, is to use sparse reconstruction techniques from CS. Bypassing the problem by introducing sparseness offers the usage of a novel class of optimizers that can be applied for this problem type. These algorithms are problem specific optimizers that are considerd to be among the fastest optimization strategies in CS.

Within the scope of ITP, the demand of sparsity yields treatment plans that consist of a sparse representation of dwell-positions and needles. This approach leads to two major benefits. Firstly, less needles reduce the risk of an infection. Secondly, less needles and seeds reduces the overall time of the intervention. Hence, both clinic and patients benefit from this approach. Introducing the sparsity aspect leads to interesting research questions:

1. What are the properties of using sparsity constraints on the solution with respect to the quality that is achieved?

2. What is the gain in performance using problem specific optimizers?

These questions should be answered in the following. Therefore, the feasibility of the concept is analyzed using an initial retrospective test. Based on the obtained results the ITP problem is reformulated to achieve a formulation that is structurally similar to the CS problem. Since standard optimizers from CS cannot be used for the CS ITP problem, a detailed explanation of the newly designed CS inspired solvers follows. Then the TPS, that has been developed within the scope of this thesis is introduced. A description of the retrospective study used to compare the new optimizers with state of the art methods concludes this section.

4.1 Introducing the demand of sparsity into the ITP problem

The focus of the state-of-the-art optimization strategies for ITP is subjected to minimizing different objective functions [20, 24, 26, 31, 86, 87]. As discussed in sec. 3.2, this problem can be optimized using a variety of general class optimizers. The concept of sparsity opens up the opportunity of using CS based inspired solvers to tackle the ITP problem. However, it is not intuitively clear whether this approach yields clinically acceptable plans with respect to underdosage and overdosage of PTV and OARs.
Interestingly, the request for sparse solution was implicitly raised within the context of IMRT treatment planning in order to reduce the number of beams. The aim of the research was how many intensity-modulated beams should be used to observe no practically relevant improvement of the treatment plan [113, 114, 115].

In brachytherapy planning, the question is how many dwell-positions have to be selected in order to retrieve a clinically acceptable plan?

An intial test is performed to anaylze the number of used dwell-position with respect to the total number of available dwell-positions of already applied plans. The results are summarized in tab. 4.1.

Table 4.1: Initial sparsity test for LDR and HDR treatment plans. For ten different patient cases ($P1, \ldots, P10$), '# used DP' and '# total DP' labels the number of dwell-positions which are used or available.

Modality	P1	P2	P3	P4	P5	P6	P7	P8	P9	P10
LDR										
# used DP	40	58	34	50	35	48	39	42	37	36
# total DP	207	364	192	293	198	297	213	217	234	206
HDR										
# used DP	54	93	47	58	54	62	59	68	66	53
# total DP	436	728	384	590	422	594	438	434	468	412

For LDR (17.5 ± 1.3, range: 15.8 to 19.4)% and HDR (12.6 ± 1.6, range: 9.8 to 15.7)% of the total number of dwell-positions are used to form the final plan. Since this is much less than the number of available dwell-positions, it is assumed that the concept of spare solution is applicable for brachytherapy ITP.
The request for sparsity in brachytherapy is a novel and interesting approach that

leads to the inquiry, whether it is possible to re-write the state of the art optimization problem as a formulation that incorporates the sparsity aspect. More importantly, the new formulation should have the same mathematical structure as those of CS type. This would allow the usage of the already mentioned highly efficient solvers applied in the field of CS (sec. 3.2) in the field of ITP.

4.2 Reformulation of ITP as a CS problem

The results of the feasibility test showed that the clinically acceptable plans can be represented using sparse combination of dwell-positions. This poses the question how many dwell-positions should be activated in order to achieve a demanded quality Q_0 and yields the following optimization problem:

$$\boldsymbol{x}^* = \underset{\boldsymbol{x}\in\Omega_{LDR/HDR}}{\arg\min} \|\boldsymbol{x}_0\|_0 \qquad s.t. \qquad \mathcal{Q}(\boldsymbol{x}) \leq Q_0, \tag{P1}$$

where $\Omega_{LDR} = \{0,1\}^s$ represents the domain of all potentials solutions for LDR and $\Omega_{HDR} = \{\mathbb{R}^+\}^s$ the domain of all potentials solutions for HDR for a given number of dwell-positions s. In addition, $\|\boldsymbol{x}\|_0 = \{\#i \in \mathbb{I}|x_i \neq 0\}$ is the l_0 seminorm which counts the number of nonzero elements of $\boldsymbol{x}$ as defined in eq. (2.27). Since the difference between LDR and HDR optimization exists only in the domain of all potential solutions, the subscripts LDR and HDR are dropped in the following section.
For ITP optimization, it has to be differentiated between optimizing a fixed needle configuration, where all possible dwell-positions should be taken into account or an optimization problem where the goal is to additionally optimize the number of used needles. These are two optimization problems with different complexities and thus the reformulation is split into an optimization problem with and one without needle optimization.
In order to highlight the CS inspired optimization problems, those are labeled with a 'P'.

4.2.1 Without needle optimization

The question arises, whether the ITP problem (2.5) can be reformulated, such that it is of CS type (eq. (2.26)) .
In addition, the system matrix is also bound to fulfills the exact recovery condition (ERC)[78]. However, the latter is hard or even impossible to evaluate for a given matrix[1][75]. Therefore, the focus is to reformulate the ITP problem as an

[1]There are special designed matrices that fulfill the ERC but this is beyond the scope of this thesis in computational medical physics.

LP problem and empirically show that the returned solutions of the CS inspired algorithms are near the global optimum.
Hence, the important step is to rewrite the standard ITP optimization problem as an LP problem and transform it into the CS inspired problem equivalent to eq. (2.26). In the following, a general reformulation for the LDR and the HDR problem without needled optimization is presented.

Let us denote $\boldsymbol{D}^{\nu} \in \{\mathbb{R}^{+}\}^{m \times n}$ as a dose dictionary, where ν labels the organs and structures. Each element of the dose matrix $\boldsymbol{D}^{\nu}_{ij}$ represents the dose at a given dose point i introduced by a seed placed at a dwell-position j. The dose $\boldsymbol{D}^{\nu}_{ij}$ is determined by eq. (2.11). For simplicity, we drop the organ index ν, keeping in mind that at the end the DBOF value q is the sum of the results over the different organs. Finally, for a given treatment plan, represented by a solution vector $\boldsymbol{x}$, the accumulated dose at all DPs $\boldsymbol{d}$ is determined by the linear equation:

$$\boldsymbol{D}\boldsymbol{x} = \boldsymbol{d} \tag{4.1}$$

To rewrite the DBOF using matrix notation the penalty terms f_L (eq. (2.13)) and f_U (eq. (2.14)) have to be rewritten as constraints of the LP. This can be done by replacing the θ function with an inequality by introducing slack variable vectors $\boldsymbol{s}_L \geq 0$ and $\boldsymbol{s}_U \geq 0$ given by:

$$-\boldsymbol{D}\boldsymbol{x} - \boldsymbol{s}_L \leq -\boldsymbol{t}_L, \tag{4.2}$$

$$\boldsymbol{D}\boldsymbol{x} - \boldsymbol{s}_U \leq \boldsymbol{t}_U, \tag{4.3}$$

where $\boldsymbol{t}_L$ is the lower and $\boldsymbol{t}_U$ is the upper dose threshold. If the given thresholds cannot be reached, the deviation is compensated with the slack variable vectors to fulfill the inequality. In contrast, if the constraints are reached the slack variables are set to zero. Hence, eq. (4.2) and eq. (4.3) are a valid substitute for eq. (2.13) and eq. (2.14), respectively.
In addition eq. (2.15) is replaced with a scalar product of a weighting vector $(\boldsymbol{w}_L, \boldsymbol{w}_U)$ where each element consists of the weighting factors w_L and w_U divided by the number of dose points of the given dictionary times the slack variable vector $(\boldsymbol{s}_L, \boldsymbol{s}_U)$. The objective function value q is given by:

$$q = (\boldsymbol{w}_L, \boldsymbol{w}_U) \cdot (\boldsymbol{s}_L, \boldsymbol{s}_U)^T \tag{4.4}$$

Finally, the ITP optimization problem using matrix notation can be written as:

$$\min((\boldsymbol{w}_L, \boldsymbol{w}_U) \cdot (\boldsymbol{s}_L, \boldsymbol{s}_U)^T) \quad s.t. \quad \begin{pmatrix} -\boldsymbol{D} & -\boldsymbol{I} & \boldsymbol{0} \\ \boldsymbol{D} & \boldsymbol{0} & -\boldsymbol{I} \end{pmatrix} \cdot \begin{pmatrix} \boldsymbol{x} \\ \boldsymbol{s}_L \\ \boldsymbol{s}_U \end{pmatrix} \leq \begin{pmatrix} \boldsymbol{t}_L \\ \boldsymbol{t}_U \end{pmatrix}, \quad (4.5)$$
$$\boldsymbol{x} \in \Omega$$
$$\boldsymbol{s}_{L/U} \in \{\mathbb{R}^+\}$$

where $\boldsymbol{I} \in \mathbb{R}^{m \times m}$ is a unit matrix, $\boldsymbol{0} \in \mathbb{R}^{m \times m}$ is a zero matrix, and Ω is the domain of all potential solutions. The optimization problem can further be simplified by defining $\tilde{\boldsymbol{D}} = (-\boldsymbol{D}, \boldsymbol{D})$, $\hat{\boldsymbol{t}} = (\boldsymbol{t}_L, \boldsymbol{t}_U)$, $\boldsymbol{s} = (\boldsymbol{s}_U, \boldsymbol{s}_L)$, $\boldsymbol{w} = (\boldsymbol{w}_U, \boldsymbol{w}_L)$, and $\hat{\boldsymbol{I}} \in \mathbb{R}^{2m \times 2m}$ to obtain:

$$\min(\boldsymbol{w}^T \cdot \boldsymbol{s}) \quad s.t. \quad \begin{pmatrix} \hat{\boldsymbol{D}} & -\hat{\boldsymbol{I}} \end{pmatrix} \cdot \begin{pmatrix} \boldsymbol{x} \\ \boldsymbol{s} \end{pmatrix} \leq \hat{\boldsymbol{t}} \quad (4.6)$$
$$\boldsymbol{x} \in \Omega$$
$$\boldsymbol{s} \geq 0$$

This is the general reformulation of the ITP problem for LDR and HDR which can be optimized using MILP and LP solvers, respectively.
Analog to the reformulation of optimization problem eq. (2.15) into form of P1, the objective is to get a sparse representation while achieving a certain plan quality Q_0. Hence, $\boldsymbol{w}^T \cdot \boldsymbol{s}$ is replaced with the l_0-semi-norm $\|x\|_0$ and an additional quality constraint is added. The CS form is:

$$\min(\|\boldsymbol{x}\|_0) \quad s.t. \quad \begin{pmatrix} \tilde{\boldsymbol{D}} & -\hat{\boldsymbol{I}} \end{pmatrix} \cdot \begin{pmatrix} \boldsymbol{x} \\ \boldsymbol{s} \end{pmatrix} \leq \tilde{\boldsymbol{t}} \quad (4.7)$$
$$\boldsymbol{x} \in \Omega$$
$$\boldsymbol{s} \geq 0$$
$$\boldsymbol{w}^T \cdot \boldsymbol{s} \leq Q_0$$

And in a compact form this reads as:

$$\min(\|\boldsymbol{x}\|_0) \quad s.t. \quad \begin{pmatrix} \tilde{\boldsymbol{D}} & -\hat{\boldsymbol{I}} \\ \boldsymbol{0} & \boldsymbol{w}^T \end{pmatrix} \cdot \begin{pmatrix} \boldsymbol{x} \\ \boldsymbol{s} \end{pmatrix} \leq \begin{pmatrix} \tilde{\boldsymbol{t}} \\ Q_0 \end{pmatrix} \quad (4.8)$$
$$\boldsymbol{x} \in \Omega$$
$$\boldsymbol{s} \geq 0$$

Using $\boldsymbol{A} = \begin{pmatrix} \tilde{\boldsymbol{D}} & -\boldsymbol{I} \\ \boldsymbol{0} & \boldsymbol{w}^T \end{pmatrix}$, $\boldsymbol{g} = \begin{pmatrix} \tilde{\boldsymbol{D}} \\ Q_0 \end{pmatrix}$ and $\boldsymbol{f} = \begin{pmatrix} \boldsymbol{x} \\ \boldsymbol{s} \end{pmatrix}$, the problem in matrix notation reads:

$$\min \|\boldsymbol{W}\boldsymbol{f}\|_0 \qquad s.t. \qquad \boldsymbol{A}\boldsymbol{f} \leq \boldsymbol{g}, \tag{P2}$$

where $\boldsymbol{W}$ is a weighting matrix that fulills the equation $\begin{pmatrix} \boldsymbol{x} \\ \boldsymbol{0} \end{pmatrix} = \boldsymbol{W}\boldsymbol{f}$. This is the standard compressed sensing problem well known from literature [75], where $\boldsymbol{A}$ is the basis, $\boldsymbol{f}$ is a measured, and $\boldsymbol{g}$ is the signal.

Since the ITP problem can be cast as a linear problem, it is concluded that it has the same mathematical structure as the CS problem and is henceforth called the CS-ITP problem. This justifies the use of CS solvers for the ITP problem without needle optimization.

4.2.2 Needle optimization

For needle optimization, the state-of-the-art approaches is to use the DBOF with an additional cost per needle term (eq. (2.16)). Instead of penalizing $\mathcal{N}(\boldsymbol{x})$, the problem can be cast as a constrained optimization problem, where an additional needle constraint η, i.e. the number of maximally allowable needles, is added to problem P1. This formulation leads to a problem that should also be structurally similar to CS, i.e.:

$$\begin{aligned} \boldsymbol{x}^* = \arg\min_{\boldsymbol{x}\in\Omega} \|\boldsymbol{x}_0\|_0 \qquad s.t. \qquad & \mathcal{Q}(\boldsymbol{x}) \leq Q_0 \\ & \mathcal{N}(\boldsymbol{x}) \leq \eta \end{aligned} \tag{4.9}$$

As demonstrated in the previous section, the DBOF constraint can be cast as an LP problem and hence, the only remainder is to show that needle optimization can also be rewritten as an LP problem. Thus, the goal is to rewrite the ITP problem into an LP problem having the same form as eq. (2.26). Introducing two additional constraints lead to the following:

Firstly, for a given needle configuration $\boldsymbol{n} \in \{0,1\}^n$, where n is the total number of needles, only dwell-positions at those needles should be considered for dwell-time optimization. Whereby a used needle i is labeled with $\boldsymbol{n}_i = 1$ and $\boldsymbol{n}_i = 0$ otherwise. This constraint can be written as an inequality that reads as:

$$\begin{pmatrix} \boldsymbol{N} & -\boldsymbol{G} \end{pmatrix} \cdot \begin{pmatrix} \boldsymbol{x} \\ \boldsymbol{n} \end{pmatrix} \leq 0, \tag{4.10}$$

where $\boldsymbol{N} \in \{0,1\}^{n \times s}$ is a matrix defined as:

$$\boldsymbol{N}_{ij} = \begin{cases} 1, & \forall j \in \boldsymbol{\Upsilon}_i \\ 0, & \text{otherwise} \end{cases}, \tag{4.11}$$

and assigns each dwell-positions to a needle, $\boldsymbol{G}^{n \times n}$ is a diagonal matrix where the elements can be interpreted as maximally allowed accumulated number of dwell-positions per needle for LDR and HDR, respectively. The threshold should be chosen such that it does not influence the result. However, it can be used as an additional constraint to reduce the number of dwell-positions per needle for LDR, and does reduce the accumulated treatment time per channel for HDR. It can be seen that for a given needle configuration $\boldsymbol{n}$ the inequality can only be fulfilled if all elements of $\boldsymbol{x}$ which are not part of the given needle configuration are set to zero.

The second constraint is that the used number of needles, i.e. the number of elements of $\boldsymbol{n}$ which are non-zero, have to be equal to or less than a predefined number η. This constraint is again written as an inequality:

$$\begin{pmatrix} \boldsymbol{0} & \boldsymbol{1} \end{pmatrix} \cdot \begin{pmatrix} \boldsymbol{x} \\ \boldsymbol{n} \end{pmatrix} \leq \eta, \tag{4.12}$$

with $\boldsymbol{0}^{1 \times s}$ being a zero matrix and $\boldsymbol{1}^{1 \times n}$ being a all-ones matrix. Finally, the MILP optimization problem reads as:

$$\min(\|\boldsymbol{x}\|_0) \qquad s.t. \qquad \begin{pmatrix} \tilde{\boldsymbol{D}} & -\hat{\boldsymbol{I}} & \boldsymbol{0} \\ \boldsymbol{0} & \boldsymbol{w}^T & \boldsymbol{0} \\ \boldsymbol{N} & \boldsymbol{0} & -\boldsymbol{G} \\ \boldsymbol{0} & \boldsymbol{0} & -\boldsymbol{1} \end{pmatrix} \cdot \begin{pmatrix} \boldsymbol{x} \\ \boldsymbol{s} \\ \boldsymbol{n} \end{pmatrix} \leq \begin{pmatrix} \tilde{\boldsymbol{t}} \\ Q_0 \\ 0 \\ \eta \end{pmatrix} \tag{4.13}$$

$$\boldsymbol{x} \in \Omega \tag{4.14}$$

$$\boldsymbol{s} \geq 0 \tag{4.15}$$

$$\boldsymbol{n} \in \{0,1\}^n$$

Further simplification using $\tilde{\boldsymbol{A}} = \begin{pmatrix} \tilde{\boldsymbol{D}} & -\hat{\boldsymbol{I}} & \boldsymbol{0} \\ \boldsymbol{0} & \boldsymbol{w}^T & \boldsymbol{0} \\ \boldsymbol{N} & \boldsymbol{0} & -\boldsymbol{G} \\ \boldsymbol{0} & \boldsymbol{0} & -\boldsymbol{1} \end{pmatrix}$, $\tilde{\boldsymbol{f}} = \begin{pmatrix} \boldsymbol{x} \\ \boldsymbol{s} \\ \boldsymbol{n} \end{pmatrix}$, and $\tilde{\boldsymbol{g}} = \begin{pmatrix} \tilde{\boldsymbol{t}} \\ Q_0 \\ 0 \\ \eta \end{pmatrix}$ yields a problem which is structurally similar to CS, i.e.:

$$\min \|\boldsymbol{W}\tilde{\boldsymbol{f}}\|_0 \qquad s.t. \qquad \tilde{\boldsymbol{A}}\tilde{\boldsymbol{f}} \leq \tilde{\boldsymbol{g}}, \tag{P3}$$

where $\boldsymbol{W}$ is the weighting matrix as defined in the previous. Since the needle optimization problem can be cast into a linear problem, it is again concluded that the algorithms used for CS can also be applied to solve problem P3.

4.2.3 Relaxation of the ITP problem

As shown within the last two subsections the ITP optimization is structurally equivalent to the problems well known in the field of CS. The focus was to introduce a sparse optimization technique based on minimization of the l_0-norm. Due to the l_0-norm the problem is NP-hard and thus difficult to solve (sec. 2.3.1).
Another popular strategy is to relax the problem by replacing the l_0-norm with the l_1-norm. Under certain conditions the solutions retrieved using the l_1-relaxation is with a high probability equivalent to the l_0-norm solution [116]. The problem is found to be:

$$\min \|\boldsymbol{W}\tilde{\boldsymbol{f}}\|_1 \qquad s.t. \qquad \tilde{\boldsymbol{A}}\tilde{\boldsymbol{f}} \leq \tilde{\boldsymbol{g}} \tag{P4}$$

Alternatively, the $l1$-regularization optimization problem reads as follows:

$$\boldsymbol{x}^* = \arg\min_{\boldsymbol{x}\in\Omega} \|\boldsymbol{x}\|_1 + \lambda_Q \cdot \|\mathcal{Q}(\boldsymbol{x}) - Q_0\|_2^2 + \lambda_N \cdot \|\mathcal{N}(\boldsymbol{x}) - \eta\|_2^2 \tag{P5}$$

The l_1-relaxation is a good approximation which allows the use of many LP optimization tools or gradient based optimization techniques. However, those methods are computationally more expensive than greedy algorithms.

4.3 Algorithms for ITP

In the last two sections the concept of sparsity was introduced and ITP problem was reformulated into a problem that has the same mathematical structure as CS problems. It is concluded that the algorithms well known in the field of CS can therefore be used to solve the reformulated ITP problem.
The optimization problem itself can be divided into l_0 and l_1 optimization problems which can be tackled with a variety of efficient algorithms, depending on their principle, as greedy algorithms and numerical algorithms. For the former, examples are MP, OMP, weak matching pursuit (wMP), and a multitude of variants thereof [75]. For the latter, examples are interior-point-methods and simplex methods [104].
Both share that the returned solutions of the CS problem are only approximations either due to the pursuit strategy or due to relaxation. These approximation

lead to a huge decrease in optimization time. The golden rule for CS in practice is:

"If it is easy to find a nearly optimal solution, there is no reason to waste a lot of time and resources to reach the ne plus ultra" [78].

Choosing between the different methods and finding appropriate optimizers depend on the application. Important factors which have to be considered, are the complexity of the problem and the required accuracy of the solution.
Within the context of the ITP problems, the domain of all potential solutions defines the complexity of LDR and HDR problem. Thus, the problem of finding an effective algorithm is divided into LDR and HDR treatment planning.
This raises the question whether standard CS optimization algorithms can be used to optimize the ITP problem.
For both methods state-of-the-art optimizers cannot be used due to the restricted domain of the ITP problem for LDR and HDR ITP. The standard algorithms assume an unrestricted domain, i.e. $\boldsymbol{x} \in \mathbb{R}^s$, which leads to errors when trying to solve the ITP problem. From experience it is known that using OMP to solve the ITP inevitably leads to the selection of negative amplitudes when updating the support and additional selection steps are therefore necessary. Apart from that the standard algorithm may be inefficient. For example, in LDR treatment planning it is unnecessary to determine the pseudo-inverse to update the provisional solution.
Hence, it is decided to develop algorithms for the ITP problem which are inspired by the state of the art algorithms used to solve the CSP. The focus is to develop fast and efficient solvers that are tailored to the underlying structure of the ITP problem. In the following, different algorithms are proposed starting from low complexity towards more sophisticated methods. The goal is to determine algorithms that allow real-time ITP while achieving the same quality as the state of the art methods.
For simplicity, the formulation as an unconstrained optimization problem using the functional representation of the DBOF is used, which was shown to be equivalent to the matrix notation.

4.3.1 LDR treatment planning without needle optimization

For LDR treatment planning, all novel algorithms are presented in the following, tarting with a simple thresholding algorithm towards more complex greedy algorithms.

Algorithm 1 LDR thresholding algorithm

Input:
$\mathcal{Q}(\cdot)$, s, σ
Initialization:
$\boldsymbol{x} = \mathbf{0}$
Iteration:
for $i = 1$ to s **do**
$\hat{\boldsymbol{x}} = \boldsymbol{x}$
$\hat{\boldsymbol{x}}_i = 1$
$\boldsymbol{q}_i = \mathcal{Q}(\hat{\boldsymbol{x}})$
end for
$\boldsymbol{x}^* = shrink^{bin}_{min}(\boldsymbol{q}, \gamma(\sigma))$
Output:
$\boldsymbol{x} = \boldsymbol{x}^*$, $Q = \mathcal{Q}(\boldsymbol{x})$

Thresholding

Thresholding is one of the greedy algorithms that can be used for LDR ITP. The idea is to choose the final dwell-position configuration solely using the first projection alone.
For the CS-ITP problem, the first projection $\boldsymbol{q}$ can be calculated using s independent DBOF iterations, i.e. one per potential dwell-position. The i-th test is given by:

$$\boldsymbol{q}_i = \mathcal{Q}(\boldsymbol{x}^{(i)}) \tag{4.16}$$

where $\boldsymbol{q}_i$ as the resulting DBOF value. In addition, $\boldsymbol{x}^{(i)}$ is a potential solution vector given by $\boldsymbol{x}^{(i)}_j = \delta_{ij}$, $j \in \{1, \ldots, s\}$, δ_{ij} is the Kronecker delta, and s is the number of potential dwell-positions.
The thresholding can be explicitly computed by using a binary shrinkage operator which is defined as an element-wise operation:

$$shrink^{bin}_{min}(u, \gamma) = 1 - \frac{\max(|u| - \gamma, 0)}{|u| - \gamma}, \tag{4.17}$$

where u is the input, i.e. the result of a single projection $\boldsymbol{q}_i$, and γ is a threshold. The subscript *min* labels that only elements smaller than the given thresholds are nonzero and the superscript *bin* imposes a binary solution. For the ITP problem the threshold depends on the number of desired dwell-positions σ and on the range of all possible elements in $\boldsymbol{q}$ and is in the following referred to as $\gamma(\sigma)$.

A pseudo code of the introduced algorithm is presented in alg. 1 and is henceforth referred to as "LDR thresholding algorithm (LTA)". The proposed algorithm is

Algorithm 2 LDR orthorgonal matching pursuit

Input:
$\mathcal{Q}(\cdot)$, Q_0, s
Initialization:
$x^{(0)} = \mathbf{0}$, $\mathcal{S}^{(0)}$, $\hat{\mathcal{S}} = \{1, \ldots, s\}$, $k = 0$
Iteration:
do
$k = k + 1$
$j^* = \arg\min_{j \in \hat{\mathcal{S}} \setminus \mathcal{S}^{(k-1)}} \mathcal{Q}(\boldsymbol{x}^{(k-1)} + \boldsymbol{e}^{(j)})$
$\boldsymbol{x}^{(k)} = \boldsymbol{x}^{(k-1)} + \boldsymbol{e}^{(j^*)}$
$\mathcal{S}^{(k)} = \mathcal{S}^{(k-1)} \cup \{j^*\}$
while $Q_0 \leq \mathcal{Q}(\boldsymbol{x}^{(k)})$ & $\mathcal{Q}(\boldsymbol{x}^{(k)}) < \mathcal{Q}(\boldsymbol{x}^{(k-1)})$
Output:
$\boldsymbol{x} = \boldsymbol{x}^{(k-1)}$, $Q = \mathcal{Q}(\boldsymbol{x})$, $\mathcal{S} = \mathcal{S}^{(k-1)}$

one of the simplest that can be used for ITP. The final shrinkage operation requires only a few operations per elements and thus the optimization time is determined by the time required to evaluate s independent DBOF values.
Note that the LTA assumes that the number of used dwell-positions σ is defined as an input parameter. Alternatively, the number of used dwell-positions can be increased until a certain quality of the DBOF is reached.

Matching pursuit inspired algorithm

Other alternatives to tackle the LDR ITP problem are more sophisticated greedy algorithms. One type of algorithms which is extensively used in the field of image processing, is matching pursuit and its variants.
The basic strategy of matching pursuit-based algorithms is to construct the solution iteratively, by selecting one dwell-position per iteration step. In the following, this is called expansion step. The differences between variations of MP-inspired strategies are essentially related to the selection of dwell-positions (e.g. wMP) or to the updated process of the intermediate solution (e.g. OMP). The new dwell-position at the k-th iteration is chosen such that it minimizes the quality function $\mathcal{Q}(\cdot)$ the most. The index of the new dwell-position is stored as element of the so-called dwell-position support $\mathcal{S}$. The support containing all potential dwell-positions is given by $\hat{\mathcal{S}} = \{1, \cdots, s\}$. To fit the LDR ITP problem an algorithm, which is inspired by OMP, is implemented as follows:
Starting with an initially empty solution $\boldsymbol{x}^{(0)} = \mathbf{0}$ the set of active dwell-positions is expanded forming an intermediate solution $\boldsymbol{x}^{(k)}$ as well as the intermediate support $\mathcal{S}^{(k)}$ based on the solution $\boldsymbol{x}^{(k-1)}$ of iteration k-1. The new dwell-position

$j \in \hat{\mathcal{S}} \backslash \mathcal{S}^{(k-1)}$ is chosen such that it minimizes the quality function according to:

$$j^* = \underset{j \in \hat{\mathcal{S}} \backslash \mathcal{S}^{(k)}}{\arg\min} \mathcal{Q}(\boldsymbol{x}^{(k-1)} + \boldsymbol{e}^{(j)}), \tag{4.18}$$

whereby $\boldsymbol{e}^{(j)}$ is defined as:

$$\boldsymbol{e}^{(j)}; \qquad \boldsymbol{e}_i^{(j)} = \begin{cases} 1, & i = j \\ 0, & \text{otherwise} \end{cases}, \forall i \in \hat{\mathcal{S}} \backslash \mathcal{S}^{(k)} \tag{4.19}$$

To avoid the selection of dwell-positions that are already part of the support $\mathcal{S}^{(k)}$ they are excluded from the search space of the expansion step and thus $j \in \hat{\mathcal{S}} \backslash \mathcal{S}^{(k)}$. This guarantees a binary solution and is an important difference compared to the strategies MP and wMP. Here, already selected elements can be chosen again to further improve the objective function.
Finally, the expansion step leads to the complete update $\boldsymbol{x}^{(k)} = \boldsymbol{x}^*(k-1) + \boldsymbol{e}^{(j^*)}$. If no $\boldsymbol{e}^{(j^*)}$ is found that decreases the objective function or the quality bound Q_0 is reached, the iteration stops.

Since the algorithm is inspired by OMP it is called "LDR orthogonal matching pursuit (LOMA)" and a description in pseudo code is given in alg. 2. When compared to alg. 1, an improvement in accuracy is expected at the expense of growing complexity. To obtain a σ sparse solution, where σ is the number of used dwell-positions, a total of $\sum_{i=0}^{l}(s-i) = \frac{1}{2}(2s-l)(l+1)$ evaluations of the objective function have to be completed.

LDR subspace pursuit algorithm

The main drawback of LOMA (alg. 2), the number of dwell-positions grows continuously. This may yield suboptimal solutions with respect to sparsity and DBOF value. In CS, methods as SP or CoSaMP are able to overcome these limitations. Both methods are capable to identify erroneously chosen components and excluding their contribution from the solution found so far. Resulting in guaranteed improvement in accuracy [84, 83].
Therefore, the ideas of the used mechanisms for the removal of on-support elements are tailored to the binary LDR ITP problem. The following strategy is implemented.
The algorithm starts again with an empty support $\mathcal{S}^{(0)} = \emptyset$ and with an initial solution $\boldsymbol{x}^{(0)} = \boldsymbol{0}$. During each iteration, the same expansions step as used in alg. 3 is performed to form an intermediate solution $\boldsymbol{x}^{(k)}$ and intermediate support $\mathcal{S}^{(k)}$. In contrast to LOMA, a reduction step follows directly after the expansion. In this reduction step, the one element r^* from the previously chosen dwell-positions is

Algorithm 3 LDR subspace pursuit algorithm

Input:
$\mathcal{Q}(\cdot)$, Q_0, s
Initialization:
$x^{(0)} = \mathbf{0}$, $\mathcal{S}^{(0)}$, $\hat{\mathcal{S}} = \{1, \ldots, s\}$
Iteration:
do
$k = k + 1$
$j^* = \arg\min_{j \in \hat{\mathcal{S}} \setminus \mathcal{S}^{(k-1)}} \mathcal{Q}(x^{(k-1)} + \boldsymbol{e}^{(j)})$
$\boldsymbol{x}^{(k)} = \boldsymbol{x}^{(k-1)} + \boldsymbol{e}^{(j^*)}, \qquad \mathcal{S}^{(k)} = \mathcal{S}^{(k-1)} \cup \{j^*\}$
$r^* = \arg\min_{r \in \mathcal{S}^{(k-1)}} \mathcal{Q}(\boldsymbol{x}^{(k)} - \boldsymbol{e}^{(r)})$
if $\mathcal{Q}(\boldsymbol{x}^{(k)} - \boldsymbol{e}^{(r^*)}) \leq \mathcal{Q}(\boldsymbol{x}^{(k-1)})$ **then**
$\boldsymbol{x}^{(k)} = \boldsymbol{x}^{(k-1)} - \boldsymbol{e}^{(r^*)}, \qquad \mathcal{S}^{(k)} = \mathcal{S}^{(k-1)} \setminus \{r^*\}$
end if
while $Q_0 \leq \mathcal{Q}(\boldsymbol{x}^{(k)}) \quad \& \quad \mathcal{Q}(\boldsymbol{x}^{(k)}) < \mathcal{Q}(\boldsymbol{x}^{(k-1)})$
Output:
$\boldsymbol{x} = \boldsymbol{x}^{(k-1)}, \qquad Q = \mathcal{Q}(\boldsymbol{x}), \qquad \mathcal{S} = \mathcal{S}^{(k-1)}$

removed that reduces the objective function the most and simultaneously guarantees that after the removal the obtained objective function value is still less than the previous one, i.e.:

$$r^* = \underset{r \in \mathcal{S}^k}{\arg\min}\, \mathcal{Q}(\boldsymbol{x}^{(k)} - \boldsymbol{e}^{(r)}) \quad s.t. \quad \mathcal{Q}(\boldsymbol{x}^{(k)} - \boldsymbol{e}^{(r)}) \leq \mathcal{Q}(x^{(k-1)}) \tag{4.20}$$

If the reduction step does not improve the objective function value its result is omitted. The iteration stops either if the quality bound Q_0 is reached or the objective function cannot be further reduced[2].
A pseudo code of the introduced algorithm is presented as "LDR subspace pursuit (LSUP)" (alg. 3). To obtain a σ sparse solution at least
$s + \sum_{i=1}^{l}\{(s-i) + (i-1)\} = l(s-1) + s$ evaluations of the objective function have to be carried out.

4.3.2 LDR treatment planning including needle optimization

For needle optimization problem as stated in eq. (2.16) the previously discussed algorithms can be used without any restrictions. However, due to the realization of the greediness, i.e. inability to correct previous steps, the accuracy of LTA and LOMA might not be sufficient.
The focus in the following is to develop efficient needle optimization algorithms.

[2]This algorithm was published under the acronym "MPIP" by Guthier et al. in 2015 [35].

Algorithm 4 LDR split thresholding algorithm

Input:
$\mathcal{Q}(\cdot)$, s, n, η
Initialization:
$\mathcal{S}^{(0)} = \{1, \ldots, s\}$, $\mathcal{S}^{(f)} = \emptyset$
Iteration:
$\boldsymbol{x}^* = \arg\min_{\boldsymbol{x}} \mathcal{Q}(\boldsymbol{x})$
$\boldsymbol{q} = \mathcal{Q}(\boldsymbol{C}\boldsymbol{x}^*)$
$\boldsymbol{u} = sort(\boldsymbol{q})$
for $i = 1$ to n **do**
$\mathcal{S}^{(f)} = \mathcal{S}^{(f)} \cup \boldsymbol{\Upsilon}_{\boldsymbol{u}_i}$
end for
$\boldsymbol{x}^* = \arg\min_{\boldsymbol{x}} \mathcal{Q}(\boldsymbol{x}_{|\mathcal{S}^{(0)} \setminus \mathcal{S}^{(f)}})$
Output:
$\boldsymbol{x} = \boldsymbol{x}^*$, $Q = \mathcal{Q}(\boldsymbol{x})$

The main principle is to decouple needle from dwell-position optimization for needle optimization in LDR ITP.

Split thresholding for LDR needle optimization

As for the LDR ITP, the simplest algorithm to determine a final needle configuration is thresholding.
The idea is to obtain an initial dwell-position configuration using one of the discussed algorithms 1-3 and applying thresholding to find a final needle configuration. Afterwards, the obtained configuration is used and the final solution is obtained via re-optimizing the dwell-position configuration with respect to the new subset of dwell-positions.

The proposed algorithm is named "LDR split thresholding algorithm (LST)" and its strategy is described in the following:
It starts with a full dwell-position support $\mathcal{S}^{(0)} = \{1, \cdots, s\}$, meaning that all possible dwell-position points are considered for optimization. An initial solution $\boldsymbol{x}^*$ is obtained by minimizing:

$$\boldsymbol{x}^* = \arg\min_{\boldsymbol{x}} \mathcal{Q}(\boldsymbol{x}) \tag{4.21}$$

which can be optimized using alg. 1-3. Subsequently, the contribution $\boldsymbol{q}_i$ of needle i to the final objective function is evaluated according to:

$$\boldsymbol{q}_i = \mathcal{Q}(\boldsymbol{C}\boldsymbol{x}^*), \tag{4.22}$$

where $\boldsymbol{C}$ is a $n \times s$ matrix where the elements are given by:

$$\boldsymbol{C}_{ij} = \begin{cases} 0, & \forall j \in \boldsymbol{\Upsilon}_i \\ 1, & \text{otherwise} \end{cases} \tag{4.23}$$

As defined ine eq. (2.9),$\boldsymbol{\Upsilon}_i$ is the index set of dwell-position points at needle i. From this, the η largest elements, where η is defined as the maximum number of needles, are selected with the help of a sorting algorithm referred as *sort*. The result is assumed to be a set of indices describing the new arrangement. These form the final needle support $\mathcal{N}^{(f)}$. The dwell-position support that constrains the optimization can be obtained with $\mathcal{S}^{(f)} = \bigcup_{i \in \mathcal{N}^{(f)}} \boldsymbol{\Upsilon}_i$. Finally, the solution can be obtained via:

$$\boldsymbol{x}^* = \underset{x \in \Omega_{LDR}}{\arg\min}\, \mathcal{Q}(\boldsymbol{x}) \qquad s.t. \qquad \boldsymbol{x}_i = \begin{cases} 0, & \forall i \in \mathcal{S}^{(0)} \backslash \mathcal{S}^{(f)} \\ 1, & \text{oterhwise} \end{cases} \tag{4.24}$$

For readability this problem (eq. (4.24)) is henceforth used as

$$\boldsymbol{x}^* = \underset{\boldsymbol{x}}{\arg\min}\, \mathcal{Q}(\boldsymbol{x}_{|\tilde{\mathcal{S}}}), \tag{4.25}$$

whereby $\tilde{\mathcal{S}} = \mathcal{S}^{(0)} \backslash \mathcal{S}^{(f)}$ for the given problem. A pseudo code of this algorithm is presented in alg. 4. Since in total only n additional evaluations of the objective function are necessary, the runtime is comparable to that of LTA or LOMA algorithms. In addition, similar to LTA the number of used needles η can be increased until a certain quality is reached.

Splitting inspired subspace pursuit for needle optimization

Another way to tackle the needle optimization problem for LDR is a matching pursuit inspired strategy incorporating the splitting idea for needle minimization. Therefore, the proposed algorithm is based on alg. 3 and is extended to iteratively minimize the objective function with respect to dwell-position - and, if necessary, needle - configuration.
The algorithm starts with an empty dwell-position support $\mathcal{S}^{(0)}$. Furthermore, each element of the support can be related to a needle forming a needle support $\mathcal{N}^{(0)}$. At the beginning this support is again empty. During each iteration k, the algorithm performs the following steps: Let $\boldsymbol{x}^{(k-1)}$, $\mathcal{S}^{(k-1)}$, and $\mathcal{N}^{(k-1)}$ be the solution and support vectors at iteration $k-1$. Similar to LSUP, during the expansion and reduction step an intermediate solution $\boldsymbol{x}^{(k)} = \boldsymbol{x}^{(k-1)} + \boldsymbol{e}^{(j^*)} - \boldsymbol{e}^{(r^*)}$ is formed. In addition, the support is updated according to the indices j^* and r^* where the given index is added or removed, respectively. Considering $\mathcal{N}(\boldsymbol{x})$, a function that returns the indices of the used needles, an intermediate needle support $\mathcal{N}^{(k)} = \mathcal{N}(\boldsymbol{x}^{(k-1)})$ is obtained. If, however, the number of elements of

Algorithm 5 LDR splitting inspired subspace pursuit algorithm

Input:
$\mathcal{Q}(\cdot)$, $\mathcal{N}(\cdot)$, Q_0, s, η
Initialization:
$\boldsymbol{x}^{(0)} = \mathbf{0}$, $\mathcal{S}^{(0)} = \emptyset$, $\hat{\mathcal{S}} = \{1, \ldots, s\}$, $\mathcal{N}^{(0)} = \emptyset$
Iteration:
do
$k = k + 1$
$j^* = \arg\min_{j \in \hat{\mathcal{S}} \setminus \mathcal{S}^{(k-1)}} \mathcal{Q}(\boldsymbol{x}^{(k-1)} + \boldsymbol{e}^{(j)})$
$\boldsymbol{x}^{(k)} = \boldsymbol{x}^{(k-1)} + \boldsymbol{e}^{(j^*)}, \qquad \mathcal{S}^{(k)} = \mathcal{S}^{(k-1)} \cup \{j^*\}$
$r^* = \arg\min_{\mathcal{S}^{(k-1)}} \mathcal{Q}(\boldsymbol{x}^{(k)} - \boldsymbol{e}^{(r)})$
if $\mathcal{Q}(\boldsymbol{x}^{(k)} - \boldsymbol{e}^{(r^*)}) \leq \mathcal{Q}(\boldsymbol{x}^{(k-1)})$ **then**
$\boldsymbol{x}^{(k)} = \boldsymbol{x}^{(k-1)} - \boldsymbol{e}^{(r^*)}, \qquad \mathcal{S}^{(k)} = \mathcal{S}^{(k-1)} \setminus \{r^*\}$
end if
$\mathcal{N}^{(k)} = \mathcal{N}(\boldsymbol{x}^{(k)})$
if $\|\mathcal{N}^{(k)}\|_0 > \eta$ **then**
$c^* = \arg\min Q(\boldsymbol{x}_{|c})$
$\mathcal{S}^{(k)} = \mathcal{S}^{(k)} \setminus c^*$
for i in $\boldsymbol{\Upsilon}_{c^*}$ **do**
$\boldsymbol{x}_i^{(k)} = 0$
end for
$\mathcal{N}^{(k)} = \hat{\mathcal{N}}(\boldsymbol{x}^{(k)})$
end if
while $Q_0 \leq \mathcal{Q}(\boldsymbol{x}^{(k)}) \quad \& \quad \mathcal{Q}(\boldsymbol{x}^{(k)}) < \mathcal{Q}(\boldsymbol{x}^{(k-1)})$
Output:
$\boldsymbol{x} = \boldsymbol{x}^{(k-1)}, \qquad Q = \mathcal{Q}(\boldsymbol{x}), \qquad \mathcal{S} = \mathcal{S}^{(k-1)}$

$\mathcal{N}^{(k)}$ exceeds the maximum number of needles an additional reduction step is performed. In this step the one element c^* that reduces the objective function the most is removed to from the given needle configuration $\mathcal{S}^{(k-1)}$:

$$c^* = \arg\min_{c \in \mathcal{N}} Q(\boldsymbol{x}) \quad s.t. \quad \boldsymbol{x}_i = \begin{cases} \boldsymbol{x}_i, & \forall i \in \mathcal{S}^{(k)} \setminus c \\ 0, & \text{otherwise} \end{cases} \tag{4.26}$$

This leads to the final update of the needle support $N^{(k)} = N^{(k)} \setminus c^*$ and dwell-position support $S^{(k)} = S^{(k)} \setminus \boldsymbol{\Upsilon}_c^*$. For readability, eq. (4.26) is henceforth used as:

$$c^* = \arg\min Q(\boldsymbol{x}_{|c}) \tag{4.27}$$

In addition, all elements i of the update $\boldsymbol{x}^{(k)}$ which are not a part of the final support are set to zero. The iteration continues until either the quality bound Q_0 is reached or the objective function value cannot be further reduced.

The presented algorithm is summarized using pseudo-code in alg. 5 and is referred as "LDR splitting inspired subspace pursuit algorithm (LSPA)". The complexity is almost the same as for LSUP plus the additional objective function evaluations. For a single needle reduction step this adds η additional objective function evaluations.

4.3.3 HDR treatment planning

The HDR ITP without needle optimization problem P2, i.e. problem with domain $\Omega = \{\mathbb{R}^+\}$, can be solved with standard non-negative CS solvers. Examples are fast non-negative orthogonal matching pursuit and the reformulation as a BP problem [79, 117]. In addition, the standard problem can be efficiently solved using an LP algorithm. Thus, the CS inspired approach would not yield a beneficial improvement with respect to calculation time.
However, there is no efficient solver for problem P3 and related problems. The CS inspired approach could enable fast and efficient needle optimization. As demonstrated in the previous section, the decoupling of needle and dwell-time selection[3] leads to techniques which are less complex than approaches like HIPO or MILP.
Therefore, the goal of the following section is to introduce new optimizers that allow fast needle optimization by combining the discussed approaches.

Thresholding

The first and easiest method for needle optimization is a thresholding approach. In contrast to LDR treatment planning, the focus is on needle selection rather than dwell-position selection. Hence, the thresholding is applied to the accumulated dwell time per needle. Needles with a large contribution to the overall treatment time have a high influence to the final plan quality and thus have to be chosen to form the final needle configuration.
The algorithm first optimizes the standard HDR ITP problem with all needles and dwell-position active. This forms an initial approximation $\boldsymbol{x}^{(0)} = \arg\min_{\boldsymbol{x}} \mathcal{Q}(\boldsymbol{x})$. With this solution, the accumulated dwell-time $\boldsymbol{x}_i^{(acc)}$ per needle with index i can be calculated according to $\boldsymbol{x}_i^{(acc)} = \sum_{j \in \boldsymbol{\Upsilon}_i} \boldsymbol{x}_j$. Afterwards, the final needle configuration is determined using a shrinkage operator to select η needles with the largest contribution to the treatment time given by:

$$shrink_{max}(u, \gamma(\eta)) = \frac{u \cdot \max(|u| - \gamma(\eta), 0)}{|u| - \gamma(\eta)} \tag{4.28}$$

[3] Instead of optimizing a dwell-position configuration the dwell-times connected to dwell-positions are optimized in HDR.

Algorithm 6 HDR thresholding algorithm

Input:
$\mathcal{Q}(\cdot)$, s, n, γ
Initialization:
$\mathcal{S}^{(0)} = \{1, \ldots, s\}$
Iteration:
$\boldsymbol{x}^* = \arg\min_{\boldsymbol{x}}(Q(\boldsymbol{x}))$
for $i = 1$ to n **do**
$\boldsymbol{x}_i^{(acc)} = \sum_{j=\Gamma_i} \boldsymbol{x}_j$
end for
$\boldsymbol{x}^{(\boldsymbol{acc})} = shrink(\boldsymbol{x}^{(acc)}, \gamma)$
$\mathcal{S}^{(f)} = \mathcal{S}^{(0)}$
for $i = 1$ to n **do**
if $\boldsymbol{x}_i^{(acc)} == 0$ **then**
$\mathcal{S}^f = \mathcal{S}^f \backslash \boldsymbol{\Upsilon}_{\mathcal{N}_i^{(f)}}$
end if
end for
$\boldsymbol{x}^* = \arg\min_{\boldsymbol{x}} \mathcal{Q}(\boldsymbol{x}_{|\mathcal{S}^{(0)} \backslash \mathcal{S}^{(f)}})$
Output:
$\boldsymbol{x} = \boldsymbol{x}^*$, $Q = \mathcal{Q}(\boldsymbol{x}^*)$

The shrinkage is an element-wise operation, where the threshold $\gamma(\eta)$ depends on the demanded sparsity of the needle configuration, i.e. maximum number of needles η. Elements which are greater than zero are chosen to form the final subset of needles represented by the needle support $\mathcal{N}^{(f)}$. From this all possible dwell-positions are selected according to $\mathcal{S}^{(f)} = \bigcup_{i \in \mathcal{N}^f} \boldsymbol{\Upsilon}_i$. The final dwell-times $\boldsymbol{x}^{(f)}$ are obtained by solving the standard CS ITP (P4) with the constraint that all elements of $\boldsymbol{x}$ that are not part of support $\mathcal{S}^{(f)}$ equal zero.

A summary of the presented algorithm named "HDR thresholding algorithm (HTA)" as pseudo code is presented in alg. 6. The proposed method has the advantage that in order to get the final result only two BP-inspired problems have to be solved. The complexity is determined by the complexity of the BP problem, i.e. relaxation as an LP problem, which is proportional to the cube of the number of free variables. Since only a small subset of all possible dwell-positions are considered for optimization, the contribution of the second optimization step to the overall execution time is in most cases negligible. A good estimate is that we consider only 10% of all available dwell-positions.

Needle Selection

Another approach is similar to alg. 5. Its principle is a greedy heuristic that decouples needle from dwell-time optimization. However, for HDR ITP the dwell-times have to be updated during each expansion step, which leads to a more complex algorithm. To reduce the number of updates, more than one dwell-position is included into the support to form the intermediate solution per iteration step. Those elements are selected using a shrinkage operation. In contrast to thresholding, the shrinkage operation is performed during each iteration and thus the algorithm also resembles the iterative-shrinkage methods for l_1-optimization problems. Therefore, the algorithm is a union of two commonly used techniques in CS.

In detail, the above mentioned approach is implemented as follows: The algorithm starts with an empty support $\mathcal{S}^{(0)} = \emptyset$ and the initial solution is $\boldsymbol{x}^{(0)} = \mathbf{0}$. During the expansion at iteration $k-1$ an estimation of the amplitudes $\boldsymbol{z}_j$ of all dwell-positions j which are not part of the support $\mathcal{S}^{(k-1)}$ has to be performed. This is necessary because the contribution of single dwell-positions to the final objective function value can only be calculated with a valid estimation. The estimation is the projection of the contribution of a single dwell-position to the residual, i.e. difference between actual and prescribed dose:

$$\boldsymbol{z} = (\boldsymbol{D}^{PTV})^T \cdot (\boldsymbol{t}_L^{PTV} - \boldsymbol{D}^{PTV}\boldsymbol{x}^{(k-1)}), \tag{4.29}$$

where $\boldsymbol{D}$ is the dose dictionary and $\boldsymbol{t}$ is the vector representing the lower threshold (i.e. prescribed dose). In addition, the superscript PTV labels that only the PTV is considered for the intermediate amplitude estimation. Only the PTV is used in order to reduce the complexity of this intermediate step. Now, new dwell-positions are selected according to their objective function values $\mathcal{Q}(\boldsymbol{x}^{(k-1)} + \boldsymbol{e}^{(j)} \cdot \boldsymbol{z}_j)$. From this the κ smallest elements j^* are chosen to from the intermediate support $\mathcal{S}^{(k)}$ and the amplitudes are updated according to:

$$\boldsymbol{x}^{(k)} = \arg\min_{\boldsymbol{x}} \mathcal{Q}(\boldsymbol{x}_{|\mathcal{S}\setminus\mathcal{S}^{(k)}}) \tag{4.30}$$

Based on this solution, the needle support $\mathcal{N}^{(k)}$ is updated. If the number of used needles exceeds the number of maximally allowed needles, a reduction step is performed. In this step, out of all needles inside support $\mathcal{N}^{(k)}$ the needle that has the largest contribution to the final objective function value is removed. For a needle j, this leads to the following optimization problem:

$$\boldsymbol{x}^{(k)} = \arg\min_{\boldsymbol{x}} \mathcal{Q}(\boldsymbol{x}_{|\mathcal{S}^{(k)}\setminus\boldsymbol{\Upsilon}_j}) \tag{4.31}$$

This reduction step continues until the number of selected needles is equal to the number of maximally allowable needles. The iteration stops if either the quality bound is reached or the objective function cannot be reduced further.

Algorithm 7 HDR splitting inspired subspace pursuit algorithm

Input:
$\mathcal{Q}(\cdot)$, Q_0, n, η, κ
Initialization:
$x^{(0)} = \mathbf{0}$, $\mathcal{S}^{(0)}$, $\hat{\mathcal{S}} = \{1, \ldots, n\}$, $\mathcal{N}^{(0)} = \emptyset$, $\hat{\mathcal{N}}^{(0)} = \emptyset$
Iteration:
do
$k = k + 1$
$\boldsymbol{z} = (\boldsymbol{D}^{PTV})^T \cdot (\boldsymbol{t}_L^{PTV} - \boldsymbol{D}^{PTV} \cdot \boldsymbol{x}^{(k-1)})$
for j in $\hat{\mathcal{S}} \backslash \mathcal{S}^{(k-1)}$ **do**
$\boldsymbol{q}_j = \mathcal{Q}(\boldsymbol{x}^{(k-1)} + \boldsymbol{z}_j \cdot \boldsymbol{e}^{(j)})$
end for
$\boldsymbol{q} = shrink_{min}^{bin}(\boldsymbol{q}, \gamma(\eta))$
$\boldsymbol{u} = sort(\boldsymbol{q})$
for $j = 1$ to κ **do**
$S^{(k)} = S^{(k)} \bigcup \boldsymbol{u}_j$
end for
$\boldsymbol{x^{(k)}} = \arg\min_{\boldsymbol{x}} \mathcal{Q}(\boldsymbol{x}_{|\mathcal{S}^{(0)} \backslash \mathcal{S}^{(k)}})$
$\mathcal{N}^{(k)} = \hat{\mathcal{N}}(\boldsymbol{x}^{(k)})$
while $\|\mathcal{N}^{(k)}\|_0 > \eta$ **do**
for j in $\mathcal{N}^{(k)}$ **do**
$\boldsymbol{x'}^{(j)} = \arg\min_{\boldsymbol{x}} \mathcal{Q}(\boldsymbol{x}_{|\mathcal{S}^{(k)} \backslash \boldsymbol{\Upsilon}_j})$
$\boldsymbol{q}_j = \mathcal{Q}(\boldsymbol{x'}^{(j)})$
end for
$j^* = \arg\min_{j \in \mathcal{N}^{(k)}} \boldsymbol{q}$
$S^{(k)} = S^{(k)} \backslash \boldsymbol{\Upsilon}_{j^*}$
$\boldsymbol{x}^{(k)} = \boldsymbol{x'}^{(j)}$
$\mathcal{N}^{(k)} = \hat{\mathcal{N}}(\boldsymbol{x}^{(k)})$
end while
while $Q_0 \leq \mathcal{Q}(\boldsymbol{x}^{(k)}) \quad \& \quad \mathcal{Q}(\boldsymbol{x}^{(k)}) < \mathcal{Q}(\boldsymbol{x}^{(k-1)})$
Output:
$\boldsymbol{x} = \boldsymbol{x}^{(k-1)}, \qquad Q = \mathcal{Q}(\boldsymbol{x}), \qquad \mathcal{S} = \mathcal{S}^{(k-1)}$

A summary using pseudo code is presented as alg. 7. The algorithm is named "HDR splitting iterative subspace pursuit algorithm (HSIS)". The complexity of the algorithm is determined by the complexity of the LP problem. Hence, the overall optimization time depends on the time needed to solve the different LP sub-problems.

4.3.4 Generalized algorithm for treatment planning

So far, all introduced algorithms are especially designed for either solving LDR or HDR problems. In this section, a general algorithm is proposed that can be used to solve both ITP needle optimization problems.

Split iterative shrinkage algorithm for needle optimization

The main idea is based on the reformulation of the ITP into a l_1-regularization optimization problem as discussed in sec. 4.2. Even though those problems are usually difficult to solve, it has been shown that there are very efficient solvers for CS problems.
Usually, when iteratively solving generalized constraint optimization problems in the form of eq. (2.38) the Lagrange multiplier increases sequentially. But if $\lambda_k \to \infty$, the problem arises that the condition number of the Hessian approaches infinity. This makes it impractical for fast iterative methods. However, there are techniques to overcome this issue by using sequences of unconstrained problems. Algorithms to tackle this problem efficiently are iterative-shrinkage or based on the split Bregman iteration scheme.
The idea of splitting is used to optimize the brachytherapy ITP problem. This yields an iterative algorithm, which is implemented as follows:
In contrast to all algorithms mentioned before, the developed method starts with all dwell-positions active and thus $\mathcal{N}^{(0)} = I$ and $\mathcal{S}^{(0)} = \bigcup_{i \in N^{(0)}} \boldsymbol{\Upsilon}_i$. In addition, an initial solution $\boldsymbol{x}^{(k)}$ is obtained according to optimization problem P2.
During each iteration, a needle reduction step and an optimization of dwell-times are executed consecutively. Let $\boldsymbol{x}^{(k-1)}$ be the solution after iteration $k-1$ with related supports $\mathcal{N}^{(k-1)}$ and $\mathcal{S}^{(k-1)}$.
In the reduction step the needle that has the least influence to the overall treatment time is erased. The accumulated dwell-times per needle $j \in N^{(k-1)}$ can be calculated as $\boldsymbol{x}^{(acc)} = \boldsymbol{N}\boldsymbol{x}^k$, where $\boldsymbol{N}$ is defined according to eq. (4.11). The new needle configuration is determined using a shrinkage operation $\boldsymbol{x}^{(acc)} = shrink(\boldsymbol{x}^{(acc)}, \eta)$, where only η needles with largest accumulated dwell-times are kept and thus form the intermediate supports $N^{(k)}$ and $S^{(k)}$. In addition, the parameter η depends on the number of iteration and is therefore termed $\eta(n-k)$. Subsequently, the dwell-times are updated according to the sub-problems P2 for LDR and HDR. Those decoupled problems can be solved using the presented algorithms for LDR or the BP approach for HDR. In addition, an alternative approach for the HDR sub-problem is discussed in the following section.
The iteration stops, if either the desired quality Q_0 is achieved or the number of needles inside the support $N^{(k)}$ is equal to the number of maximally allowable needles.
The presented algorithm is referred as "split iterative shrinkage algorithm (SISA)"

Algorithm 8 Split iterative shrinkage algorithm

Input:
$\mathcal{Q}(\cdot)$, Q_0, s, n, η
Initialization:
$\mathcal{S}^{(0)} = \{1, \ldots, s\}$, $\mathcal{N}^{(0)} = \{1, \ldots, n\}$, $k = 0$, $l = n$
Iteration:
$\boldsymbol{x}^{(0)} = \arg\min_{\boldsymbol{x}\in\Omega} \mathcal{Q}(\boldsymbol{x})$
do
$k = k + 1$
$\boldsymbol{x}^{(acc)} = \boldsymbol{N} \cdot \boldsymbol{x}^{(k)}$
$\boldsymbol{x}^{(acc)} = shrink(\boldsymbol{x}^{(acc)}, \gamma(n-k))$
$\mathcal{N}^{(k)} = \mathcal{N}^{(k-1)}$
for i in $\mathcal{N}_{(k-1)}$ **do**
if $\boldsymbol{x}_i^{(acc)} == 0$ **then**
$S^{(k)} = S^{(k)} \backslash \boldsymbol{\Upsilon}_{\mathcal{N}_i^{(k)}}$
$\mathcal{N}^{(k)} = \mathcal{N}^{(k)} \backslash i$
end if
end for
$\boldsymbol{x}^{(k)} = \arg\min_{\boldsymbol{x}\in\Omega_{HDR}} \mathcal{Q}(\boldsymbol{x}) \quad s.t. \quad x_{\hat{\mathcal{S}}\backslash\mathcal{S}^{(k)}} = 0$
while $n - k > \eta \quad \& \quad Q_0 \leq \mathcal{Q}(\boldsymbol{x}^{(k)})$
Results:
$\boldsymbol{x} = \boldsymbol{x}^*$, $Q = \mathcal{Q}(\boldsymbol{x})$

and summarized using pseudo code in alg. 8. Since the needle reduction step is of low complexity, the optimization time is determined by the time needed to solve the $n - \eta$ sub-problems.

Acceleration using gradient techniques for HDR

Until now, the LP formulation of the objective function has been considered for the optimization of dwell-times. However, by introducing a smooth approximation of the Heaviside step function θ the optimization problem (eq.(2.5)) can also be tackled with various classic iterative optimization-algorithms, e.g. Steepest-Descent or conjugate gradient methods.
A surrogate is the logistic function $\theta(y) = 0.5(1 + tanh(\varsigma \cdot y))$. It leads to a smooth surrogate of the stepping function, where ς represents the steepness of the curve. Assuming that DBOF $Q(\boldsymbol{x})$ only consists of the lower bound of the PTV, (eq. (2.15)) can be rewritten as:

$$\tilde{\mathcal{Q}}(\boldsymbol{x}) = w \cdot \{1 + \tanh\left[\varsigma \cdot (\boldsymbol{t} - \boldsymbol{D}\cdot\boldsymbol{x})\right]\}^T \cdot \{\boldsymbol{t} - \boldsymbol{D} \cdot \boldsymbol{x}\}, \tag{4.32}$$

where w is the weighting factor, $\boldsymbol{D}$ the dose dictionary, and $\boldsymbol{t}$ is a given threshold, i.e. the prescribed dose. The advantage of this formulation is that $\tilde{Q}(\boldsymbol{x})$ is continuously differentiable. Assuming $\hat{\mathcal{Q}}(\boldsymbol{x}) = \|\boldsymbol{x}\|_1 + \lambda_Q \cdot \|\tilde{\mathcal{Q}}(\boldsymbol{x}) - Q_0\|_2^2$ the l_1-regularized optimization problem is found to be:

$$\boldsymbol{x}^* = \arg\min_{\boldsymbol{x}\in\Omega} \hat{\mathcal{Q}}(\boldsymbol{x}), \tag{4.33}$$

where the gradient of the objective function is given by:

$$\begin{aligned}\nabla\hat{\mathcal{Q}}(\boldsymbol{x}) = 1 + \lambda_Q \cdot (\tilde{\mathcal{Q}}(\boldsymbol{x}) - Q_0) \\ \cdot \Big\{\varsigma \cdot \boldsymbol{D}^T \cdot sech(\boldsymbol{t} - \boldsymbol{D}\cdot\boldsymbol{x}) \odot sech(\boldsymbol{t} - \boldsymbol{D}\cdot\boldsymbol{x}) \odot (\boldsymbol{t} - \boldsymbol{D}\cdot\boldsymbol{x}) \\ + \boldsymbol{D}^T \cdot [1 + \tanh(\varsigma \cdot (\boldsymbol{t} - \boldsymbol{D}\cdot\boldsymbol{x}))]\Big\},\end{aligned} \tag{4.34}$$

where $\odot$ labels element-wise vector multiplication. Taking advantage of the gradient, the problem can be efficiently solved using the Limited-memory L-BFGS algorithm. This algorithm provides an extremely fast convergence rate and can be used as a substitute of the more extensive interior-point algorithm.

4.3.5 Summary - treatment planning

Different optimizers to tackle LDR and HDR ITP problems have been introduced. Starting from simple thresholding algorithms towards more sophisticated greedy heuristics.
They offer improvements either in accuracy, complexity, or both. It is assumed that all discussed strategies are faster than the state of the art methods. However, due to greedy their nature, all algorithms return approximations, where the convergence to a global optimum cannot be guaranteed. An overview of all developed algorithms with the expected performance is presented in tab 4.2.
The question raises whether it can be proven that the algorithms perform reliably for ITP. This will be answered by a series of comparative experiments.

4.4 New objective functions

Up to now, the ITP problem was solely subjected minimizing the DBOF. However, recently more effort has been made to develop more practical objective functions. For example, during intra-operative treatment planning the DBOF parameters have to be tailored to the patients anatomy. These parameters are considered to be not intuitive. Thus finding the right parameter set usually takes several attempts. A time-consuming trial-and-error method to determine the right set is not suitable for intraoperative planning.

Table 4.2: Overview of the developed CS inspired algorithms. 'x' marks the treatment modality for which it can be used. '(x)' denotes that the algorithm can be used, but is not specially designed for the given problem. The expected efficiency and quality is rated with the number of '+'.

Algorithm	LDR	HDR	needle optimzation	efficiency	quality
LTA	x			+++	+
LOMA	x		(x)	++	++
LSUP	x		(x)	+	+++
LST	x		x	+++	+
LSPA	x		x	+	+++
HTA		x	x	+++	+
HSIS		x	x	++	++
SISA	x	x	x	+	+++

As a consequence, the goal is either to have optimizers that are capable of real-time planning (previous section), more realistic models or both, which allows a more intuitive steering of the plan quality.

Even though the DBOF is the basis of the discussed reformulation, it is assumed that all objective functions having the same structure can also be optimized with the presented methods.
Since the contribution of organ ν to the total DBOF can be subdivided into the weighted sum of the product of two independent functions $f_\nu(\boldsymbol{x})$ and $g_\nu(\boldsymbol{x})$, a general formulation can be obtained:

$$\mathcal{Q}(\boldsymbol{x}) = \sum_\nu w_\nu \cdot \theta(\boldsymbol{D}_\nu \cdot \boldsymbol{x} - \boldsymbol{t}_\nu) \cdot (\boldsymbol{D}_\nu \cdot \boldsymbol{x} - \boldsymbol{t}_\nu) = \sum_\nu w_\nu \cdot f_\nu(\boldsymbol{x}) \cdot g_\nu(\boldsymbol{x}) \tag{4.35}$$

Where $f_\nu(\boldsymbol{x})$ is a function that evaluates whether a certain objective is fulfilled, e.g. the stepping function or its surrogates. In addition, $g_\nu(\boldsymbol{x})$ is a measure of the deviation between objective and achieved value. If necessary for the optimization, the gradient is given by:

$$\nabla\mathcal{Q}(\boldsymbol{x}) = \sum_\nu w_\nu \cdot (f'_\nu(\boldsymbol{x}) \cdot g_\nu(\boldsymbol{x}) + f_\nu(\boldsymbol{x}) \cdot g'_\nu(\boldsymbol{x})) \tag{4.36}$$

In the following, two different objective functions are introduced that have the mentioned structure. Firstly, a function incorporating criteria based treatment

planning and secondly, a biological model based objective function. To validate those they are later compared against competitive methods.

4.4.1 Dosimetric criteria based objective function

A treatment plan is assumed to be clinically acceptable if certain dosimetric criteria are fulfilled. The formulation of optimizing those leads to MILP problems which are thought to be computationally expensive and hence not feasible for treatment planning.
However, when considering the general formulation of the ITP an equivalent objective function can easily be derived. Assuming that an optimal plan meets all planning criteria, this leads to the following penalty terms:

$$p^{\kappa 1}(\boldsymbol{x}) = \theta\left(\mathcal{C}^{\kappa 1}(\boldsymbol{x}) - t_C^{\kappa 1}\right) \cdot \left(t_C^{\kappa 1} - \mathcal{C}^{\kappa 1}(\boldsymbol{x})\right), \tag{4.37}$$

and

$$p^{\kappa 2}(\boldsymbol{x}) = \theta\left(t_C^{\kappa 2} - \mathcal{C}^{\kappa 2}(\boldsymbol{x})\right) \cdot \left(t_C^{\kappa 2} - \mathcal{C}^{\kappa 2}(\boldsymbol{x})\right), \tag{4.38}$$

where $\mathcal{C}(\boldsymbol{x})$ is the value of the considered criterion given the solution $\boldsymbol{x}$ and t_C are thresholds for the dosimetric criteria. The different criteria are labeled κ_1 and κ_2 denoting the upper and lower bounds, respectively. Using the recommendations of the AAPM $\kappa_1 = \{V150,\ UD10,\ UD30,\ RD0.1cc,\ RD02.0cc\}$ for LDR and $\kappa_1 = \{V150,\ UD0.1cc,\ UD02.0cc,\ RD0.1cc,\ RD02.0cc\}$ for HDR. Whereas κ_2 is equal to $V100$ for both methods. In analogy to the DBOF, the contribution of values $C(\boldsymbol{x})$ that meet the criteria are suppressed using the Heaviside step function. Finally, the criteria based objective function (CBOF) is a weighted sum of the penalty terms:

$$\mathcal{Q}_{DB}(\boldsymbol{x}) = \sum_{\kappa 1} w^{\kappa 1} \cdot p^{\kappa 1}(\boldsymbol{x}) + w^{\kappa 2} \cdot p^{\kappa 2}(\boldsymbol{x}) \tag{4.39}$$

This formulation is equivalent to the general formulation (eq. 4.35) and thus, it is assumed that the CBOF can also be optimized using the novel optimizers.
When compared to existing methods, the combination between the developed algorithms and the new objective function would for the first time allow dosimetric criteria based treatment planning with needle optimization.

4.4.2 Biological model based treatment planning

The general aim of radiation therapy is a high TCP while at the same time reducing the NTCPs. Both are usually described using biological models that predict the response of the tissue. The concept of taking biological consequences into account for plan evaluation rather than only considering dosimetric criteria is well

established [61, 118, 119, 120, 121].
However, due to the complexity of biological models, they are exclusively considered for evaluation purposes. Since with novel optimizers, a major increase in speed is expected, biological based treatment planning may be in reach. Therefore, the question raises whether biological treatment planning can be formulated such that it has the same structure as eq. (4.35).
Assuming, for a given plan $\boldsymbol{x}$ the TCP and NTCP can be determined using the function $\mathcal{P}(\boldsymbol{x})$. In addition, the objectives are to minimize the distance to a desired TCP specified by $t_P^{\kappa 3}$ and the distance to an acceptable NTCP defined by $t_P^{\kappa 4}$. The superscript κ labels what organs are considered for TCP and for NTCP calculations. For prostate brachytherapy, $\kappa 3 = PTV$ and $\kappa 4 = \{urethra, rectum\}$. This leads to two different constraint functionals, which are given by:

$$p^{\kappa 3} = \theta \left(t_P^{\kappa 3} - \mathcal{P}^{\kappa 3}(\boldsymbol{x}) \right) \cdot \left(t_P^{\kappa 3} - \mathcal{P}^{\kappa 3}\boldsymbol{x}) \right) \tag{4.40}$$

and

$$p^{\kappa 4} = \theta \left(\mathcal{P}^{\kappa 4}(\boldsymbol{x}) - t_P^{\kappa 4} \right) \cdot \left(\mathcal{P}^{\kappa 4}(\boldsymbol{x}) - t_P^{\kappa 4}) \right). \tag{4.41}$$

Finally, the biological based objective function (BBOF), taking all constraints into account, is the weighted sum of the individual penalty functions:

$$\mathcal{Q}_{BB}(\boldsymbol{x}) = w_{TCP} \cdot p^{TCP}(\boldsymbol{x}) + \sum_{\kappa 4} w_{\kappa 4} \cdot p^{\kappa 4}(\boldsymbol{x}) \tag{4.42}$$

Due to its construction the biological based ITP problem can be optimized with the developed CS inspired solvers. Even though the BBOF is designed to cope with biological responses and is thus expected to be more realistic, it should be evaluated whether the gain in quality compensates an increased optimization time.

4.5 The treatment planning system

The novel ITP system is explained in detail in the following. Although the main focus of the system is interstitial brachytherapy, it should be flexible enough to be extended for different treatment modalities in future.

4.5.1 Details of the ITP

The ITP was implemented in Matlab® R2013a (Matlab) [122] using an object oriented programming concept. The system is designed to run on Mac OS X and Windows.
To allow the communication with standard software used in clinical routine the system provides a complete DICOM support. This includes import and export

of treatment plans and image data obtained via computed tomography, magnetic resonance imaging and ultrasound.
The user can choose between predefined optimization settings or adapt them according to the particular needs. For different brachytherapy sources, an importer is available that is able to handle the calibration data provided by the vendors. For dose calculation, the code is based on AAPM's TG-43 recommendations as explained in sec. 2.2.2. The calculation accuracy in terms of the mean squared error was found to be $(0.9 \pm 1.1) \times 10^{-4}$ with a minimum of 5.3×10^{-6} and a maximum of 3.5×10^{-3} when compared to the quality assurance files available from the vendor.
Furthermore, the system provides complete pre- and post-processing of the data. For all generated plans, isodose lines can be obtained or DVHs generated. In addition, plans can be analyzed by calculating COIN, EUD, TCP, NTCPs, and dosimetric criteria.
From initial DICOM files the volume of interests (VOIs), needles, and if available source information are extracted and stored in particular classes `VOIs`, `Needles` and `Source`. Given these classes the necessary pre-processing, i.e. generation of dwell-positions and dose points, can be performed. Subsequently, the dose dictionary can be calculated. Together with the parameters describing the used objective function and/or biological models the dictionary initializes a class called `Organ`. After optimization, the generated plan is stored as a structurer called `Plan` and the necessary post-processing is performed.
Using this modular class structure with well-defined interfaces, the system is highly adaptable and can easily be improved and extended in future. A flow diagram of the class structure is presented in fig. 4.1. For example by interchanging the dose-calculation engine of the source a Monte-Carlo based ITP is possible without the need for modification of the remaining modules.
The ITP system can either be used script based (fig. 4.2), which allows to perform automatic testing, or controlled using a GUI (fig. 4.3). The script-based example shows a LDR treatment planning for one representative patient. As source, the Amersham 6733 source description is used. The settings, e.g. sampling densities, source strength, and DBOF parameters are retrieved from the DICOM file. After optimization using LOMA as the optimizer, the generated plan is analyzed and exported as a new plan.
All computations are performed on a 2013 MacBook Pro using an Intel® Core™ i7-3829QM CPU with 2.7GHz and 8GB RAM. The operation system was OS X 10.8.4.

4.5.2 Implementation of the algorithms

For treatment planning, all novel solvers as well as the state of the art optimizers previously described have been implemented. The implementations itself consist

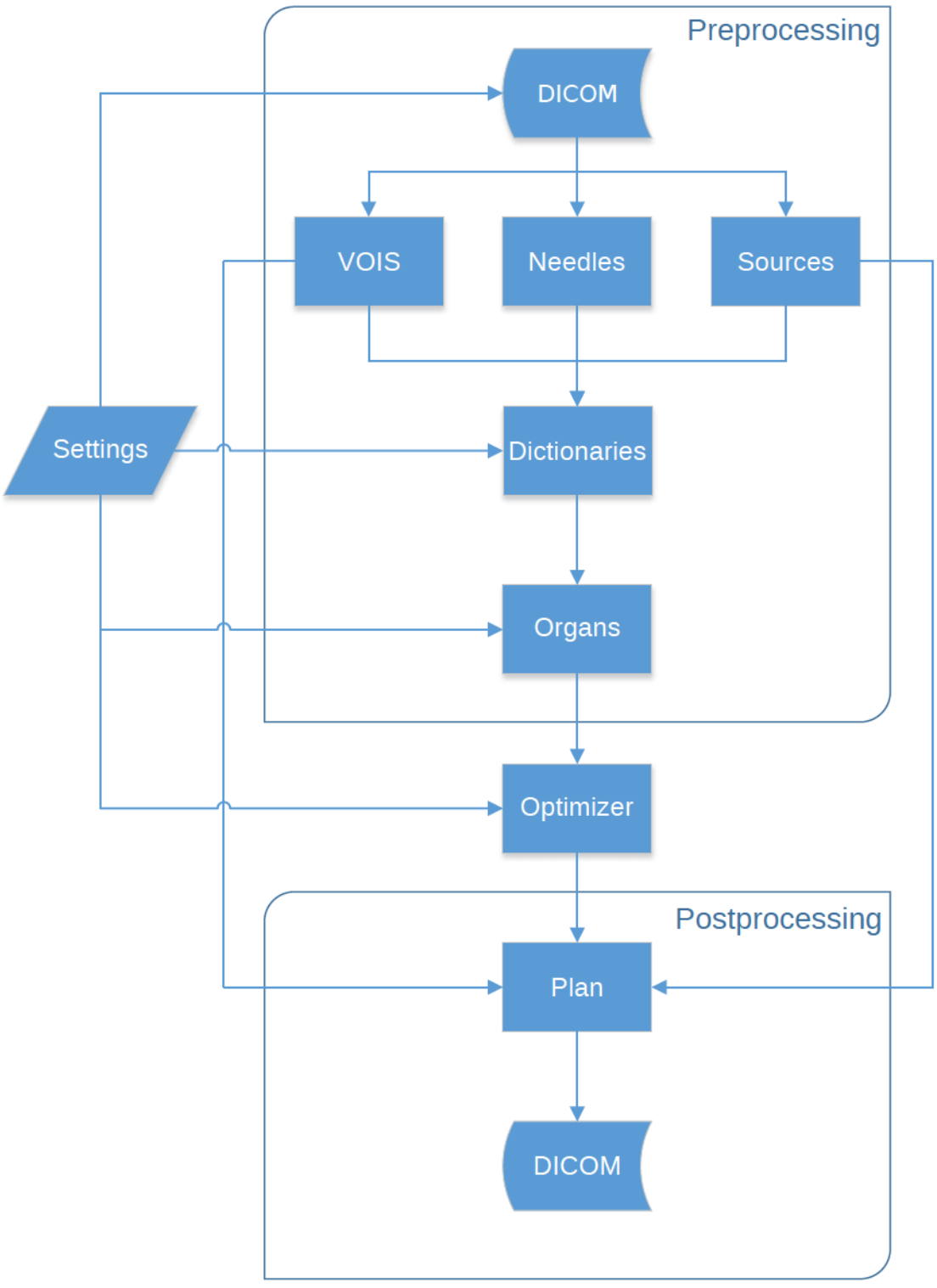

Figure 4.1: Flow diagram of the class structure. The diagram shows the evolving class structure from the input of a DICOM file to the output of the final plan stored again using the DICOM format.

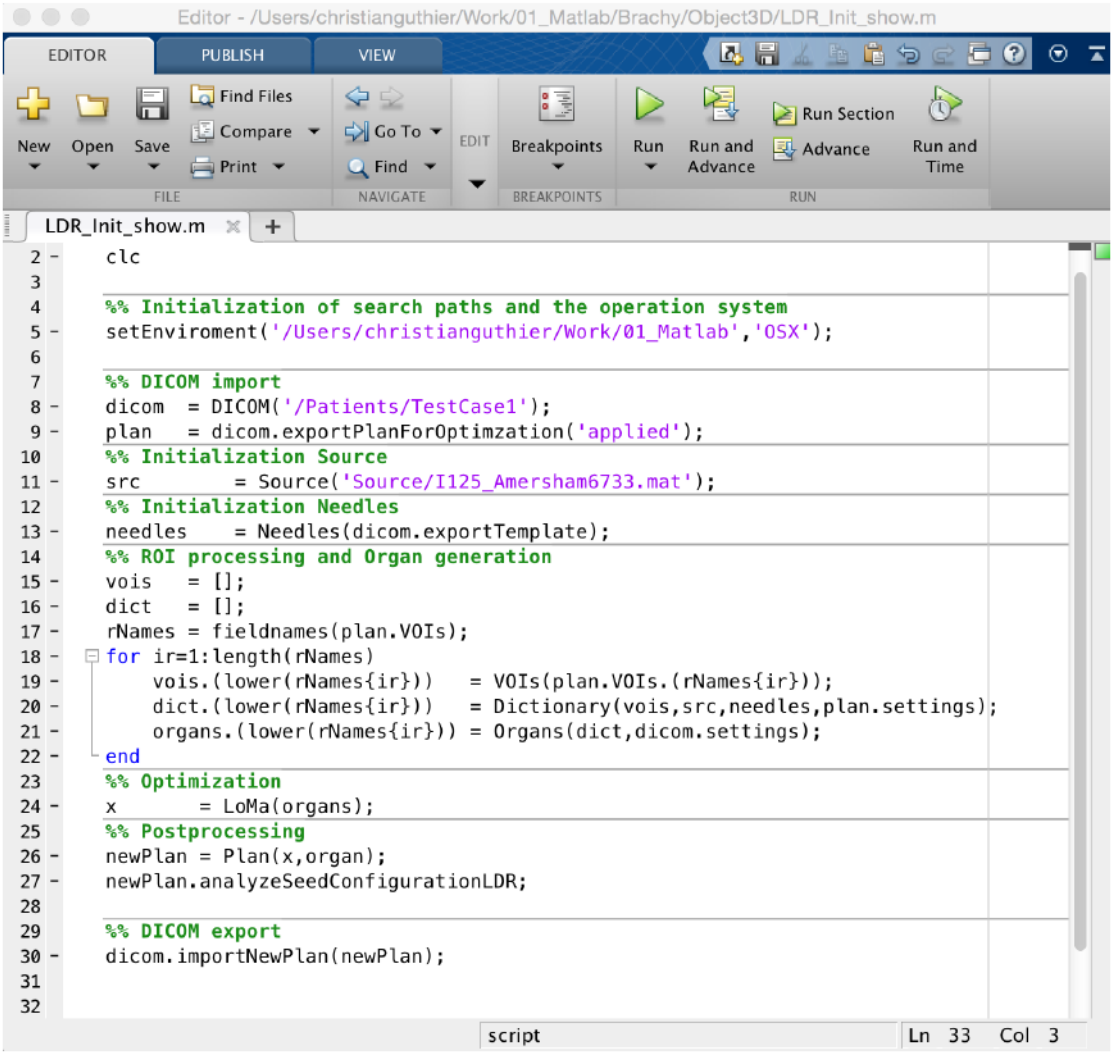

Figure 4.2: An example of the Matlab script to optimize the plan of one single patient with LOMA.

of three different programming levels: Matlab, Mex-file, and C++.
The Matlab level is used to test the algorithms and to analyze the time complexity of each algorithm. Afterwards, time-critical structures are identified and re-implemented in C++. The communication between C++ and Matlab is realized using Mex-files. This enables the use of C++ routine, as if they are built-in function of Matlab.
For C++, either existing optimization libraries are used or ones that are specially designed for the algorithms are implemented.
For solving the different LPs, an interface for IBM ILOG CPLEX Optimization Studio is incorporated. CPLEX was chosen since it performs best when compared

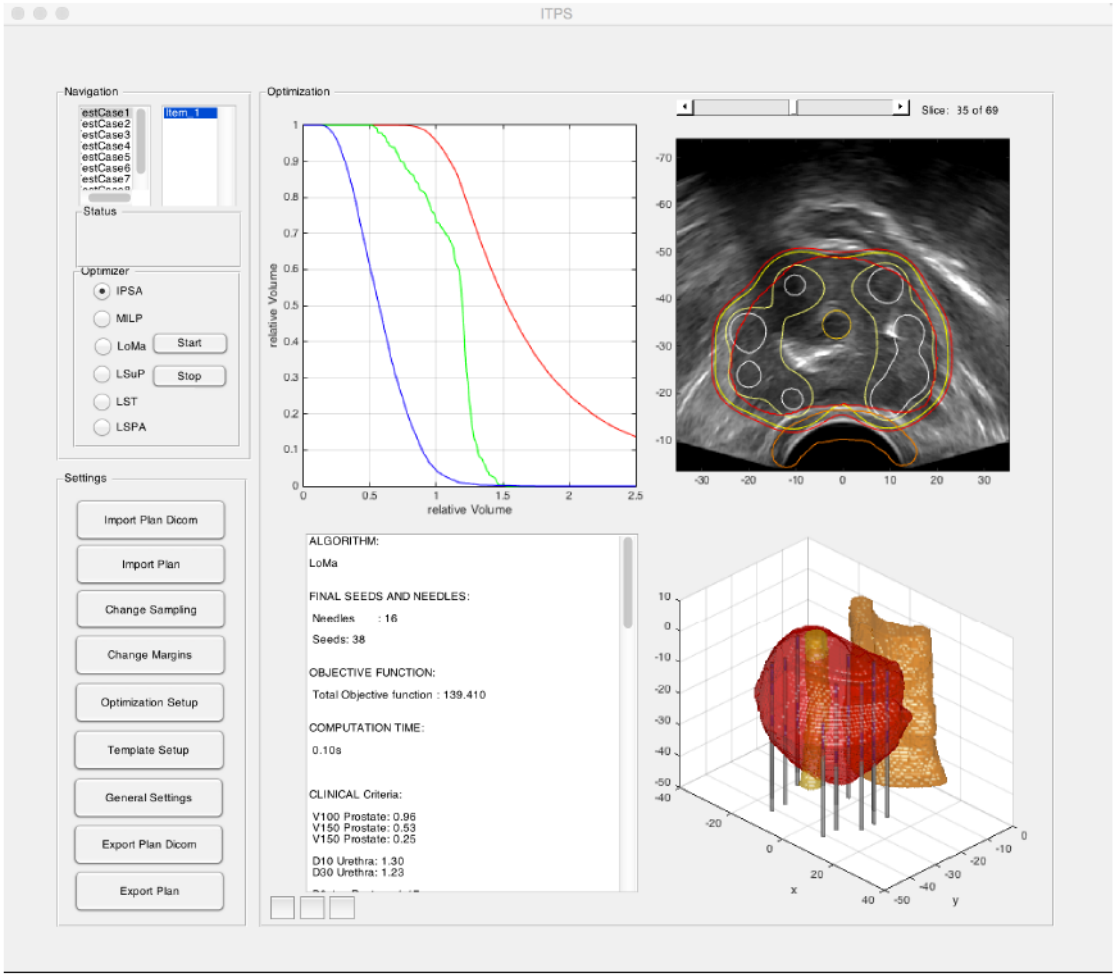

Figure 4.3: The graphical user interface of the novel ITP. The example shows the DVHs (upper left), a transversal slice (upper right), a plan report (lower left) and an overview (lower right) for a plan obtained with LOMA.

to other libraries such as GLPK, LPSOLVE, CLP, or GUROBI [123]. For LDR ITP, this was also confirmed by Guthier et. al in 2014 [28].

Furthermore, to solve unconstrained optimization problems the ALGLIB (www.alglib.net, Sergey Bochkanov) library is used. ALGLIB is chosen since when compared to other existing libraries, e.g. GNU Scientific Library (GSL) it shows a better performance.
To additionally gain performance, the Streaming SIMD Extensions (SSE) instruction set is used. This allows that the same operation is performed on multiple data and thus increases the floating-point operations per cycle. SSE leads to a

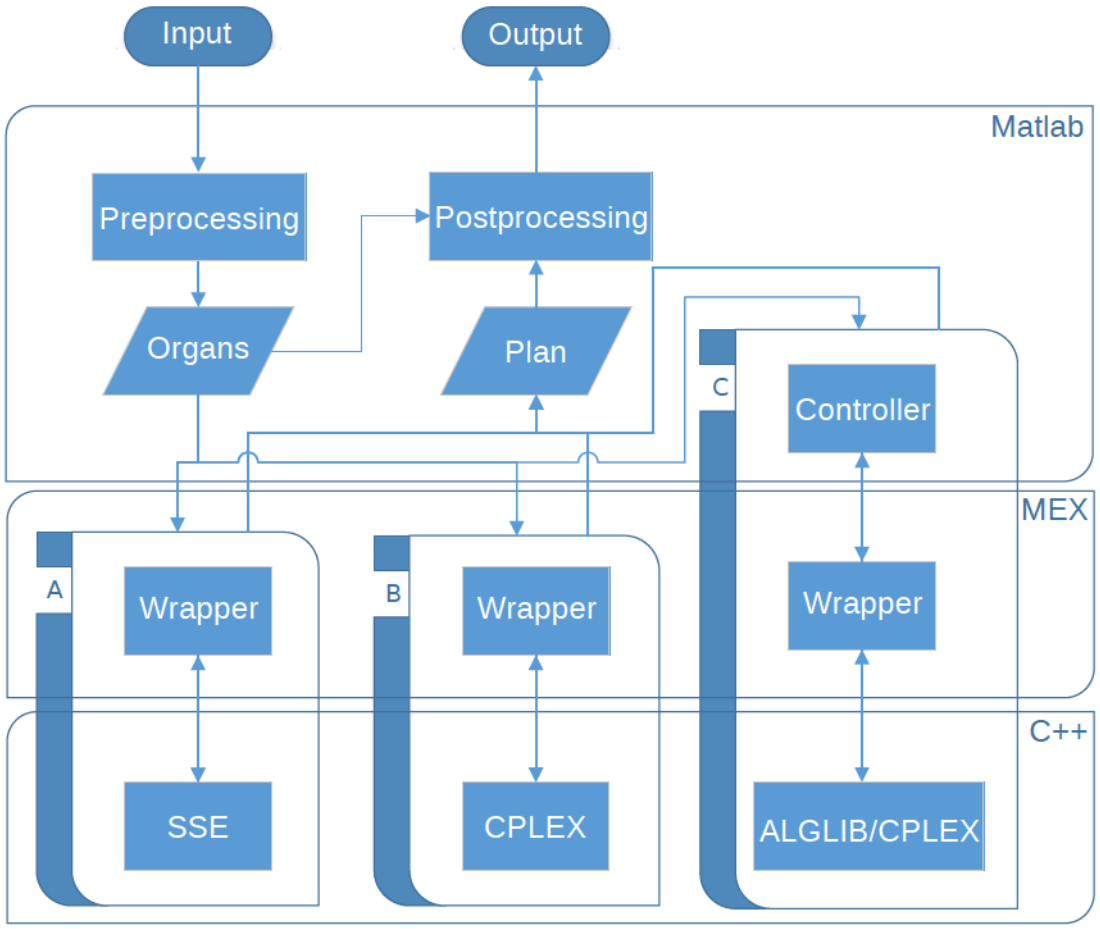

Figure 4.4: The different programming levels of the developed ITP.

theoretical acceleration of the evaluation of the objective function, for a given dose distribution, by a factor of four.
To summarize, for the final versions of the optimizers IPSA, LTA, LOMA, LSUP, LST, and LSPA highly efficient C++ based implementations incorporating SSE are used. The unconstrained sub problems during the iterations of HIPO and SISA are tackled with LBFGS optimizers provided by the ALGLIB library. In addition, the different LP problems are solved with the CPLEX Optimization Studio. A schematic drawing of the different layers is presented in fig. 4.4.
When comparing the re-implemented version of IPSA and HIPO it became clear that they are more efficient than the implementations of the commercially available TPS Oncentra, Elekta AB. An initial benchmarking showed that the re-implemented versions of IPSA and HIPO are a factor of (5.3 ± 4.2, range 2.1 ± 13.6) and (3.9 ± 2.3, range 2.0 ± 8.8) faster. Simultaneously, no statistically significant difference in retrieved plan quality ($p = 0.36$) is observed.

4.6 Patient study

To test the newly developed optimizers, the comparative studies are explained in detail. All necessary parameters and settings which are used to carry out the benchmarking, are presented. The retrospective studies for benchmarking are introduced.

4.6.1 Patient data sets and optimization settings

For this study, ten patient cases where retrospectively examined. These are all available patient cases at the University Medical Center of Mannheim. The prostatic volume ranged from $43.0\,cm^3$ to $77.0\,cm^3$. A detailed description containing the volume of the prostate gland V and source strength S_k is given in appendix tab. A.2.

Contouring and dose prescription

For the PTV for LDR brachytherapy, the visible contour of the prostate plus a margin of $3\,mm$ was used to define the clinical target volume [10]. The planning target volume is equal to the CTV. Further margins do not need to be taken into account since the $3\,mm$ margin already covers systematic errors, e.g. seed displacement and seed migration and the presence of edema directly after the intervention. The dosimetric criteria used are the recommendations of the AAPM TG-143 and are summarized in tab.A.3.
The prescribed dose varies between $120\,Gy$ and $140\,Gy$ and was assigned by experienced radio-oncologists. In general, the recommendation on dose prescription from AAPM TG-143 is $140\,Gy$ for ^{125}I [10]. The used LDR seeds are the Amersham EchoSeed 6733.
For HDR treatment planning, the CTV is defined as the prostate capsule without any margins around its surface. This is in accordance with the recommendations of the American Brachytherapy Society for HDR prostate therapy for tumor stages T1c-T2. Again, the CTV is set as PTV. The dose prescription is assumed to be $10.5\,Gy$ per fraction, with a total number of three fractions for all patient cases. Since the University Medical Center of Mannheim has no experience with HDR brachytherapy, a set of parameters found in literature was used. In addition, those parameters were discussed with colleagues from the Würzburg Medical Center who have an expertise in HDR brachytherapy. For plan evaluation, the recommendations from the GEC ESTRO where used [60]. A summary can be found in tab.A.3. The HDR source is assumed to be the 192Ir-HDR Nucletron mHDR-v2 source commonly used with the MicroSelectron after-loader from Elekta AB, Sweden. A summary of the prescribed doses, number of fractions, and source

strength can be found in appendix tab. A.2.

Point sampling

For both modalities, the generation of dose-points is exactly. The VOIs are sampled from a uniform grid with a spacing of $2.5\,mm$. In addition, the contours are sampled at a resolution of $2\,mm$. With those assumptions, the number of dose points is between 5286 and 7769.
In contrast to DBOF, DCOF and BBOF based ITP considers only the dose-points inside the VOI for optimization. The dose points are generated using a random sampling with sampling density of $50\,cm^{-3}$ according to the uniformly dose-point generation algorithm from Lahanas et al. [124]. This leads to a total number of dose points ranging from $14,367$ to $23,710$.
For dwell-positions, the set of available needles is sampled with a resolution of $4.5\,mm$ for LDR and $2.5\,mm$ for HDR. An additional margin of $2.0\,mm$ is subtracted from the surface in LDR in order to ensure that the seeds are inside the prostate capsule. A margin of $5\,mm$ is added to the caudal end of the prostate in HDR to account for the fact that dwell-points can also be located outside.

Objective functions

The DBOF based plans for LDR and HDR are optimized using the standard optimization parameters summarized in tab. A.5. Those are the de-facto standard settings in clinical routine at the Mannheim University Medical center. They are recommended by the vendor of the commercial planning system Oncentra Prostate, Elekta AB, Sweden. This parameter set delivers applicable clinical plans with respect to the planning criteria for almost all patient cases.
The cost per needle for IPSA, LOMA, and LSUP for LDR treatment planning was set to $\lambda > 7.5$, which was determined in the following way: For each patient, plans with $\lambda \in [0,\ 20]$ and a step size of 0.5 were optimized using IPSA. The resulting configuration was analyzed qualitatively as a function of λ. As an example the DVHs and the number of used needles as a function of λ for one patient are exemplary presented in fig. 4.5. This shows that for $\lambda = 7.5$ the number of used needles is almost constant. In addition, comparing the resulting DVHs between $\lambda = 0$ and $\lambda = 7.5$ only a slight deviation is visible, which is clinically not significant. Thus, this seems to be a viable compromise between number of used needles and plan quality.
For dosimetric criteria based optimization, the constraints are extracted from the recommendations for the given dosimetric criteria for the different modalities [60, 10]. The weights for the new objective function are taken from recommendations

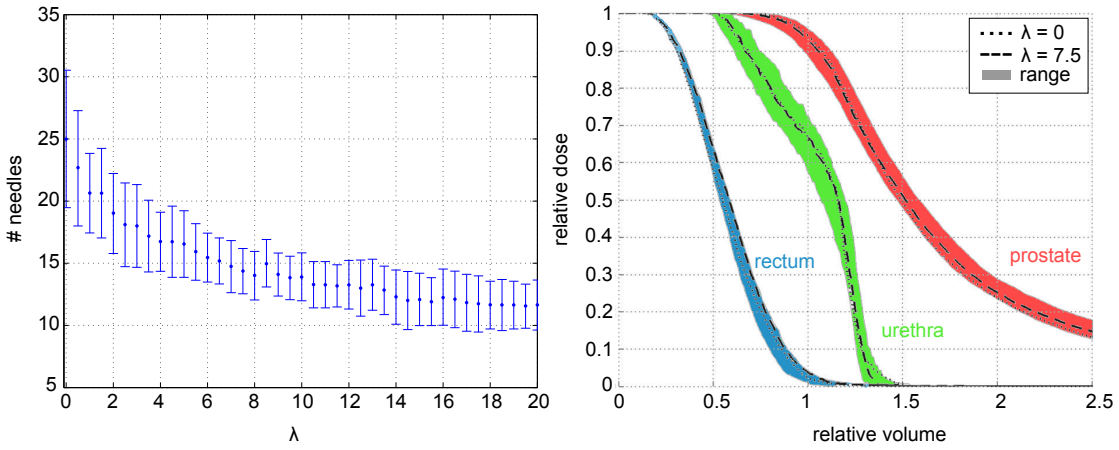

(a) number of needles **(b) DVH**

Figure 4.5: Number of used needles as a function of the cost per needle penalty λ for all patients (a). Resulting DVHs for the different cost per needles(b). The shadowed area shows the range of the DVHs for all patients. Exemplary the DVHs for patient 1 for $\lambda = 0$ and $\lambda = 7.5$ are shown [35].

from HIPO. This was chosen as a reference since the used weighting for prostate, urethra, and rectum provides a good compromise between tumor coverage and sparing of OARs.
Furthermore, for biological based optimization, the desired TCP for LDR and HDR is assigned to be 95% and 100%. These thresholds are obtained by analyzing the estimated biological outcome of the initially applied plans as depicted in fig. 4.6. Therefore, the TCP for LDR ITP is set to 95% to achieve a compromise between tumor control and occurrence of side effects. In contrast, for HDR a TCP of 100% seems applicable without sacrificing the OARs. The accompanying weightings are set the same as for the dosimetric criteria based ITP.
For HIPO and IPSA the standard setup parameters for the optimizers are chosen. Those are the standard settings in the University Medical Center Mannheim and are provided by the vendor [30].
The quality tolerance Q_0 specifies a targeted plan quality defined by the user, where the smaller Q_0 represents the better plan quality. A value of $Q_0 = 1 \times 10^{-3}$ is selected for optimization. If this quality cannot be reached, the optimizer returns the solution closest to Q_0.

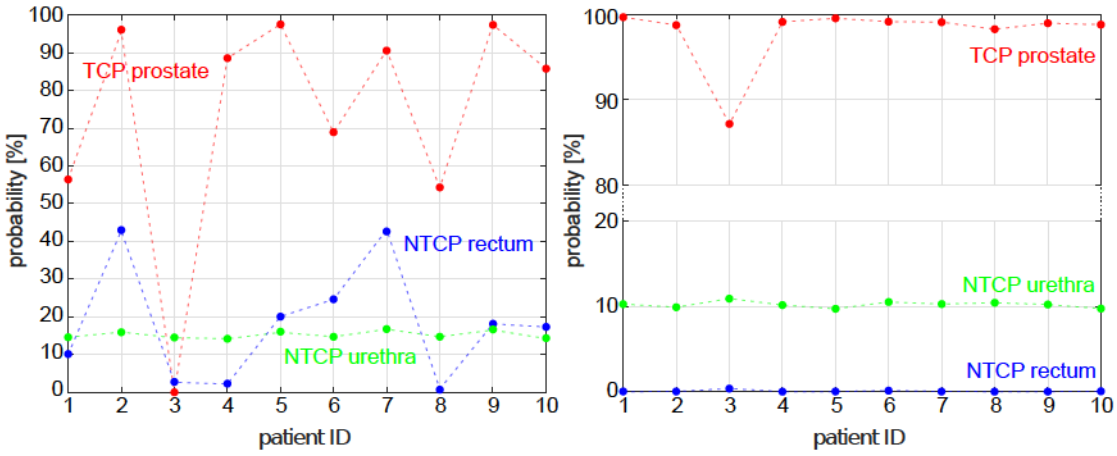

(a) LDR **(b) HDR**

Figure 4.6: Retrospective comparison of the biological outcome for the two different modalities LDR (a) and HDR (b).

4.6.2 Comparative Tests

Each patient study was exported from Oncentra Prostate™ [30] as DICOM file and afterwards re-imported into the novel TPS as described in sec. 4.5.1. Depending on the method, the optimization parameters are set as described in the previous section. The comparative tests are performed as follows:

LDR treatment planning

As an initial benchmark of the applicability of CS inspired optimization, the different algorithms for a predefined needle configuration for LDR treatment planning are applied. The subset of needles is determined by a experienced radiation oncologist of the University Medical Center Mannheim. Defining a needle configuration prior to the optimization is one of the standard approaches in intraoperative ITP. After optimization, the performance of the CS-inspired solvers LTA, LOMA, and LSUP is compared. In addition, the results are evaluated against the state of the art solution IPSA and the lower bound provided by MILP. The main focus is on the final DBOF value, optimization time, and the sparsity of the solution. For clinical rating, EUD and COIN are considered.

LDR treatment planning including needle optimization

As an alternative approach, a comparative study of the algorithms capable of LDR ITP including needle optimization is performed. The CS inspired solvers LST, LSUP, and LSPA are compared against the state-of-the-art methods. As

a reference, the plan generated with IPSA and the manually re-optimized and applied plan (APP), are considered. MILP provides an estimation of the lower bound of the solution. In general, MILP is able to provide the optimal solution, but due to the complexity of the problem, this is hardly reachable in acceptable time. Thus, it is decided to stop the MILP after a runtime of $12\,h$.
The generated plans are rated according to their performance with respect to calculation time, final DBOF value, sparsity of the seeds, and number of used needles. For the latter, it is decided to use a maximum number of needles as used for APP. This allows a fair comparison of the returned DBOF value. The plans are further rated according to clinically relevant parameters such as dosimetric criteria, COIN, and EUD.

HDR treatment planning

Since optimization of a given needle configuration can be optimized in less than one second using L-BFGS, the focus of this comparison is on HDR ITP including needle optimization.
This problem is usually being tackeled using the reformulation as an MILP or with HIPO heuristic. Another possibility is to manually select a needle configuration followed by an optimization of the dwell-times.
The retrieved plans are compared to those obtained via HTA, HSIS, and SISA. For the benchmarking, DBOF value, the number of active dwell-positions, dosimetric criteria, COIN, and EUD are taken into account.
For the CS-inspired solvers, HIPO and MILP, the number of maximally allowable needles was set to the number defined by the physicians during manual needle placement. This again ensures a fair rating of the plan quality.

Dosimetric treatment planning

For the dosimetric criteria-based planning, the reference for both treatment modalities is again the applied plan APP.
For LDR, the results obtained using a reformulation into a BILP problem is used as a reference. This based on the IPIP problem introduced by Siauw et al. [31] with the additional constraint of a binary solution vector. Those are compared to the results obtained using the best performing CS-inspired solver with and without needle selection using the CBOF as objective function. The obtained plans are labeled with LDR criteria based optimization LCB and LCB*.
For HDR, the dosimetric criteria-based MILP problem, i.e. eq. (2.5) and eq. (4.39), and the heuristic IPIP [31] are used as a reference. For the CS-inspired approach, two different solutions, with HDR criteria based optimization (HCB) and without needle optimization (HCB*).
For comparison of the plans, the number of active dwell-positions, the optimiza-

tion time, the dosimetric criteria, EUD, and COIN are considered.

Biological treatment planning

As a final comparative test, the biological based optimization using the BBOF is analyzed. Since there is no existing optimization strategy available, only APP is considered as a reference. For LDR and HDR the plans are refereed as LDR biological based optimization (LBio) and HDR biological based optimization (HBio), respectively.
For LDR, optimization strategies for biological ITP are considered. LBIO labels the plans where the same needle configuration as for APP is re-optimized using the BBOF. LBIO* labels the plans where a sub-set with the same number of used needles as for APP is retrieved out of all available needles.
Since for biological ITP, the gradients for the generalized HDR problem have to be calculated numerically, the optimization of amplitudes is more complex than for LDR. For HDR the two strategies with and without needle optimization are labeled as HBIO* and HBIO.
The different methods are compared using optimization time, number of used active dwell-positions, TCP, NTCP of the urethra (NTCPU), NTCP of the rectum (NTCPR), COIN, and EUD are considered.

Statistical analysis and data representation

To test if the evaluated parameters differ statistically, a one-sided paired Wilcoxon signed-rank test is used. This test can be used when the groups cannot be assumed to be normally distributed. The different levels of significance are labeled with *($p < 0,5$), ** ($p < 0.01$), and *** ($p < 0.001$).
For visualization, boxplots are used. In each box, the median is marked as the central line. The edges of the box represent 25th and 75th percentiles and the whiskers extend to the most extreme data points. In addition, outliers are plotted separately.
If the MILP or BILP solution was not found within the pre-defined optimization time the time is labeled as N/A*. In addition, if runtime information are not available, i.e. the time used for intra-operative forward planning is usually not recorded, it is labeled with N/A.
The ratio between the difference of the resulting objective function values and the reference value $\mathcal{Q}_{MILP}(\boldsymbol{x})$ is employed as a measure of quality:

$$\epsilon = \frac{Q_i(\boldsymbol{x}) - Q_{MILP}(\boldsymbol{x})}{Q_{MILP}(\boldsymbol{x})}, \tag{4.43}$$

where the index i labels the used algorithm.

5 Results

In this chapter, the benchmarking of the novel CS inspired solvers is presented followed by the study regarding criteria based and biological model based treatment planning. The comparative studies are performed according to the protocol described in the previous chapter.

5.1 Comparative study of the optimizers

In order to test the practicability of the optimizers introduced in this work, their performance is compared against state of the art algorithms. Benchmarking criteria are the final objective function values, optimization time, and clinical rating of the treatment plans. The tests are divided into three parts, LDR ITP with and without needle optimization and HDR treatment planning with needle optimization.

5.1.1 LDR treatment planning without needle optimization

In the following, the comparative study of the algorithms that can be used to solve the LDR ITP problem without needle optimization is presented. As commonly done in clinical intra-operative brachytherapy treatment planning, the needle configuration is assigned by an experienced physician. The set of standard optimization settings defined in tab. A.5 are applied for each patient case. To evaluate the quality of the optimization, MILP is used as a reference as it provides a lower bound of the solution. The objective function value of the solution $Q(x)$, the runtime $t[s]$, the number of dwell-position $\#DP$, EUD, and COIN are used for comparison of the algorithms. For each parameter, mean value μ, standard deviation σ, minimum min, and maximum max are calculated from the set of all patients. A summary of the results is presented in tab. 5.1.
For the quality measure stated in eq. (4.43) $i = \{LTA, LOMA, LSUP, SA\}$ is used and depicted in fig. 5.1. The results obtained with LSUP are closer to the expected lower bound than the results obtained using SA. LSUP returns results near the global optimum and small deviation (< 0.01) is an indication of the robustness of the solver.
A similar situation can be observed when comparing LSUP and SA against MILP with ($p > 0.05$) and ($p > 0.05$), respectively. In contrast, the results of LTA

Table 5.1: Comparison of the different optimization algorithms for LDR without needle optimization. $Q(x)$ is the objective function value, t the optimization time, $\#DP$ the number of used dwell-positions. For plan rating EUD and COIN are calculated. For each parameter mean value μ, standard deviation σ, minimum min, and maximum max are given. Underlined values are the best found values.

Algorithm	$\mathcal{Q}(\boldsymbol{x})$	t [s]	#DP	EUD	COIN
MILP (ref)					
μ	151.23	409.80	40	59.79	0.59
σ	16.50	239.30	4	3.01	0.02
min	124.05	34.67	35	54.79	0.55
max	179.56	N/A*	50	65.41	0.63
LTA					
μ	244.31	<u>0.01</u>	40	<u>64.37</u>	0.58
σ	87.39	0.00	4	5.52	0.02
min	168.14	0.00	35	54.96	0.54
max	413.92	0.01	50	72.62	0.62
LOMA					
μ	183.60	0.02	<u>38</u>	56.94	<u>0.59</u>
σ	24.60	0.01	4	3.40	0.02
min	129.66	0.01	34	52.32	0.56
max	216.85	0.03	47	65.48	0.63
LSUP					
μ	<u>153.75</u>	0.11	40	59.46	0.58
σ	16.84	0.10	4	3.02	0.02
min	124.35	0.03	35	54.75	0.55
max	182.60	0.32	49	65.47	0.63
SA					
μ	163.95	4.78	40	58.83	0.58
σ	21.57	3.12	5	3.56	0.02
min	124.50	1.08	35	53.74	0.55
max	211.01	9.83	53	65.27	0.62

($p < 0.001$) and LOMA ($p < 0.01$) with respect to obtained objective function value are significantly worse.
For a total of six cases, the runtime of the MILP exceeds the maximum allowable optimization time. Since MILP is not used in clinical routine, the reference for benchmarking the performance of the novel algorithms is SA, a state of the art method with a mean optimization time of $(4.78 \pm 3.12)s$. The mean runtime

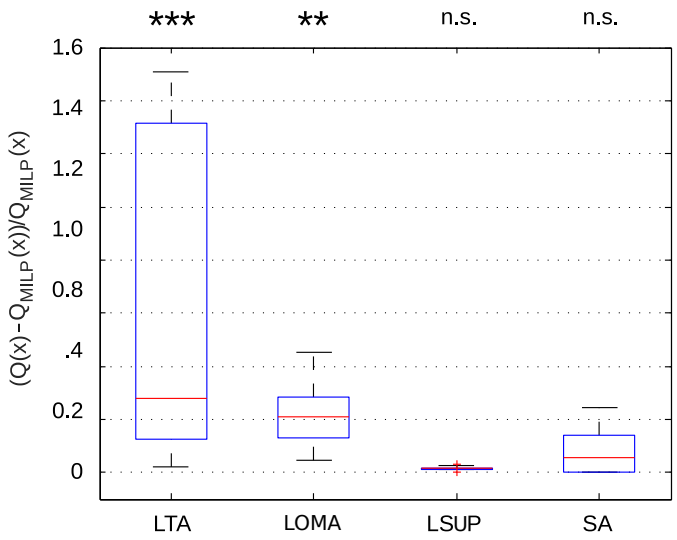

Figure 5.1: Box-and-whisker plot of the ratio between the different strategies for LDR without needle optimization. The reference function value is obtained via MILP. The different levels of significance are labeled with '$***$' ($p < 0.001$), '$**$' ($p < 0.01$), and 'n.s'. ($p > 0.05$).

of LSUP was $(0.11 \pm 0.10)s$ and, thus, the new CS inspired solver is $(104 \pm 112$, range: 8 to 329) times faster. In addition, LOMA $(338 \pm 311$, range: 62 to 969) is faster than SA. For LTA a speed-up of $(1181 \pm 1.213$, range: 154 to 3526) is observed. In summary, the newly introduced optimizers have a significantly ($p < 0.001$) reduced optimization time.
Considering the number of dwell-positions, the obtained results do not differ significantly ($p > 0.05$) from the reference. However, comparing the number of used dwell-positions using SA and LSUP show that the sparsity approach reduces the number of dwell-positions in six out of ten cases. For the remaining cases, the number of dwell-positions remains the same. Using COIN and EUD as a measure for the quality of the treatment plan, the obtained results using LOMA, LSUP, and SA showed statistically significant differences ($p > 0.05$ and $p > 0.05$).
When benchmarking the overall performance of the CS inspired solvers it is obvious that LSUP performs better than LTA and LOMA with respect to the objective function value, but vice-versa for the optimization time.

5.1.2 LDR treatment planning including needle optimization

In order to assess the practical applicability of the proposed CS inspired algorithms comparative tests including needle optimization are presented in the following. The focus of this assessment is to compare objective function value, runtime, number of used dwell-positions and needles, as well as the rating of plans using

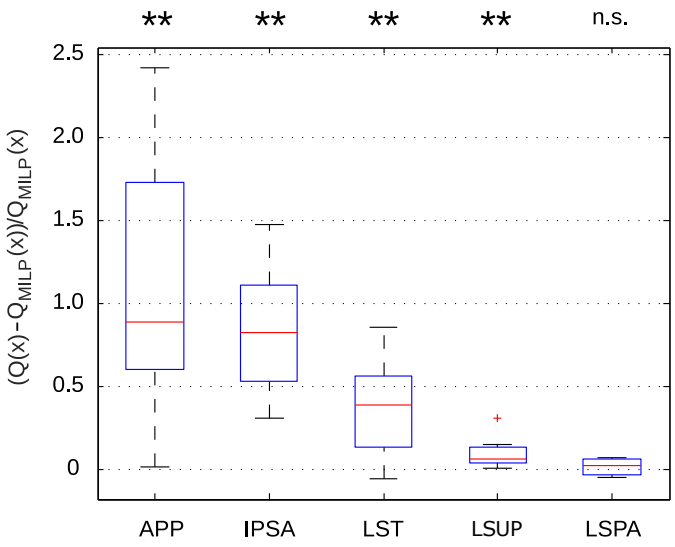

Figure 5.2: Box-and-whisker plot of the ratio between the different strategies for LDR including needle optimization. The reference function value is obtained via MILP. The different levels of significance are labeled with '$**$' ($p < 0.01$), and 'n.s.' ($p > 0.05$).

AAPM criteria. As additional parameters for plan evaluation EUD and COIN are presented.
Again MILP provides a lower bound of the objective function value and all algorithms are compared against this solution. However, when comparing the performance with respect to optimization time, IPSA is used as a reference because it is the fastest state-of-the-art algorithm capable of LDR ITP including needle optimization. The results are sumarized in tab. 5.2.
The comparison of the algorithms with respect to the resulting objective function value is again based on eq. (4.43) with $i = \{APP, IPSA, LST, LSUP, LSPA\}$ and depicted in fig. 5.2. The resulting objective function value obtained via LSPA does not show a significant difference ($p > 0.05$) when compared to MILP. The same accounts for LSUP with ($p > 0.05$). In contrast, the results of the remaining methods are significantly worse. In detail, the level of significance is $p < 0.001$ for APP, $p < 0.001$ for IPSA, and $p < 0.01$ for LST.
Exemplarily, the resulting plans for the patients with the largest deviation in the resulting objective function value for LSPA vs. IPSA and LSPA vs. MILP are depicted in fig. 5.3. While for LSPA vs. IPSA it shows patient 2, it is patient 1 for LSPA vs. MILP. The illustration shows the DVHs as well as the isodose curves of the central transversal slice of the prostate.
The CS inspired solvers reduce the optimization time dramatically. The speed-up for LTA, LSUP, LSPA compared to IPSA was (104 ± 50, range 28 to 213), (169 ± 48, range 110 to 256), and (117 ± 106, range 17 to 312), respectively. The

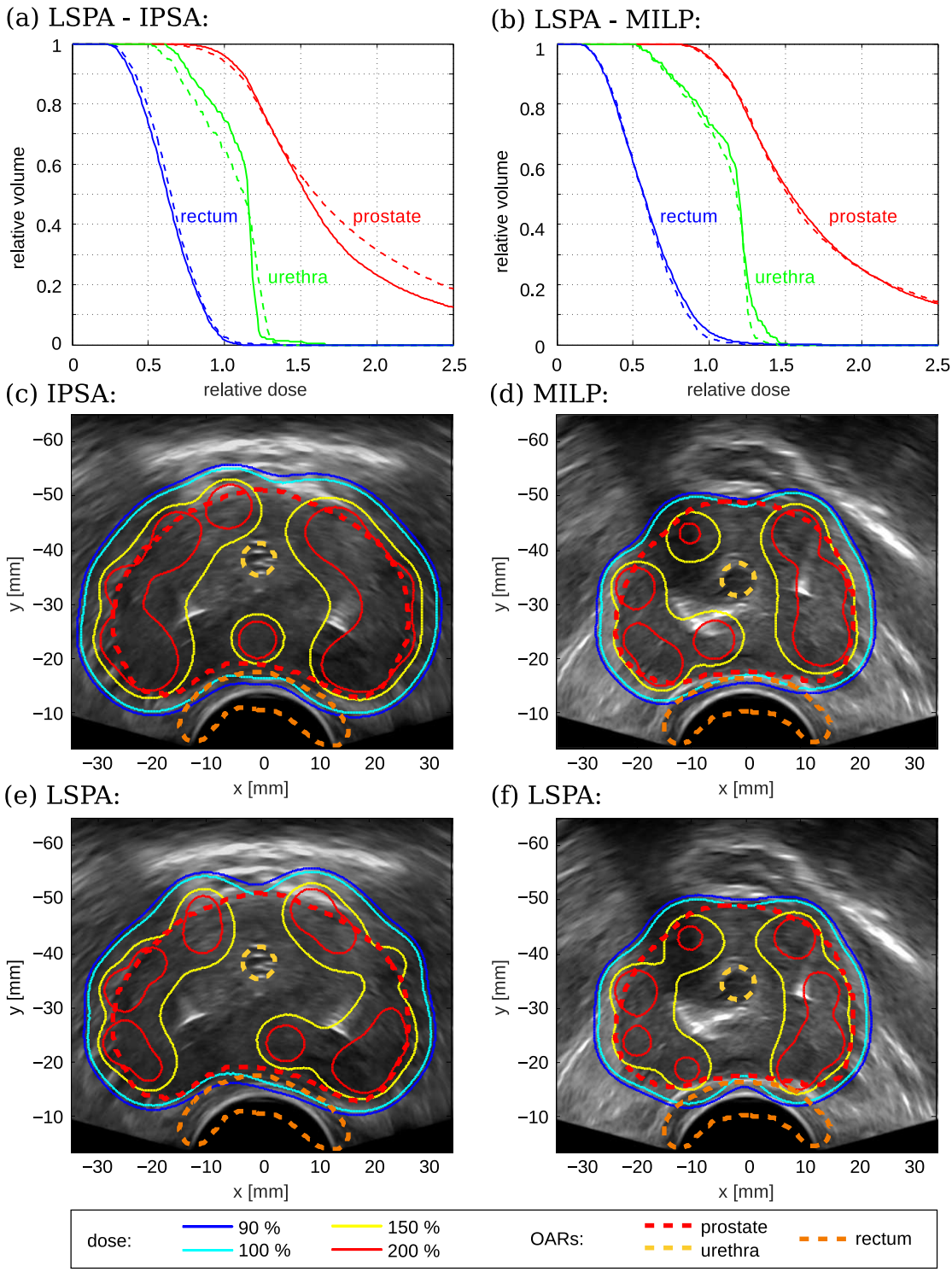

Figure 5.3: Comparison of the different optimization methods. DVHs and isodose lines for the cases with the largest deviation in $\mathcal{Q}(\boldsymbol{x})$ for LSPA vs. IPSA (a,c,e) and LSPA vs. MILP (b,d,f) are shown. The DVHs of references IPSA and MILP are drawn as dashed lines. In addition, the DVHs of LSPA are shown as solid-lines.

Table 5.2: Comparison of the different optimization algorithms for LDR including needle optimization.

Algorithm	$\mathcal{Q}(\boldsymbol{x})$	t [s]	#DP	#N	V100	V150	V200	UD10	UD30	RD0.1cc	RD2.0cc	COIN	EUD
MILP (ref)													
μ	123.6	N/A	42	17	95.3	54.5	26.4	125.3	121.5	99.8	71.4	0.63	69.88
σ	14.9	N/A	8	3	1.6	2.9	2.4	1.4	1.5	8.1	6.8	0.02	8.96
min	109.5	N/A	34	13	91.9	50.5	23.1	123.5	119.6	89.2	58.8	0.58	54.48
max	162.8	N/A	58	24	97.9	59.8	31.1	127.5	124.5	116.7	83.3	0.67	86.39
APP (ref)													
μ	255.2	N/A*	46	17	93.5	61.8	36.4	131.2	124.9	106.1	75.9	0.58	63.30
σ	80.5	N/A*	8	3	1.4	3.5	3.0	3.8	3.9	14.9	9.1	0.02	4.56
min	166.0	N/A*	37	13	90.6	55.7	31.6	125.5	117.6	86.3	61.8	0.53	57.23
max	415.7	N/A*	62	25	95.1	67.9	40.6	136.3	130.4	139.2	93.1	0.61	70.08
IPSA													
μ	224.2	7.18	44.7	16.5	92.8	58.0	32.7	135.3	125.8	96.9	68.8	0.58	62.45
σ	40.8	1.81	8.3	1.9	1.8	2.4	1.6	7.5	3.2	8.3	6.7	0.02	6.34
min	159.5	3.96	36	14	89.8	54.5	30.3	127.2	122.0	80.4	56.2	0.52	50.81
max	306.4	10.21	63	20	96.2	62.6	35.6	148.3	132.2	108.6	78.6	0.60	71.76
LST													
μ	172.7	0.26	41.9	17.1	93.8	53.0	26.5	128.7	122.0	106.5	72.8	0.61	66.31
σ	47.7	0.12	7.4	3.3	1.8	2.5	2.5	13.1	8.7	12.6	7.1	0.03	8.35
min	109.4	0.11	34	13	91.4	49.0	24.0	119.6	113.7	87.3	57.8	0.57	54.13
max	284.5	0.52	58	25	96.5	57.2	31.4	165.7	145.1	123.5	82.4	0.66	79.68
LSUP													
μ	134.8	0.14	41.7	16.3	94.6	53.5	25.9	124.6	119.5	105.4	72.2	0.62	68.55
σ	16.4	0.05	7.4	3.0	1.7	3.1	2.8	3.2	3.0	8.8	7.2	0.03	9.10
min	110.9	0.09	34	12	91.7	49.5	22.4	118.6	114.7	93.1	56.9	0.57	54.52
max	171.1	0.24	58	22	97.6	60.0	32.1	130.4	123.5	117.6	82.4	0.66	83.87
LSPA													
μ	125.9	0.47	41.6	17.2	94.9	53.5	25.0	125.6	120.3	105.2	71.6	0.63	69.29
σ	15.0	0.44	7.9	3.3	1.8	2.2	1.5	3.1	2.9	12.8	6.7	0.02	9.42
min	105.7	0.08	33	13	91.6	50.6	22.5	120.6	116.7	88.2	58.8	0.58	53.91
max	163.5	1.50	58	25	97.9	58.6	27.5	130.4	126.5	132.4	82.4	0.66	86.50

time for APP is not available since the planning is a trial-and-error method and not well documented. Usually the time varies from minutes up to one hour and thus being several orders of magnitudes slower than ITP methods.
The number of dwell-positions increases significantly ($p < 0.001$) for APP and IPSA while for the remaining algorithms they do not differ ($p > 0.05$) with respect to the reference MILP. The number of needles remain the same due to design of the comparative tests.
Using MILP or LSPA and rating the plans according to AAPMs dosimetric criteria, seven out of ten patient cases are clinically acceptable at the first attempt. LSUP, LST, and IPSA lead to plans that meet the criteria in five, three, and two cases, respectively. The worst rating is shown by APP, which leads to only one single acceptable plan. When considering EUD, the CS inspired solvers do not differ significantly ($p > 0.05$) from the results obtained using MILP while for standard optimization strategies APP and IPSA they do ($p < 0.001$). However, for COIN, only LSUP and LSPA do not differ significantly ($p > 0.05$) from the reference while for the remaining strategies COIN decreases ($p < 0.05$).
A comparison between the CS inspired solvers against each other is performed. Here, LSUP and LSPA are almost equivalent for all measures. LSUP and LSPA have small advantages either in speed or quality. When compared to LST, both show a statistically significant ($p < 0.05$) improvement with respect to obtained objective function values.

5.1.3 HDR treatment planning

To test the practicability of the CS inspired solvers for HDR ITP including needle selection, the novel algorithms are compared against MILP, APP, and HIPO. The MILP formulation including needle optimization allows to compare the plans against an estimation of the lower bound of the solution. The resulting DVHs are calculated and used to evaluate the planning criteria COIN, and EUD. The obtained results are listed in tab. 5.3.
To compare the resulting objective function value of the CS algorithms against the reference, eq. (4.43) with $i = \{APP, HIPO, HTA, HSIS, SISA\}$ is used and summarized in fig. 5.4. The results of the CS inspired solvers are near to the expected global optimum obtained with MILP. In some cases, the objective function values are smaller than the estimated bound of MILP indicating that the MILP solution represents a local optimum. Comparing SISA shows the best scoring where the obtained objective function values are smaller than the estimated bound. In contrast, APP does not show any improvement. The results obtained with APP, HIPO, and HTA are significantly worse ($p < 0.01$) compared to those of MILP. In contrast, the methods HSIS and SISA do not show a significant difference to MILP ($p > 0.05$). The resulting DVHs of the plans showing the maximum difference in objective function value between SISA-MILP and SISA-HIPO are depicted

Table 5.3: Comparison of the different optimization algorithms for HDR including needle optimzation.

Algorithm	$\mathcal{Q}(\boldsymbol{x})$	t [s]	#DP	#N	V100	V150	V200	UD0.1cc	UD1.0cc	RD0.1cc	RD2.0cc	COIN	EUD
MILP (ref)													
μ	47.0	N/A*	57.5	16.6	97.1	41.7	17.9	117.5	75.8	88.0	66.3	0.83	76.5
σ	9.3	N/A*	9.8	3.1	0.4	3.4	1.4	6.1	13.8	8.5	7.0	0.01	2.4
min	34.6	N/A*	46	12	96.2	33.3	14.5	106.9	56.9	75.5	52.0	0.82	73.4
max	62.5	N/A*	83	23	97.7	46.3	19.4	126.5	100.0	104.9	77.5	0.86	80.1
APP (ref)													
μ	59.9	N/A	61.6	17.2	95.8	43.1	19.1	119.0	75.2	89.8	68.0	0.78	74.3
σ	8.4	N/A	16.6	3.3	0.5	4.7	2.0	5.4	12.1	8.3	6.9	0.02	2.0
min	45.3	N/A	43	13	95.0	35.8	15.3	109.8	57.8	75.5	52.9	0.74	71.5
max	73.3	N/A	103	25	96.8	53.2	22.9	126.5	95.1	103.9	76.5	0.82	78.5
HIPO													
μ	56.9	186.9	57.9	17.2	97.2	44.3	20.1	123.6	77.9	89.5	66.9	0.82	77.6
σ	10.6	106.2	11.4	3.3	0.2	4.0	2.1	8.5	14.3	7.6	6.4	0.02	1.6
min	40.0	30.1	46	13	96.7	36.8	16.9	109.8	57.8	77.5	52.9	0.79	75.3
max	71.0	300.7	88	25	97.6	51.0	23.1	135.3	102.0	100.0	74.5	0.86	80.0
HTA													
μ	53.6	0.6	61.1	17.1	95.8	40.8	18.6	117.0	76.8	93.7	68.4	0.80	74.6
σ	9.1	0.5	16.2	3.3	0.7	5.5	3.7	6.2	12.6	13.4	8.3	0.03	2.8
min	40.0	0.3	40	13	94.8	32.0	14.0	106.9	61.8	75.5	52.9	0.73	71.2
max	68.3	1.8	102	25	97.0	54.5	28.7	123.5	100.0	122.5	80.4	0.84	79.7
HSIS													
μ	49.7	1.2	59.6	17.1	97.1	42.1	18.9	117.3	76.1	88.8	67.0	0.82	77.0
σ	9.8	0.5	13.1	3.4	0.5	5.7	2.7	6.8	12.9	8.8	7.1	0.01	2.4
min	37.3	0.7	47	12	96.4	31.9	14.2	107.8	57.8	74.5	52.0	0.80	73.6
max	69.4	2.6	93	25	98.0	48.4	23.0	126.5	99.0	102.9	76.5	0.84	80.4
SISA													
μ	46.7	3.5	66.7	17.2	97.0	41.1	17.4	117.2	75.4	86.0	65.1	0.84	76.2
σ	9.4	2.0	15.3	3.3	0.5	4.0	1.9	5.8	14.2	7.5	7.0	0.02	2.1
min	33.3	1.9	51	13	96.3	31.6	12.7	107.8	55.9	74.5	51.0	0.81	73.2
max	63.8	8.5	106	25	97.7	48.3	20.4	124.5	102.9	98.0	74.5	0.87	79.4

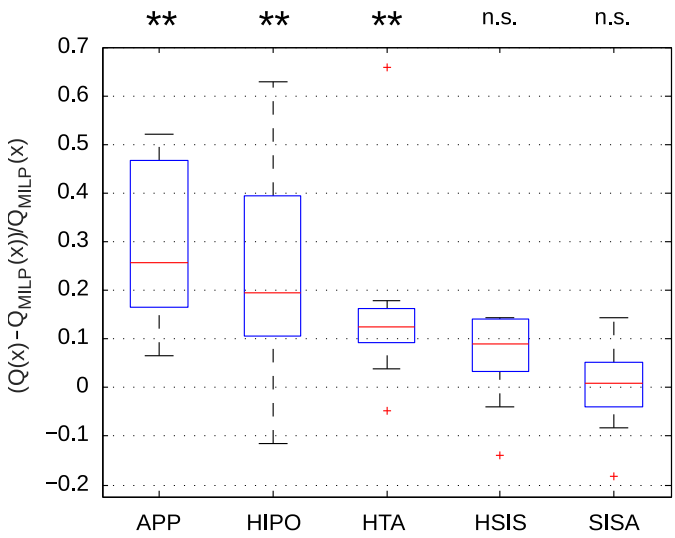

Figure 5.4: Box-and-whisker plot of the ratio between the different strategies for HDR including needle optimization. The reference function value is obtained via MILP. The different levels of significance are labeled with '**' ($p < 0.01$), and 'n.s.' ($p > 0.05$).

in fig. 5.5. No isodose lines are shown since the similar DVHs indicate a clinically non-significant change in dose distribution.
For comparison of the optimization time, the introduced strategies are compared to HIPO which is the fastest technique for needle optimization. MILP and APP are several orders of magnitudes slower and are therefore neglected. The best performance is reached in HTA being (350 ± 180, range: 100 to 637) times faster than HIPO. For HSIS and SISA a speed up of (163 ± 90, range: 27 to 303) and (56 ± 34, range: 12 to 132) was obtained, respectively.
The number of retrieved needles do not show any significant difference ($p > 0.05$). However, for the number of active dwell-positions a significant increase is observed for SISA ($p < 0.001$).
When evaluating the plans according to clinical acceptance, MILP, HSIS, and SISA show an equivalent behavior where all plans were acceptable after the first attempt. APP and HTA (acceptance rate 0.8) show a better performance than HIPO where a re-optimization would have been necessary in three cases. For EUD, the plans obtained with HIPO, HSIS, and SISA do not show a statistically significant decrease ($p > 0.05$) compared to the reference MILP. However, for the APP and HTA plans, this is observed ($p < 0.001$). Regarding COIN, a significant decrease is observed for APP ($p < 0.001$), HTA ($p < 0.01$), and HSIS ($p < 0.05$).
Finally, when comparing the introduced CS inspired solvers against each other, SISA is able to significantly reduce the obtained objective function value with respect to HTA ($p < 0.01$) and HSIS ($p < 0.01$). However, the runtime of HTA

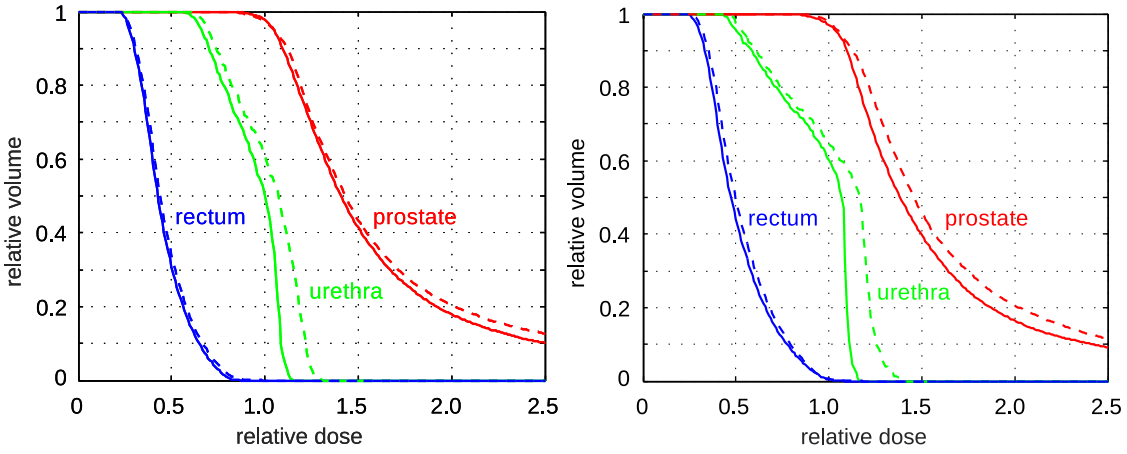

(a) SISA-MILP **(b) SISA-HIPO**

Figure 5.5: DVHs for PTV and OARs for the two cases with the largest deviation from $Q(x)$ for SISA-MILP (a) and SISA-HIPO (b). The DVHs of references MILP and HIPO are shown as dashed lines. In addition, the DVHs of SISA are labeled as solid-lines.

and HSIS is (3 ± 1) and (7 ± 1) times faster than SISA.

5.2 Study of new objective functions

In this section the newly introduced CBOF and BBOF (sec. 4.4) are evaluated. The goal is to compare the performance of both objective functions against those plans that have been clinically accepted for treatment. Finally, the question is answered whether the introduced objective functions influence the expected clinical outcome of the intervention and/or simplify the planning procedure.

5.2.1 Dosimetric criteria based objective function

In order to evaluate the practicability of the CBOF, the presentation of the results are again subdivided into LDR and HDR treatment planning. For both methods the plans are optimized with the CS inspired optimizer that shows the best compromise between objective function value and optimization time of the particular treatment modality, i.e. LSPA (LDR) and SISA (HDR).

LDR

Results for the dosimetric criteria based treatment planning are presented in tab. 5.4. For each plan, the runtime t, the number of used dwell-position $\#DP$,

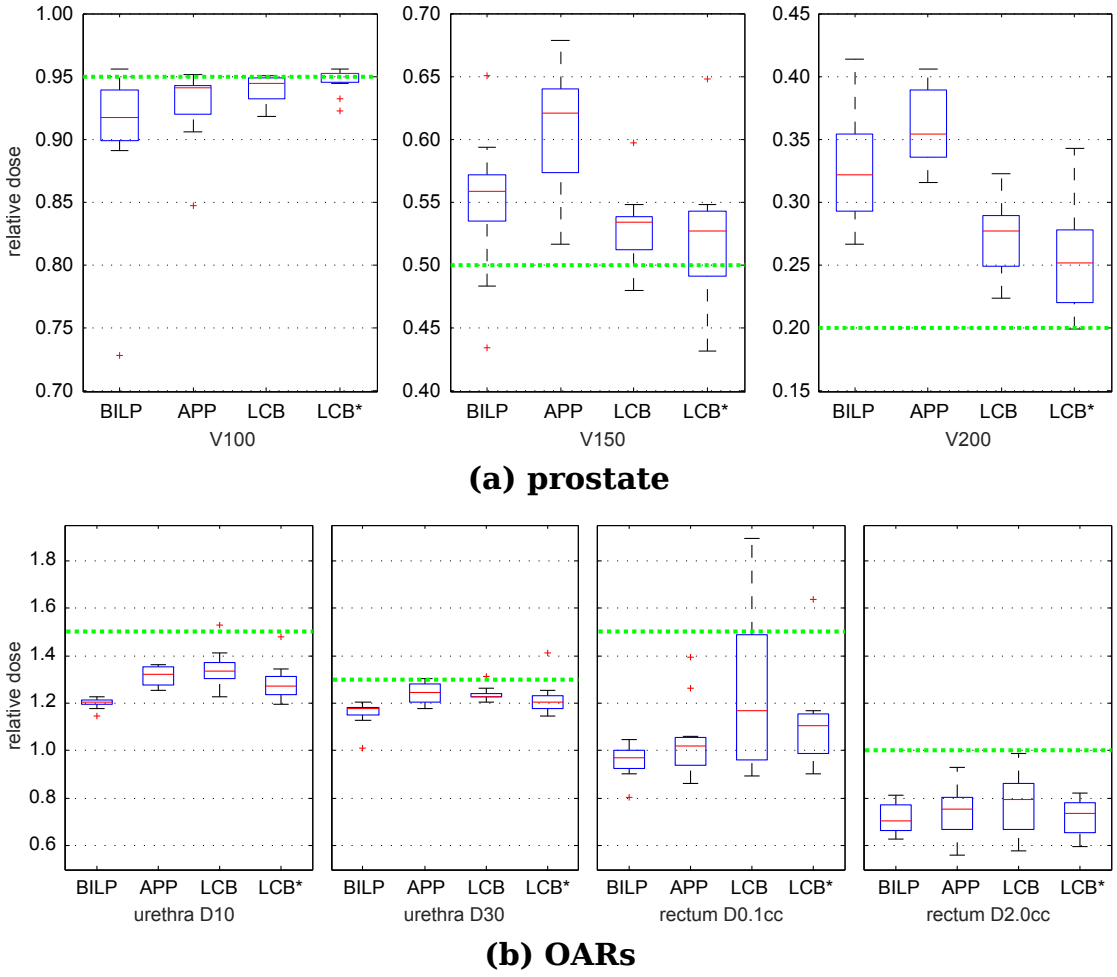

Figure 5.6: Box-and-whisker plots of the dosimetric criteria for the prostate (a) and for the OARs (b) for the different optimization strategies for LDR. The green dashed lines are the recommendations from the AAPM.

the different dosimetric criteria, as well as COIN and EUD are reported. For APP, BILP, and LCB a fixed needle configuration is used. In contrast, for LCB* all needles defined by the transperineal template that hit the PTV and miss OARs are considered for optimization.
A detailed comparison of the different methods is shown in fig. 5.6. The best performance with respect to dosimetric criteria is given by LCB*. Including needle selection, the method leads to a significant increase in the V100 criteria ($p < 0.01$) and simultaneously to a decrease in the V150 and D30 criteria ($p < 0.05$). The remaining dosimetric critera do not show a statistically significant ($p > 0.05$) improvement. In contrast, LCB only shows a significant decrease in V150 while the remaining parameters are similar to the reference. An improvement of EUD

Table 5.4: Comparison of the different optimization algorithms for the LDR dosimetric criteria based optimization.

Algorithm	$\mathcal{Q}(\boldsymbol{x})$	t [s]	#DP	#N	V100	V150	V200	UD10	UD30	RD0.1cc	RD2.0cc	COIN	EUD
APP (ref)													
μ	0.52	N/A	43.8	16.5	92.7	60.9	36.1	131.6	124.4	104.5	74.1	0.57	61.85
σ	0.27	N/A	10.2	3.8	2.8	4.4	3.0	3.9	4.0	15.0	10.4	0.04	6.32
min	0.22	N/A	24	10	84.7	51.7	31.6	125.5	117.6	86.3	55.9	0.47	47.35
max	1.16	N/A	62	25	95.1	67.9	40.6	136.3	130.4	139.2	93.1	0.61	70.08
BILP (ref)													
μ	0.61	N/A*	43.4	16.5	90.4	55.0	32.6	120.1	115.9	95.7	69.9	0.56	59.27
σ	0.55	N/A*	11.5	3.8	5.9	5.3	4.1	2.1	5.1	6.5	8.7	0.05	8.70
min	0.18	N/A*	21	10	72.9	43.5	26.7	114.7	101.0	80.4	48.0	0.43	40.72
max	2.28	N/A*	64	25	95.6	65.0	41.4	122.5	120.6	104.9	81.4	0.60	74.53
LCB													
μ	0.21	0.02	40.5	16.5	94.0	53.0	27.3	134.2	123.9	122.4	76.9	0.61	64.56
σ	0.14	0.01	8.6	3.8	1.1	2.8	2.8	7.7	2.7	31.3	12.0	0.03	6.75
min	0.05	0.00	23	10	91.8	48.0	22.4	122.5	120.6	89.2	57.8	0.54	52.79
max	0.54	0.04	57	25	95.1	59.7	32.3	152.9	131.4	189.2	99.0	0.66	76.59
LCB*													
μ	0.13	0.23	40.1	16.5	94.7	52.0	25.2	128.9	122.1	111.1	72.2	0.61	67.75
σ	0.16	0.14	8.1	3.8	1.0	5.4	4.2	7.3	6.7	18.7	7.3	0.04	8.02
min	0.00	0.04	25	10	92.3	43.2	19.9	119.6	114.7	90.2	59.8	0.53	55.17
max	0.42	0.54	57	25	95.6	64.8	34.3	148.0	141.2	163.7	82.4	0.66	80.33

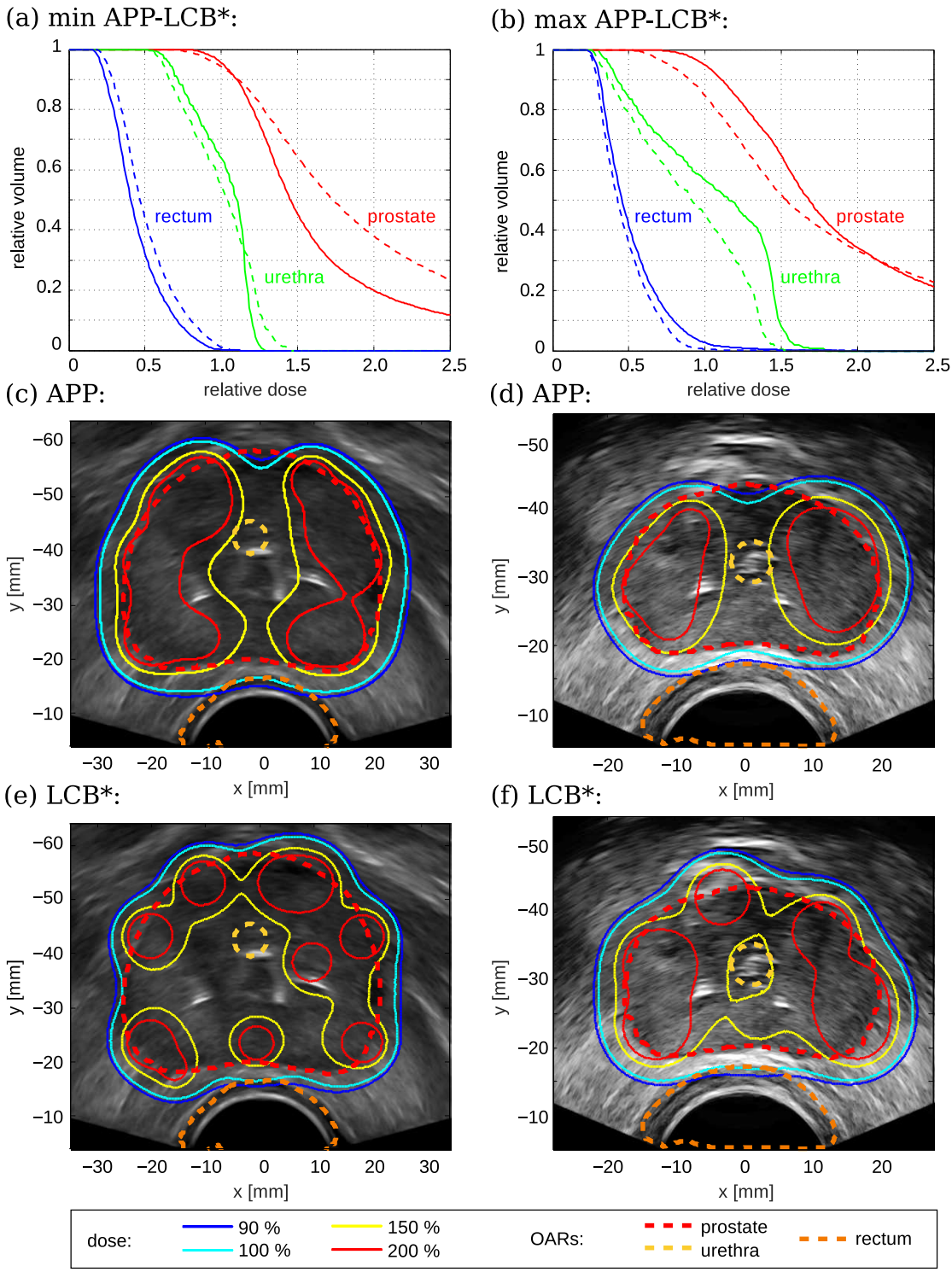

Figure 5.7: Comparison of the different optimization methods for LDR dosimetric criteria based planning. DVHs and isodose lines for the cases with the smallest (a,c,e) and largest (b,d,f) deviation in $V100$ for APP vs. LCB* are shown. The DVHs of reference APP are drawn as dashed lines and the DVHs for LCB* as solid-lines.

and COIN is observed ($p < 0.05$). Both new methods, LCB and LCB* yield a significant improvement of EUD and COIN ($p < 0.01$).
The resulting DVHs comparing APP and LCB* for Patient 3 and Patient 10 are presented in fig. 5.7. Those represent the plans with the smallest and largest deviation of the V100 criteria. In addition, the isodose lines of the transversal central slice are shown.
Using LCB*, seven out of ten patient cases are clinically acceptable at the first attempt. In contrast, APP, BILP, and LCB lead to two plans that fulfill all criteria.
The optimization times using the novel CS inspired solvers are less than $0.6s$ whereas BILP takes several days. In addition, the sparsity strategy significantly reduces the number of seeds ($p < 0.01$). In detail, LCB and LCB* save (6.9±4.0)% and $(7.6 \pm 5.3)\%$ seeds, respectively.

HDR

The results of the comparison of the different optimization strategies with CBOF for HDR treatment planning is summarized in tab. 5.5. The applied plan and the optimized plan with MILP are taken into account as a reference. Furthermore, the results are rated against the competing strategy IPIP. The focus in this comparative study is optimization time, number of active dwell positions, COIN, EUD, and dosimetric criteria. A detailed visualization of the latter is presented in fig. 5.8. When compared against the estimation of the lower bound obtained via MILP, the CS inspired algorithms and IPIP do not show a statistically significant ($p > 0.05$) improvement of the V100, V150, and D0.1cc of the rectum. However, the dosimetric criteria rating the delivered dose to the urethra is significantly improved ($p < 0.1$). The EUD is equivalent for all optimization methods ($p > 0.05$) while a significant improvement ($p < 0.05$) of COIN is observed for APP, HCB, and HCB*.
Comparing APP against IPIP and the CS inspired algorithms, a similar performance with respect to the dosimetric criteria is observed. Only for V150 and the dosimetric of the rectum, MILP, IPIP, HCB, and HCB* show a significant improvement ($p < 0.01$). In addition, EUD and COIN do show statistically significant difference ($p > 0.05$).
When rating against IPIP, the CS inspired optimization strategies improve the V100 and V150 ($p < 0.05$) criteria of the PTV. In addition, the remaining criteria are equivalent to IPIP ($p > 0.05$). Allowing needle optimization, a further significant improvement of those is observed ($p < 0.05$). Again, the EUD ($p > 0.05$) does not show a significant improvement while for the COIN ($p < 0.05$) it is observed.
As an example, the DVHs together with the isodose lines for the central transversal slice of the prostate for Patient 5 and Patient 7 are depicted in fig. 5.9. Patient

Table 5.5: Comparison of the different optimization algorithms for the HDR dosimetric criteria based optimization.

Algorithm	$\mathcal{Q}(\boldsymbol{x})$	t [s]	#DP	#N	V100	V150	V200	UD0.1cc	UD1.0cc	RD0.1cc	RD2.0cc	COIN	EUD
MILP (ref)													
μ	0.03	N/A*	39.1	16.6	95.0	37.7	17.7	122.5	84.7	76.3	61.4	0.71	76.32
σ	0.01	N/A*	11.4	3.1	2.1	4.1	2.2	1.3	12.0	2.4	2.2	0.03	4.38
min	0.01	N/A*	22	12	91.3	30.1	13.7	120.6	65.7	73.5	58.8	0.66	69.29
max	0.05	N/A*	63	23	98.0	44.0	20.8	124.5	102.0	82.4	65.7	0.75	82.67
APP (ref)													
μ	0.09	N/A	61.6	17.6	95.8	43.1	19.1	119.0	75.2	89.8	68.0	0.78	74.27
σ	0.04	N/A	16.6	3.1	0.5	4.7	2.0	5.4	12.1	8.3	6.9	0.02	1.96
min	0.04	N/A	43	13	95.0	35.8	15.3	109.8	57.8	75.5	52.9	0.74	71.48
max	0.18	N/A	103	24	96.8	53.2	22.9	126.5	95.1	103.9	76.5	0.82	78.48
IPIP													
μ	0.05	0.9	55.8	16.6	92.7	38.0	19.0	119.7	80.1	77.0	61.2	0.69	73.37
σ	0.01	0.6	14.3	3.1	2.6	3.3	3.0	1.3	12.4	2.3	2.4	0.05	3.80
min	0.03	0.4	34	12	88.0	33.0	15.1	116.7	58.8	74.5	55.9	0.59	66.64
max	0.08	2.5	87	23	97.5	44.6	24.5	121.6	100.0	83.3	64.7	0.75	81.02
HCB													
μ	0.03	0.4	49.4	16.6	94.4	36.9	17.0	113.8	79.2	75.9	60.7	0.72	74.79
σ	0.01	0.2	15.7	3.1	1.6	3.8	1.8	0.9	11.5	2.8	3.5	0.03	3.33
min	0.01	0.2	33	12	91.8	31.3	13.5	111.8	61.8	71.6	52.9	0.68	69.56
max	0.05	0.9	87	23	97.6	44.6	19.5	114.7	96.1	82.4	66.7	0.76	82.45
HCB*													
μ	0.02	2.2	73.1	17.6	95.3	37.8	17.0	112.7	77.1	75.1	59.2	0.78	74.76
σ	0.01	1.5	20.0	3.1	1.2	5.4	3.4	1.2	11.7	2.4	3.6	0.03	3.75
min	0.01	1.0	51	13	93.9	27.3	11.5	110.8	57.8	71.6	51.0	0.71	70.62
max	0.04	5.7	122	24	98.2	46.7	25.0	114.7	97.1	80.4	64.7	0.82	84.65

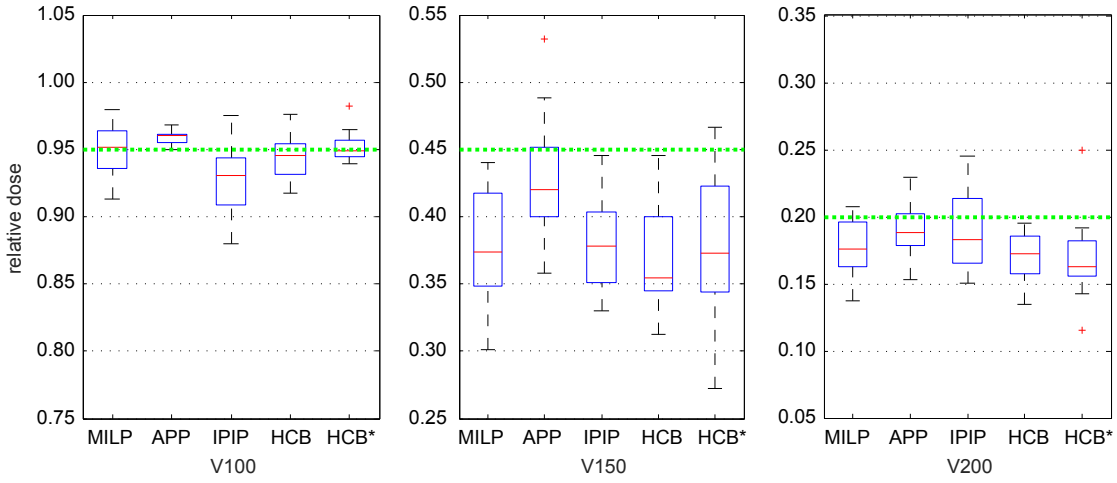

(a) prostate

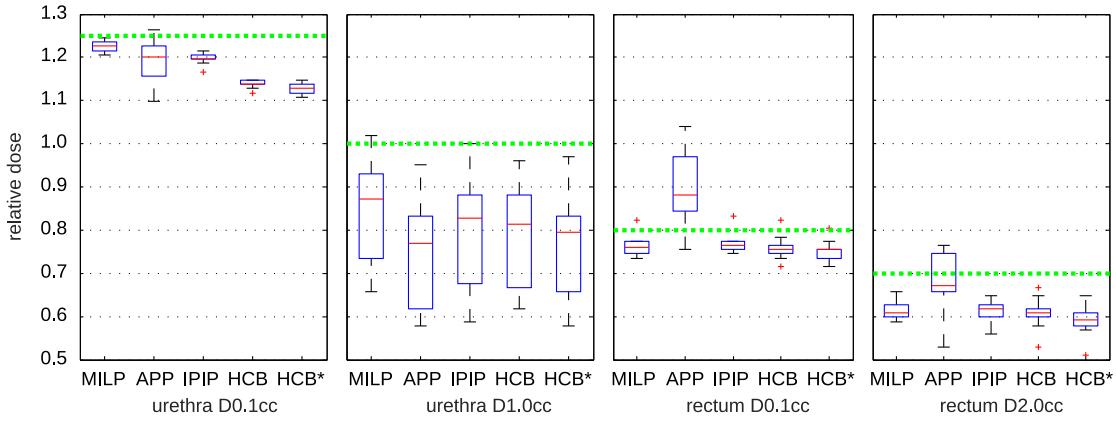

(b) OARs

Figure 5.8: Box-and-whisker plots of the dosimetric criteria for the prostate (a) and for the OARs (b) for the different optimization strategies for HDR. The green dashed lines are the recommendations from the AAPM.

5 is chosen since it represents the plan with the maximum deviation in the V100 criterium. The plan for Patient 7 exhibits the minimum deviation.
The runtime of MILP exceeds the maximum allowable time in all patient cases. Hence, only the two CS inspired methods and IPIP can be compared. With respect to IPIP, HCB improves the runtime by a factor of $(1.9 \pm 0.5$, range: 1.0 to 2.7). For HCB*, the runtime was $(2.2 \pm 1.5)s$, hence being $(2.5 \pm 1.0$, range: 1.9 to 5.0) slower than IPIP. In addition, the plans obtained with HCB* show a significant increase in number of active dwell positions ($p < 0.001$).

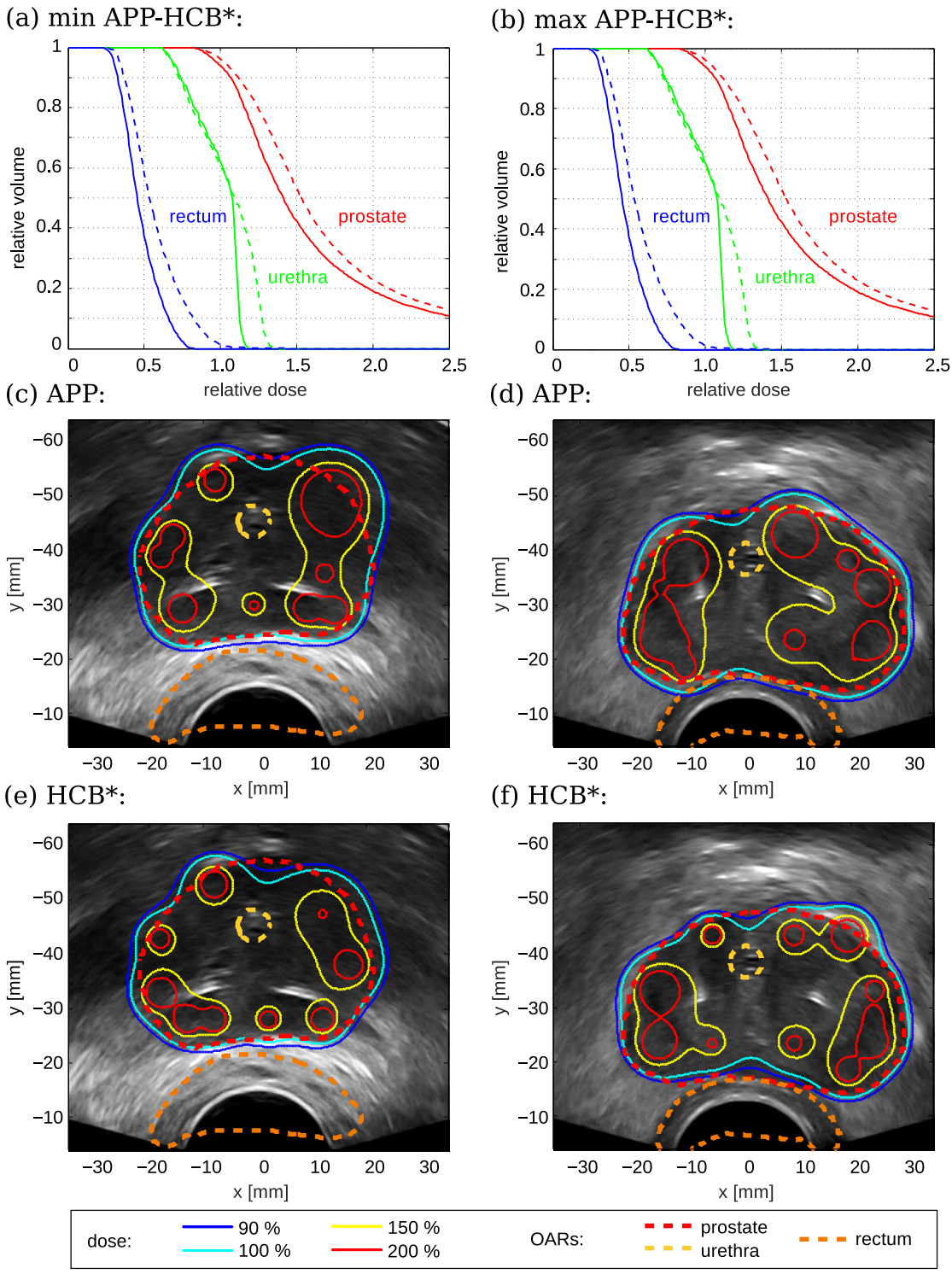

Figure 5.9: Comparison of the different optimization methods for HDR dosimetric criteria based planning. DVHs and isodose lines for the cases with the smallest (a,c,e) and largest (b,d,f) deviation in $V100$ for APP vs. HCB* are shown. In addition, the DVHs of reference APP are drawn as dashed lines and the DVHs for HCB* as solid-lines.

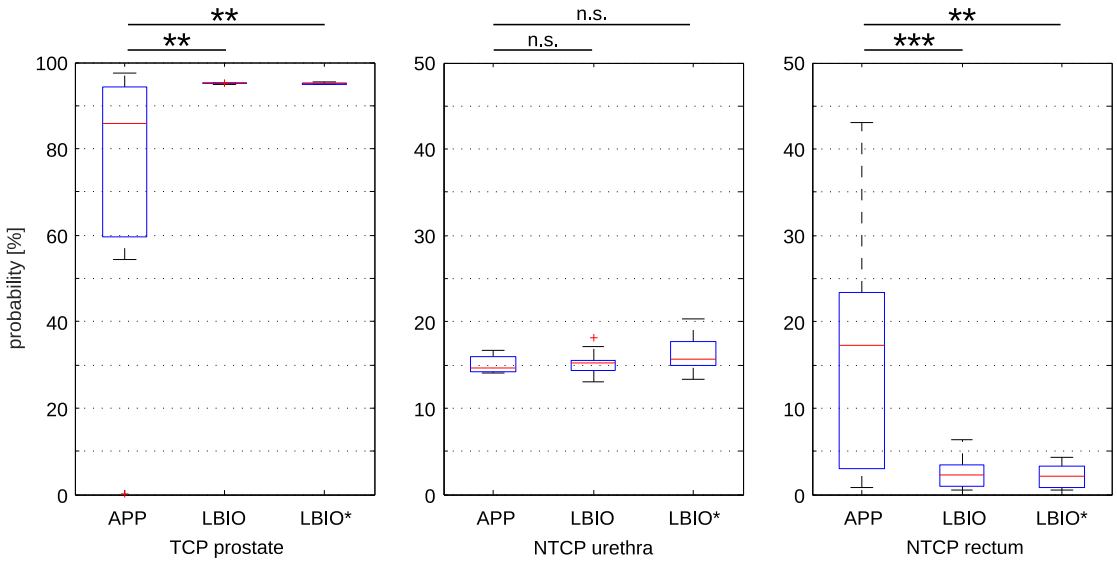

Figure 5.10: Box-and-whisker plots of the TCP and NTCPs for biological based optimization. The different levels of significance are labeled with '$***$' ($p < 0.001$), '$**$' ($p < 0.01$), and 'n.s'. ($p > 0.05$) and tests are performed for APP-LBIO (lower) and APP-LBIO* (upper).

5.2.2 Biological model based objective function

A method which so far has not been evaluated for brachytherapy treatment planning is a biological model based approach. The results of this new method are compared and evaluated against APP. The focus is the performance with respect to the TCP and the NTCPs for urethra and rectum.

LDR

The results of this study are presented in tab. 5.6. The evaluated parameters are optimization time, number of dwell-positions #DP, TCP and NTCPs, as well as COIN and EUD. As a reference, the results are compared against APP. Two different optimization strategies, LBIO and LBIO*, are presented for comparison. LBIO represents the plan with the same needle configuration as APP. LBIO* considers all needles which can potentially be used for implantation. A plan with the same number of needles as APP is generated from this configuration.
A summary of the performance of the different strategies with respect to the obtained biological parameters is presented in fig. 5.10. The CS inspired approaches result in plans that significantly increase the obtained TCP ($p < 0.01$) and decrease the NTCP of the rectum ($p < 0.01$), while at the same time providing a similar biological outcome for the urethra ($p > 0.05$). In addition, EUD and COIN show a significant improvement ($p < 0.05$) with respect to APP. Interestingly, the

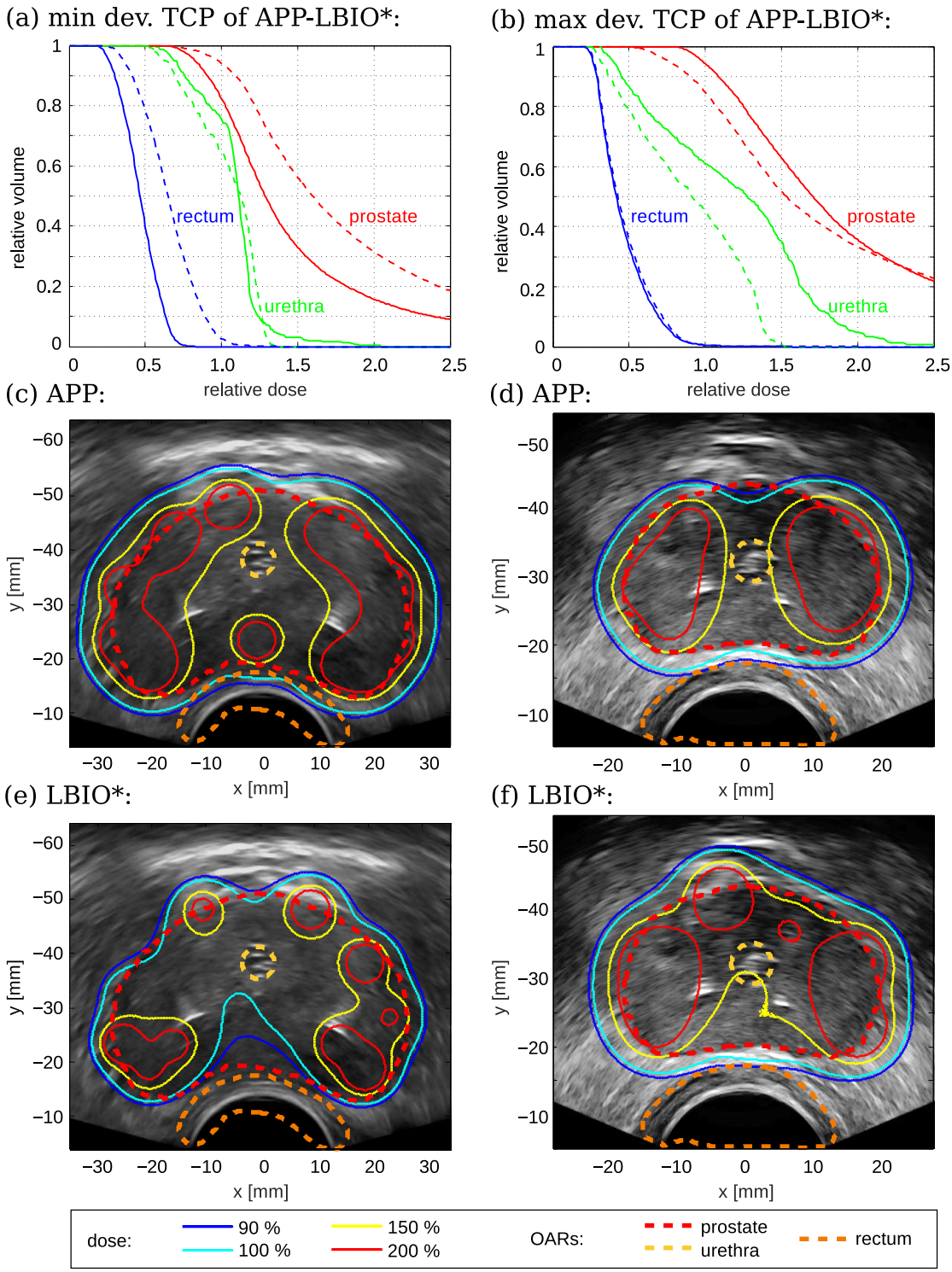

Figure 5.11: Comparison of the different optimization methods for LDR biological based planning. DVHs and isodose lines for the cases with the smallest (a,c,e) and largest (b,d,f) deviation in TCP for APP vs. LBIO* are shown. In addition, the DVHs of reference APP are drawn as dashed lines and the DVHs for LBIO* as solid-lines.

Table 5.6: Comparison of the different optimization algorithms for the LDR biological based optimization.

Algorithm	$\mathcal{Q}(\boldsymbol{x})$	t [s]	#DP	TCP	NTCPU	NTCPR	COIN	EUD
APP (ref)								
μ	2.8	N/A*	43.8	73.7	15.1	16.9	0.57	61.8
σ	2.6	N/A*	10.2	27.6	0.9	14.5	0.04	6.3
min	0.7	N/A*	24	0.1	14.1	0.8	0.47	47.4
max	9.8	N/A*	62	97.6	16.7	43.1	0.61	70.1
LBIO								
μ	0.4	51.5	38.8	95.1	15.2	2.5	0.59	67.2
σ	0.0	18.9	5.5	0.1	1.3	1.6	0.03	0.1
min	0.3	10.5	25	95.0	13.1	0.5	0.53	67.1
max	0.4	73.2	49	95.3	18.2	6.3	0.62	67.4
LBIO*								
μ	0.4	67.8	38.2	95.1	16.3	2.1	0.60	67.3
σ	0.1	30.2	5.1	0.1	1.9	1.4	0.03	0.1
min	0.3	14.7	25	95.0	13.3	0.5	0.55	67.2
max	0.5	109.8	47	95.4	20.3	4.4	0.65	67.5

CS inspired approach incorporating biological model based treatment planning leads to robust plans which show a standard deviation of less than 0.01 for TCP and EUD.
When comparing the number of seeds a significant decrease ($p < 0.01$) when using the CS inspired biological model based strategy is observed. For five patient cases, a reduction of more than 10% is observed. The runtime including needle optimization and using biological models is around one minute. This is the same order of magnitude as state-of-the-art approaches show for conventional DBOF optimization.
DVHs and isodose lines of the patients showing the largest (Patient 4) and smallest (Patient 2) deviation of the TCP compared to APP are depicted in fig. 5.11. For the plan with the smallest deviation (0.7%) the new CS inspired approach saves a total of 15 (31.9%) seeds. For the plan with the largest deviation, the CS approach yields a plan with a total TCP of 95.1% rather than 0.01% of the reference. This is achieved with almost the same number of used seeds, which is 25 (LBIO*) and 24 (APP).

HDR

In order to test the practicability of the biological model based ITP for HDR, the APP is compared against the solution of CS inspired methods optimizing

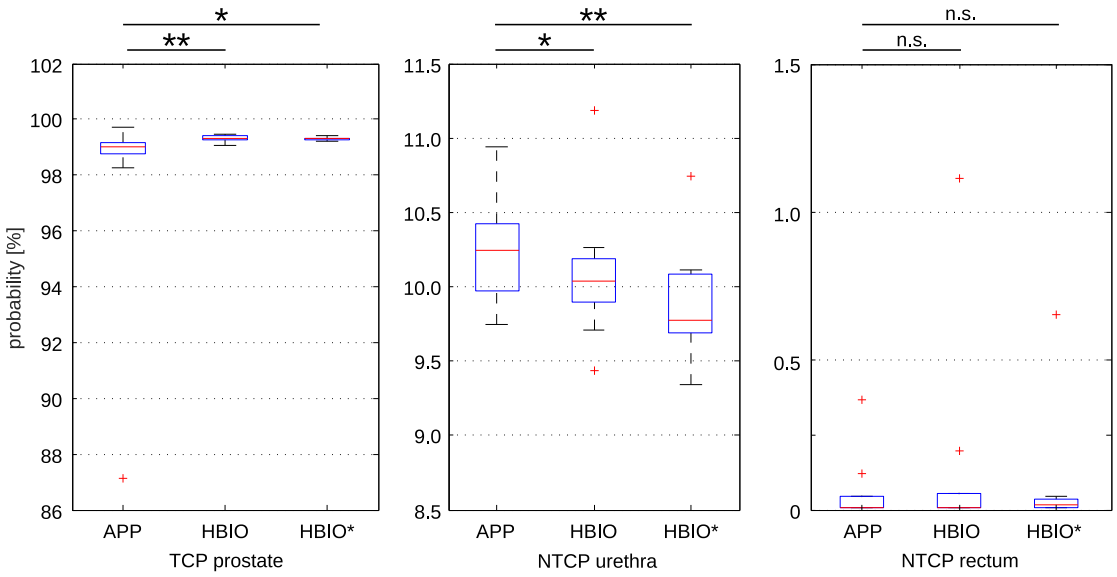

Figure 5.12: Box-and-whisker plots of the TCP and NTCPs for biological based optimization. The different levels of significance are labeled with '$***$' ($p < 0.001$),'$**$' ($p < 0.01$), and 'n.s'. ($p > 0.05$). Tests are performed for APP-HBIO (lower) and APP-HBIO* (upper).

the BBOF. HBIO labels the plan without and HBIO* with needle optimization. The resulting runtime t, number of active dwell-positions $\#DP$, the biological parameters TCP and NTCPs, as well as COIN and EUD are presented in tab. 5.7. In addition, the performance with respect to TCP and the NTCP of urethra and rectum is depicted in fig. 5.12. For both methods, the TCP for rectum significantly increases ($p < 1 \times 10^{-3}$) while the NTCP decreases ($p < 0.05$). More precisely, an increase of the TCP (1.3 ± 3.3, range: $0,3$ to 11.7)% is observed. This is however, accompanied by an increase of the probability of urethral NTCP ($p < 0.001$) of (1.7 ± 2.1, range: $-0,1$ to 5.9)%. Furthermore, a significant increase ($p < 0.01$) of COIN and EUD is recorded.
The resulting DVHs for APP and HBIO for Patient 1 and Patient 4 are depicted in fig. 5.13. Furthermore, the corresponding isodose lines for the transversal central slice of the prostate are shown. Those plans represent the largest and smallest deviation of the resulting TCP.
A maximum runtime of $2005.0\,s$ is observed which is longer than what is currently expected from state-of-the-art optimization strategies without biological optimization. In addition, the new approach yields plans with a significant increase in active dwell-positions ($p < 0.05$).

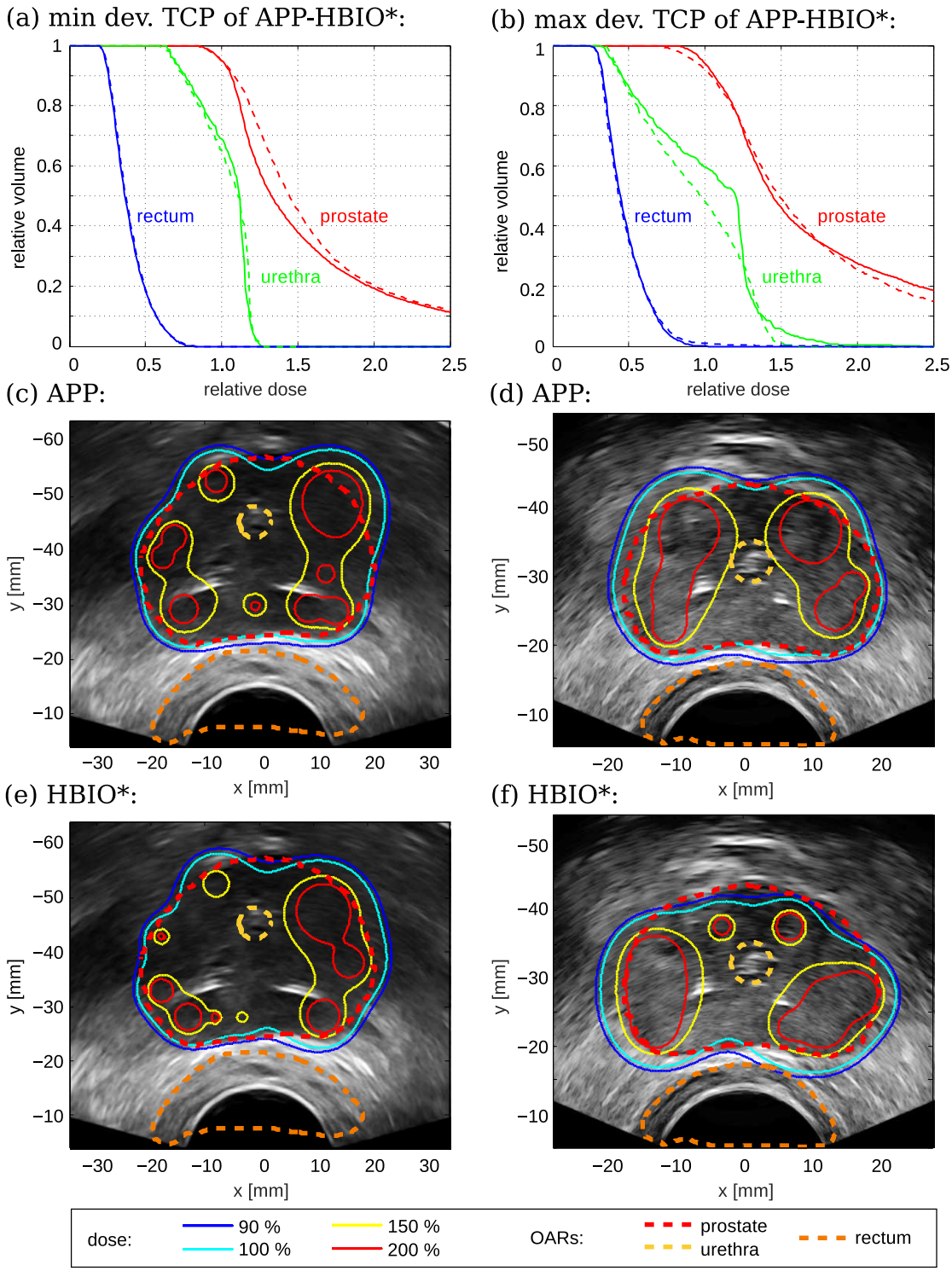

Figure 5.13: Comparison of the different optimization methods for HDR biological based planning. DVHs and isodose lines for the cases with the smallest (a,c,e) and largest (b,d,f) deviation in TCP for APP vs. HBIO* are shown. In addition, the DVHs of reference APP are drawn as dashed lines and the DVHs for HBIO* as solid-lines.

Table 5.7: Comparison of the different optimization algorithms for the HDR biological based optimization.

Algorithm	$Q(x)$	t [s]	#DP	TCP	NTCPU	NTCPR	COIN	EUD
APP (ref)								
μ	3.7	0.9	57.9	98.0	10.2	0.1	0.77	73.3
σ	4.8	0.6	19.6	3.4	0.3	0.1	0.04	3.7
min	1.9	0.1	21	87.1	9.7	0.0	0.65	63.2
max	19.0	2.6	103	99.7	10.9	0.4	0.82	78.5
HBIO								
μ	2.1	28.2	61.5	99.3	10.1	0.1	0.74	75.2
σ	0.2	13.2	20.4	0.1	0.4	0.3	0.05	0.6
min	1.8	5.3	27	99.1	9.4	0.0	0.64	74.0
max	2.6	47.8	107	99.5	11.2	1.1	0.80	76.2
HBIO*								
μ	2.0	918.5	72.0	99.3	9.9	0.1	0.74	75.1
σ	0.2	622.0	20.8	0.1	0.4	0.2	0.04	0.4
min	1.8	106.5	39	99.2	9.3	0.0	0.68	74.6
max	2.4	2005.0	118	99.4	10.7	0.7	0.79	75.9

6 Discussion

The different comparative tests showed that the reformulation of the objective function into a CS equivalent problem is a valid and successful approach. They underlined the advantages of the new methods against the state-of-the-art approach with respect to quality and efficiency.
In the following, the reasons for the gain in performance and the limitations of the demand for sparsity are discussed. A detailed discussion of the clinical relevance and how the new strategies can shorten and simplify the intra-operative planning procedure follows. Further options and application fields regarding the use, advantages, and limitations of the CS inspired optimizers in radiation therapy finishes this section.

6.1 CS inspired solvers in brachytherapy

As demonstrated, the developed optimizers based on greedy heuristics used in CS are able to solve the different ITP problems in brachytherapy.

6.1.1 Performance of the CS inspired solvers

The new approaches lead to a significant acceleration of optimization time while maintaining or even improving the quality in terms of the obtained objective function value. The idea of using CS inspired optimizers to tackle the different MILP problems lead to an increase in performance by orders of magnitude. The speed-up can be explained by the underlying heuristics of the optimizers and the efficient high-performance CPU implementations.
The CS-inspired solvers outperform IPSA (LDR) and HIPO (HDR) due to a reduction in necessary objective function evaluations. The lower number of objective function evaluations is known from the examples in CS where the corresponding strategies belong to the fastest optimization methods [33]. In contrast to the CS solvers, SA is known to require a lot of objective function evaluations in order to reach the global optimum [125].
The comparative test showed that the demand for sparse solution with the additional quality constraint leads to solutions that are near the global optimum of the state-of-the-art ITP problems. This was proven for the different brachytherapy modalities and for different linear objective functions.

6.1.2 Demand of sparsity

The key point of the new strategy is the demand of a sparse representation of dwell-positions. Assuming sparsity, a CS inspired approach is beneficial when compared to the general-purpose heuristic IPSA and HIPO or modern linear programming techniques. As sparse solution have not been used in brachytherapy. Hereby the question arises, whether they are clinically applicable.
Due to the discrete nature of seeds and the fact that only a small amount of all potential seed positions forms the final solution, the concept of sparsity is a valid approach for LDR brachytherapy. This was demonstrated in detail by the obtained results of the different comparative tests.
In HDR therapy, concerns were raised about the applicability of sparse solutions since fewer dwell-positions with longer dwell-times may introduce hot-spots and yield unknown side-effects in their proximity [109]. Consequently, different methods have been introduced which aim the reduction of long dwell-times and thus promote non-sparse solutions [107, 126]. In 2012, Holm et al. showed that the decrease in dwell-positions is enforced by the linearity of the objective function.
Since the linear DBOF is used as a reference, long dwell-times were accepted and the focus was directed to testing whether the sparsity approach can be applied and whether the new methods lead to an improvement with respect to runtime and objective function value.
Interestingly, the introduction of the new dosimetric and biological based objective functions optimized using sparse optimization techniques yields plans which show a significant increase in the number of dwell-positions and a decrease in the maximum dwell-time. At the same time, an increase in performance with respect to runtime was observed when compared to the state-of-the-art techniques. Thus, the CS inspired approach can in general be applied to solve the problem, although the degree of sparsity is comparably low.

6.2 Clinical relevance and potentials of the new approach

A detailed discussion with respect to the clinical relevance and potentials of the newly developed solvers is subdivided into the performance for the LDR and HDR ITP problem.

6.2.1 LDR treatment planning

Two different approaches were considered for LDR treatment planning: The optimization on a well-defined subset of needles and concurrent optimization of needle and seed configuration.

LDR without needle optimization

As initial test, LDR treatment planning with a predefined needle selection was performed. This strategy typcally involves the fine tuning of the seed positions based on an initial needle configuration found automatically using SA or by an experienced physician. Fine-tuning is a trial-and-error method to tailor the plan to the anatomy of the patient. Due to the long calculation time of the state-of-the-art optimizers, this step is usually performed using manual GrO[1], although it is well-known that inverse planning returns favorable plans [32, 127].
The novel strategies outperform the state-of-the-art methods by far. The solutions are near the global optimum and can be obtained in less than $0.4\,ms$. This allows for the first time a real-time inverse optimization based fine-tuning.
The strategies LTA and LOMA perform worse than the state-of-the-art method SA with respect to resulting plan quality for LDR ITP. In contrast, LSUP outperforms SA regarding the returned objective function value. In addition, the deviation from the estimated lower bound was less than 4%. SA shows a maximum deviation of 25% from MILP.
Assuming an appropriate cooling schedule and an unrestricted number of iterations SA is theoretically able to return the global optimum [92]. However, in clinical routine, a compromise between optimization time and plan quality has to be made. Another disadvantage of SA is that the user has to provide an initial estimation of the number of used seeds. This yields more seeds compared to the CS inspired solvers in 60% of the cases. An initial estimation is not needed for solvers LOMA an LSUP.
As a recommendation, LSUP should be chosen to optimize the LDR ITP problem without needle optimization.

LDR including needle optimization

The second comparative test has carried out to determine the performance of the CS inspired approach for LDR ITP including needle optimization.
Due to the computational complexity of the state-of-the-art methods treatment planning including needle optimization is performed prior to fine-tuning, in literature sometimes referred as pre-planning. Since pre-planning restricts the domain of all potential solutions this strategy is more likely to yield suboptimal plans with respect to the final objective function value. This is validated by comparing the performance of APP against the estimated lower bound obtained by MILP.
The CS inspired solvers outperform the state-of-the-art methods in quality and optimization time. The obtained solutions using the problem-specific LSUP and LSPA are near the global optimum and equivalent to MILP. The general-purpose optimizers IPSA are theoretically able to return the global optimum, but they are

[1] An interactive real-time strategy is usually expected by the user.

slow and the compromise between speed and quality limits the final outcome.
In addition, the solution obtained with the sparsity approach leads to a reduction of seeds in all patient cases. This yields a reduction of the V150 and V200 criteria of the prostate and of the received dose to the OARs. Interestingly, this reduction has no negative influence on the V100 criterion, on the contrary, even an increase was observed. A steeper gradient of the DVH of the PTV can be observed. In addition, the high dose regime shows lower DVH values for all patient cases. This is another indication that the CS inspired strategies yield more homogeneous dose distributions with less hot-spots.
Less dose received by the OARs reduces the toxicity and, thus, a reduction in side effects is expected. Hence, plans obtained using the CS inspired optimizers are more likely to be clinically accepted.
When comparing the CS inspired solvers against each other, LSUP and LSPA are recommended for optimization. Both provide a good compromise between obtained plan quality and efficiency. With optimization times of less than $0.5\,s$ LSUP and LSPA are capable of real-time ITP. Since no restriction of the domain is necessary, a decrease in the objective function of up to 20 % between the unrestricted and restricted domain of all potential solutions is observed. This is also reflected by the increase in EUD and COIN. Therefore, the fine-tuning to tailor the plans to the patients needs can be carried out using all available needles.
To conclude, LSUP and LSPA are the only algorithms which allow real-time treatment planning including needle selection for LDR treatment planning.

6.2.2 HDR treatment planning

Since real-time planning for the HDR ITP is possible using the L-BGFS [20], the focus was directed to the development of fast algorithms to tackle the needle optimization problem. HTA, HSIS, and SISA perform fast and return plans that are near the global optimum.
As expected, the CS inspired approaches show that an increased optimization time leads to an improved quality. Out of the discussed algorithms, the only one capable of real-time planning is HTA. For the remaining CS inspired algorithms, the optimization time varies between 0.5 and 9.0 seconds. Compared to HIPO, this is still a statistically significant decrease in optimization time. LSUP and SISA are between 50 and 350 times faster than HIPO. SISA shows the longest runtime of the novel optimizers. However, due to its heuristic, starting with the complete domain of possible solutions and iteratively reducing the number of seeds, the algorithm is able to return several plans in a single run. Hereby, each plan contains the number of needles equal to the maximum needles minus the number of iterations performed. To accelerate the ITP, a solution could be a more efficient sampling of the dose points. This, however, requires further investigation and is beyond the scope of this thesis.

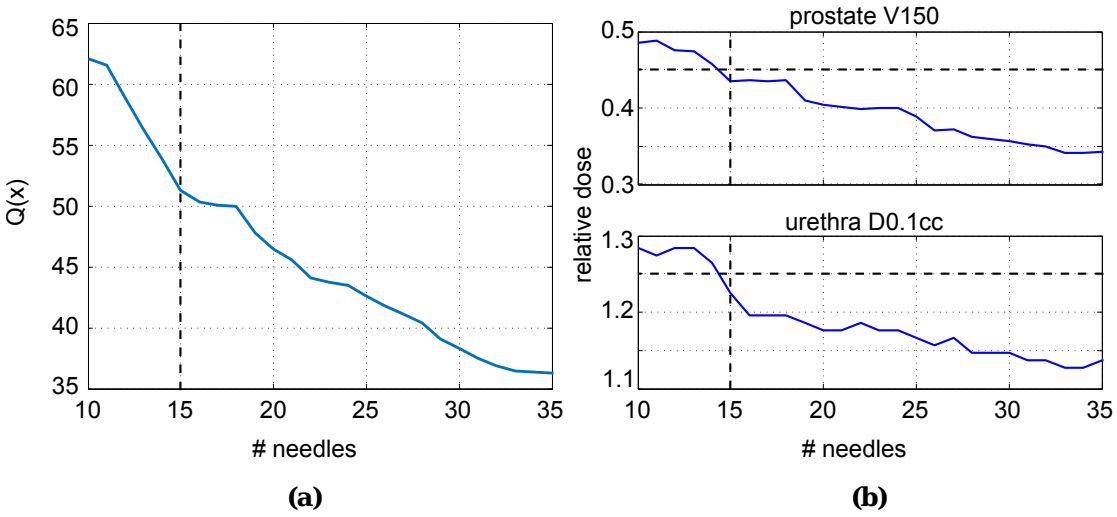

Figure 6.1: Objective function value as a function of used needles provided by SISA (a). The relevant dosimetric criteria which limit the applicability of the plan as a function of used needles (b). The remaining dosimetric criteria are fulfilled.

In fig. 6.1, the resulting DBOF value as a function of used needles and the resulting dosimetric criteria are depicted for a representative patient. For this patient, 15 needles represent a valid compromise between number of needles and dose received by the urethra (D0.1cc) and the prostate (V150), which are the limiting factors for this patient.

When comparing the solution of HTA, HSIS, and SISA against the state-of-the-art optimizers HIPO, they return a qualitatively better solution in five, two, and one of the patient cases, respectively. Thus, it is not guaranteed that the CS inspired strategy performs better than the state-of-the-art method. In general, HIPO would be able to return the global optimum. Since it is, however, based on SA, a compromise between quality and runtime has to be made.
Due to the runtime of HIPO, the needle selection is either completely omitted and done manually using GrO or once at the beginning of the intra-operative planning using a single run of HIPO. After an initial subset of needles is chosen, the plans are re-optimized on this restricted domain. However, the comparative study (sec. 5.1.3) showed that this strategy yields an increase in the returned objective function of up to $(22 \pm 10)\%$. This increase leads to a statistically significant decrease in COIN and EUD and strengthens the observation that ITP is favorable compared to GrO [29].
In terms of quality, the different CS inspired approaches for HDR ITP, SISA seems favorable, although this method is not capable of real-time planning. It provides

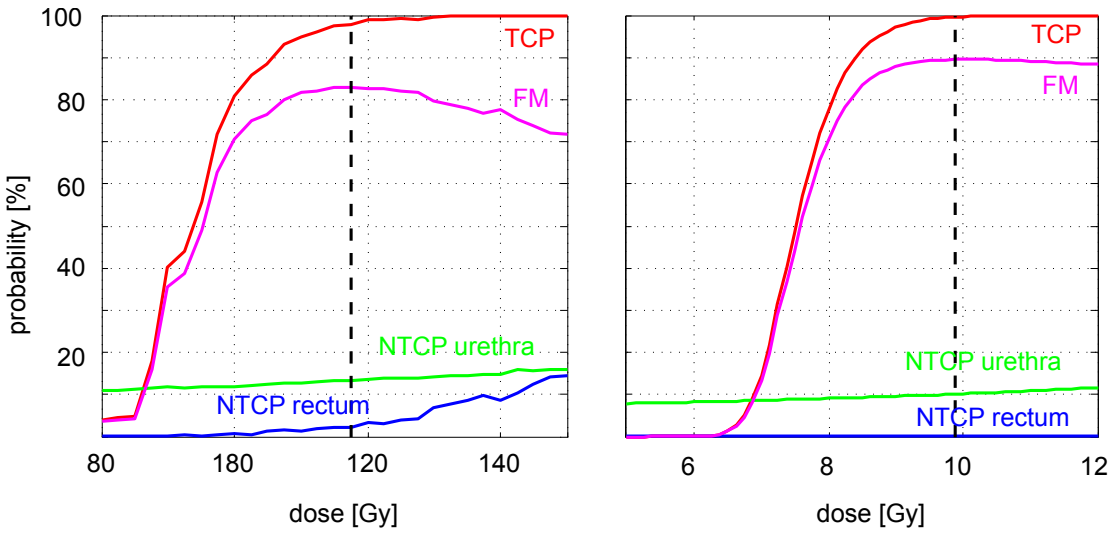

(a) LDR **(b) HDR**

Figure 6.2: Dose response curves for LDR (a) and HDR (b). The TCP, NTCPs and FM are shown for different prescribed doses.

a variety of plans from which the user can choose. This resembles the concept of multiobjective treatment planning but with an immense gain in performance [98, 100].

6.2.3 Towards individualized brachytherapy

The CS inspired algorithms open up possibilities in term of individualized brachytherapy. With state-of-the-art optimizers, the plans are already tailored to the patient specific anatomy. However, due to the trial-and-error procedure, intra-operative planning takes several minutes or, in the worst case, up to an hour. The CS inspired solvers allow for real-time planning and, thus, the fine-tuning of the plans becomes more interactive with immediate feedback to the user. The user is able to directly see the influence of changing parameters, which allows a better steering of the plan quality.
The number of used needles is usually determined by a physician and depends heavily on his or her experience [127]. To guarantee a certain quality of the plan independent of the user, an intra-operative pre-planning step can be considered. Since the CS inspired solvers are able to calculate a variety of plans with variable weightings and numbers of maximally allowable needles in parallel, different plans can be pre-planned in less than one second.
An example to determine an individualized prescribed dose for LDR and HDR planning is illustrated in fig. 6.2. The plan is evaluated according to its biological

consequences (TCP and NTCPs) as a function of the prescribed dose. A plan can be evaluated by the so-called figure of merit (FM) that quantifies to which extend the TCP is maximized while maintaining a certain NTCP. The FM is given by [128]:

$$FM = TCP \cdot \prod_{\nu=1}^{o} (1 - NTCP_\nu), \tag{6.1}$$

where ν is the organ index and o the number of OARs. The figure of merit has a maximum at the ideal prescribed dose. With respect to plans shown in fig. 6.2, an ideal dose prescription is obtained for LDR and HDR, which is approximately $115\,Gy$ and $9\,Gy$, respectively. At constant TCP, less dose can be prescribed to the PTV which simultaneously reduces the dose to the OARs and therefore NTCP.

6.2.4 Dosimetric criteria based objective function

Real-time capable optimizers allow for the introduction of more realistic objective functions. One possibility is to directly optimize the dosimetric criteria, i.e. evaluate the DVHs during each iteration step. In general, a reformulation into MILP is possible but due to the high calculation time not suitable for intra-operative ITP. Nevertheless, this was used as a reference for the obtained plan quality for LDR and HDR dosimetric based planning.
Incorporating the realistic CBOF yields a more intuitive planning. The abstract thresholds and weightings for the DBOF are replaced by dosimetric criteria and weightings. During initial tests, it was determined that for each VOI one weighting factor is sufficient. This decreases the number of parameters for optimization from 16 to 4. One parameter for each of the OARs (prostate, urethra, rectum) and one for the PTV.

LDR

The CBOF based optimization using the standard set of weightings is able to significantly reduce the obtained objective function value.
With optimization times about several milliseconds the new approach outperforms the reference BILP by far and is capable of real-time planning, while the optimization time for BILP is expected to be several days or even up to weeks.

Rating the new technique against BILP by comparing the returned values obtained for the criteria leads to plans that show small deviations in the V100 of the prostate and a clinically relevant reduction in the V150. For urethra, the obtained results for the criteria are similar with no clinically relevant difference.
A significant increase of the criteria of the rectum was observed for the method without needle optimization (LCB). Allowing the complete domain of all solutions

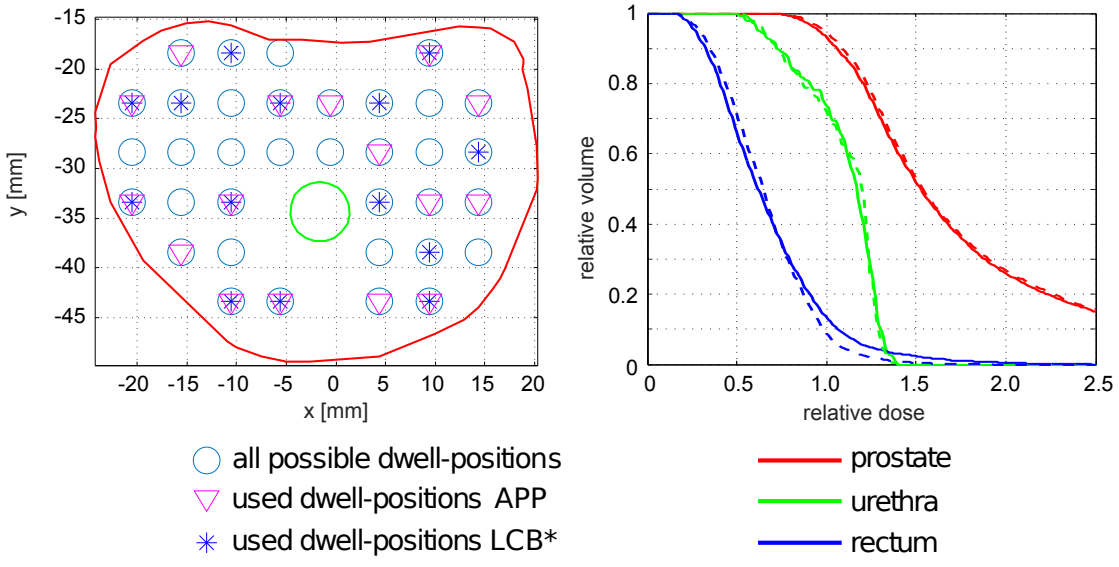

(a) needle positions **(b) DVH**

Figure 6.3: The final needle configuration for APP and LCB* (a) and the resulting DVHs (b). The DVHs of references APP are shown as dashed lines and the DVHs of LCB* are drawn as solid-lines. With LCB* a total of two needles can be spared.

(LCB*), those criteria can significantly be decreased. This indicates the advantage of ITP including needle optimization, in contrast to a fixed subset of needles.
When compared to APP, the DVHs of LCB and LCB* showed a steeper gradient and less dose in the high dose regime for the PTV. This leads to less hot-spots inside the prostate. In addition, the dose for the urethra is almost equivalent to the dose of APP.
In order to get individualized patient plans, the maximum number of needles should not be constrained during treatment planning. It is recommended that the user defines a certain range of the number of used needles and performs a fine-tuning according to the patients anatomy. Afterwards, a compromise between the number of used needles and the obtained quality can be chosen. With this strategy, unexperienced users are able to provide plans that fulfill all dosimetric criteria. In nine cases a solution with less needles were found. To demonstrate this potential such a representative case is shown in fig. 6.3.
Due to the heuristic of the CS inspired solvers for LDR ITP, many optimization problems have to be solved to obtain the solutions for different numbers of needles. Nevertheless, multi-threading on modern CPUs to calculate different plans in parallel allows real-time planning.
To conclude, the CS inspired method can also be used to solve the more realistic

CBOF in real-time. In addition, this method helps the user to generate and fine-tune the treatment plan.

HDR

The CS inspired approaches HSIS and SISA can also be used for dosimetric criteria based optimization. The returned objective function values are near the global optimum obtained by MILP. IPIP, the only existing approach that is able to generate valid plans in reasonable time, is outperformed by far by the CS inspired approaches. This can be explained by the fairly simple greediness and the relaxations used by the IPIP method [31].
Using the CS inspired solver to optimize the CBOF leads to plans that show a small deviation in the V100 criterion. For the remaining criteria of the prostate, no clinically relevant deviation was observed. The same accounts for the urethra, with a small advantage of the CS inspired optimization strategy that yields to a decrease of the dosimetric criteria. For the rectum, a deviation between the APP and the CBOF plans was observed. This indicates that the dosimetric criteria are not perfectly described by the DBOF, which also has been repeatedly discussed in literature [31, 26].
When comparing the DVHs, a reduction of the delivered dose to OARs was observed in all patient cases. In addition, a steeper gradient and less dose in the high dose regime of the prostate was observed, reducing the risk of side effects. The presented approach inherently avoids hot-spots without the need of additional constraints. This is contrary to the state-of-the-art approaches [107, 126].
The combination of the CS inspired solvers with the ability to solve the dosimetric criteria based problem leads to new possibilities in intra-operative treatment planning. Due to the underlying strategy SISA, the user can perform the fine-tuning on different needle configurations simultaneously. After the ITP, the plan with the best dosimetric outcome can be selected. Using less needles leads to a decrease in side effects linked to the trauma caused by the injection of needles. Especially erectile dysfunction is directly linked to this [129, 106].
With the discussed strategy, even an unexperienced user is able to generate treatment plans that fulfill the dosimetric criteria. In all ten patient cases, the obtained plans contained less needles than for APP. An example showing a plan where a total of four needles (25%) was saved is shown in fig. 6.4. The planning time was less than two minutes.
The CBOF based planning is an alternative which has the potential to replace the current state-of-the-art planning procedures.

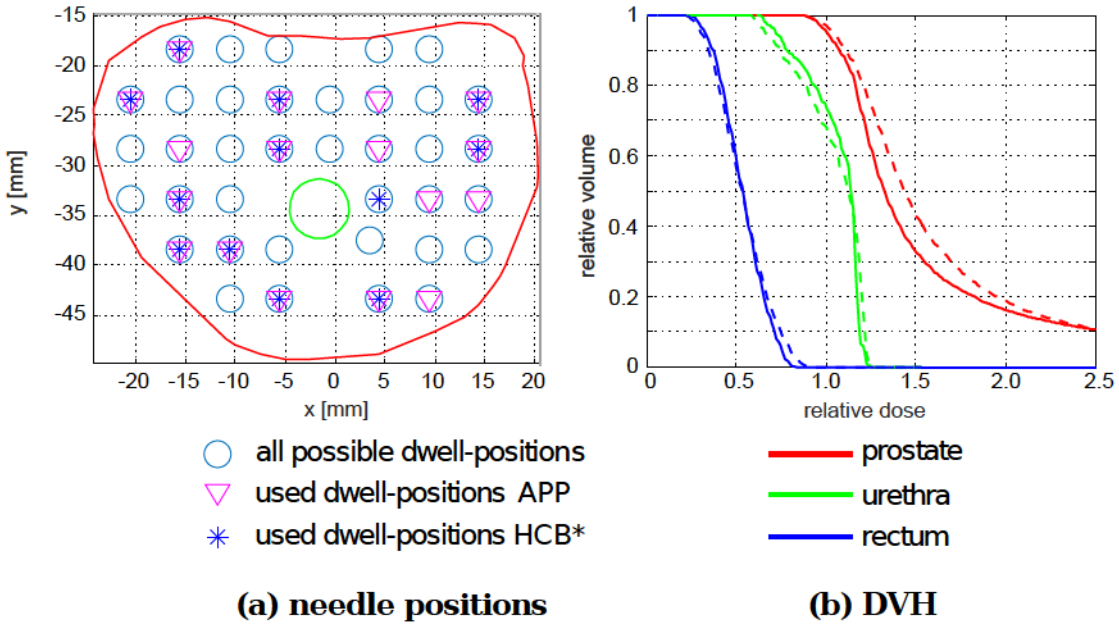

(a) needle positions **(b) DVH**

Figure 6.4: The final needle configuration for APP and HCB* (a) and the resulting DVHs (b). The DVHs of references APP are shown as dashed lines and the DVHs of HCB* are drawn as solid-lines. With HCB* a total of four needles can be spared.

6.2.5 Biological based objective function

Biological treatment planning is an important step towards more realistic objective functions. Up to now, only the evaluation of biological models is used for reporting or, in the case of retrospective studies, for comparing different treatment modalities [130, 131, 132, 61]. Since the evaluation of the objective function is too time consuming, biological optimization is not possible using the state-of-the-art optimizer.
The new class of CS inspired solvers can cope with more complex objective functions and allows for the first time biological optimization for brachytherapy. The runtime varies from a maximum of one minute for LDR and HDR without needle optimization to 15 minutes for HDR including needle optimization.
All calculations of biological parameters are performed using the standard set (e.g. parameters for the radiosensitivity of tissue) as recommended by the AAPM, which are summarized in tab. A.6. It is important to note that these are only recommendations and should not be taken as *the* biological parameters for the individual patient [10].
The expected biological outcome, based on the recommended parameters, is discussed in the following.

LDR

The biological treatment planning using the CS inspired optimizers generates plans with a TCP of $(95.0 \pm 0.1)\%$. When compared to APP with a TCP of $(73.7 \pm 10.9)\%$, which is the equivalent to the values found in literature [10], the new strategies improve the outcome of the treatment. At the same time the expected complication probability of the rectum was reduced from 17% to only 2%. The expected urethral complications do not show a clinically relevant difference. When rating the plans using DVHs and dosimetric criteria may lead to wrong decisions. For example, the plans showing the smallest deviation with respect to TCP show the largest regarding the V100 criterion. The biologically optimized plan returned a V100 of 84.1% and, thus, this criterion was not fulfilled and the plan would have never been clinically accepted. However, when considering the EUD (APP: $67.7\,Gy$ and LBIO*: $67.2\,Gy$) both plans are equivalent with respect to TCP. In addition, the biological optimized plans lead to a significant reduction of the NTCP of the rectum. Despite the worse biological rating regarding TCP, the plan was accepted for treatment.
The drawbacks of the discussed biological model is the assumption of a uniform distribution of the tumor cells within the prostate. However, there is anatomic variability in prostate cancer distribution within the gland [133]. Having the possibility to identify those regions inside the prostate would allow a more accurate calculation of the TCP. A solution might be to divide the prostate into sectors and, afterwards, assign tumor cell densities. These densities can be obtained using functional imaging such as magnetic resonance spectroscopy or single photon emission computed tomography [10].
Treatment planning with BBOF is an approach which yields robust plans with respect to TCP and NTCP. This was achieved without the need for adapting the initial parameters. The optimization time of about one minute is acceptable as long as a manual re-planning is not required. With more efficient biological models and parallelization of the algorithm for example using multi-threading or an efficient GPU implementation real-time ITP with clinically relevant biological models is in reach.

HDR

For HDR, ITP with the BBOF returns plans with small deviations in TCP and NTCP. When compared to APP, the differences are clinically not relevant in nine patient cases. Only for one patient an increase in TCP by 12.1 % was observed. The DVHs showed no clinically relevant differences for the PTV, rectum and urethra.
A benefit of biological based treatment planning is, that the prescription of a plan only contains the values for TCP, NTCPs, and a fractionation scheme. The dose

delivered to the PTV is calculated automatically. When rating the plans according to the biological parameters a re-optimization does not seem to be necessary. This simplifies the planning procedure for an unexperienced user. Two different plans for three and two fractions were obtained by an unexperienced user in less than two minutes.
A runtime of the optimizer for a fixed needle configuration of about 30 seconds is applicable for intra-operative ITP. The optimization time including needle selection of several minutes is not acceptable. However, an efficient multi-threading or a GPU implementation may yield optimization times not longer than a few seconds.

6.3 Potential and limitations

The CS inspired approach yields plans which are equivalent or better than those obtained with the state-of-the-art methods. In the following, the potential and limitations to further improve brachytherapy treatments as well as the potential with respect to radiation therapy are discussed.

6.3.1 Real-time guidance

Several benefits regarding the improvement of the intra-operative ITP using the novel approach have been proposed already.
Next to optimization, a major limitation of brachytherapy is the unavoidable inaccuracy in needle and seed placement in the prostate during insertion and implantation. Needle movement and seed migration is a problem which has been previously discussed in literature [48, 134, 135, 136]. This leads to partially severe differences between intra-operatively planned and delivered dose distributions and may cause degradation of the final outcome [137, 138, 139].
To overcome these limitations, the state-of-the-art approach is to identify the trajectory of the needles via computed tomography or ultra sound images and perform a re-planning after all needles have been injected. This is equivalent to treatment planning with a restricted domain of the solutions and may yield sub-optimal plans.
The proposed solution based on the new CS inspired optimization techniques would allow to automatically identify a potential displacement and perform a real-time re-planning during the insertion of the needle or during the implantation of the seeds. As a feedback, the expected influence of the displacement and the possible solution in terms of an update of dwell-positions and dwell-times can be intermediately provided to the user.
The discussed interactive periodical re-planning ensures the best possible plan and related outcome of the treatment.

6.3.2 Dose calculation

The major limitation in ITP is the dose calculation itself. The developed ITP system is based on the dose calculation recommended by AAPM's TG-43 which is currently the worldwide standard [58]. Even though this method is fast, it is well-known that the dose can vary by as much as a factor of ten [1]. Especially for the CS inspired approach with the tendency to select less dwell-positions this may lead to severe changes in the clinical performance of the plan.
Deviations are based on the TG-43 approach, whereby the lookup-tables to calculate the dose distribution are obtained using measurements of a single seed placed inside a homogeneous water phantom. A valid dose estimation can only be obtained for this particular setting.
To improve the ITP system, more reliable dose calculation methods considering the influence of heterogeneities of tissue and the contribution of scatter-dose, i.e. dose contributed by secondary photons, have to be incorporated. Another aspect is the attenuation between the different seeds, in literature called interseed effect. This may yield discrepancies of up to 18 % [140].
Heterogeneity correction can be applied using the 1D "effective path length" [141, 142] or more sophisticated analytical dose calculation algorithms [143, 144]. Those methods are able to account for heterogeneities including the interseed effect but are unable to describe the scatter-dose. Model-based approaches such as collapsed-cone superposition, deterministic solutions of the linear Boltzmann transport equation, or Monte Carlo simulations have to be used to simulate scattering [145, 146, 147].
For the developed ITP system the discussed strategies for more realistic models can be implemented without any restrictions, since the dose dictionary can be calculated prior to ITP. With modern GPU based Monte Carlo algorithms the dictionary can be generated in a couple of seconds which is acceptable for intra-operative planning. However, when considering the interseed effect the dictionary has to be updated during each iteration step. Even with the mentioned GPU based algorithms this adds too much time to the planning procedure and hence further modifications are necessary.

6.3.3 Applications in radiotherapy

The reformulation into a CS inspired problem and the development of new algorithms tailored to the structure of ITP yields real-time solvers for brachytherapy. Together with more realistic objective functions, dose calculation engines, and tracking devices this broadens the spectrum of brachytherapeutic approaches. In future more difficult settings such as recurrences of rectal carcinoma, spinal metastasis, head and neck tumors, and metastatic sites in patients with oligometastatic diseases could be treated with brachytherapy [148, 149, 150, 151].

Furthermore, it was shown empirically that as long as a certain sparsity of the solution can be assumed and the structure of the objective function remains linear, the novel solvers can be used to optimize different ITP objectives. The question remains whether a sparse solution can be assumed for other radiation therapy modalities and if these can be optimized using linear objective functions.

External beam Radiation Therapy

In external beam radiation therapy, intensity modulated radiation therapy is a modality that is able to deliver complex shaped dose distributions to the tumor. This is achieved by forming different intensity modulated beams and irradiating the target with multiple beams from different directions.
While first approaches assumed a high number of coplanar beams [152, 153], recent strategies promote sparse beam representations as a further increase in the number of beams does not lead to a clinically relevant improvement. A maximum number of ten intensity modulated beams was found to be sufficient [113, 114, 115].
For intensity modulated radiation therapy, there are varieties of different linear, nonlinear, and quadratic objective functions that can be considered for optimization. However, it was shown that a linear approximation of those leads to satisfactory results [154, 155]. Thus, both criteria that allow the use of the newly developed optimizers are fulfilled.
There are two different optimization strategies, direct aperture and beamlet-based optimization [156, 157, 158, 159]. According to Kim et al., the latter yields an optimization problem given by:

$$x^* = \arg\min \|\boldsymbol{W} \cdot \boldsymbol{x}\|_1 + \sum_{\nu=1}^{o} \lambda_i \|\boldsymbol{D} \cdot \boldsymbol{x} - \boldsymbol{t}\|_2^2, \tag{6.2}$$

where $\boldsymbol{x}$ is the beamlet-intensity map, $\boldsymbol{W}$ is a difference matrix, λ is a Lagrange multiplier, and $\boldsymbol{D}$ is the dose dictionary, $\boldsymbol{t}$ a dose threshold, and ν the organ index with the total number of organs o [160].
Although eq. (6.2) can be optimized using standard CS optimizers, there is a need for fast and robust solvers that address the specific issues of intensity modulated radiation therapy [160].
When comparing the formulation of (6.2) with P5, the intensity modulated radiation therapy problem is equivalent to the unconstrained HDR ITP problem. A solution for the intensity modulated radiation therapy problem could be to decouple the angle from the intensity-map optimization, which would enable the use of the introduced greedy optimizers HSIS and SISA.
The CS inspired approach can be used for the different intensity modulated modalities independent of the used particles, such as photon, proton [161], and electron

[162]. The newer technique of volumetric-modulated arc therapy cannot be performed using a sparsity approach. Instead of a step-and-shoot strategy (intensity modulated therapy) the concept of volumetric-modulated arc therapy is a continuous gantry movement [163] and, thus, a sparse angle representation of beamlets is not given.
Another strategy is the combination of external beam radiation therapy with a brachytherapy boost inside the PTV [164]. Up to now, the commercially available planning system Oncentra does not support a treatment planning for such a combined therapy [30]. Using sparse reconstruction techniques for external beam radiation therapy and brachytherapy, the developed planning system could overcome this limitation.

Intra-operative radiation therapy

A new development at the University Medical Center Mannheim, which is not yet in clinical practice, is intra-operative radiation therapy for unresectable glioblastoma. The strategy is an initial cytoreductive therapy following after a stereotactic biopsy.
The used intra-operative radiation therapy system is the Intrabeam PRS 500 System (Carl Zeiss Meditec AG, Oberkochen, Germany) for interstitial and intracavitary radiotherapy. It consists of a miniature low-energy X-ray generator $(30-50)\,kV$ with a $10\,cm$ long and $0,3\,cm$ wide drift tube emitting nearly isotropically radiation (with dose rates of $(1-2)\,Gy/min$) from its tip.
The intrabeam system is fixed onto a modified stereotactic system, which allows a stepping motion of the source along a pre-defined trajectory. The treatment goal is to deliver a sterilizing single dose of $(25-30)\,Gy$ to the tumor and to spare the OARs as much as possible. This should be achieved with sparse representation of dwell-positions, since the number of manual adjustments of the dwell-positions should be maintained as small as possible to minimize the overall treatment time. Hence, the optimization problem is equivalent to problem P3 and can be tackled with SISA. The initial results (fig. 6.5) show a good coverage of the tumor and an efficient sparing of the OARs.

Gamma knife stereotactic radio-surgery

The gamma knife stereotactic radio-surgery unit can be used for the treatment of malformations of the head. It is used for trigeminal neuralgia, arteriovenous malformations, benign tumors, and brain metastases [165].
The system, which is available at the University Medical Center Mannheim, is the Leksell Gamma Knife Icon, Elekta AB, Sweden. The system consists of 192 ^{60}Co sources that are divided into eight sectors. Each of the sectors can be controlled independently using collimators with an aperture sizes of $4\,mm$, $8\,mm$, and $16\,mm$

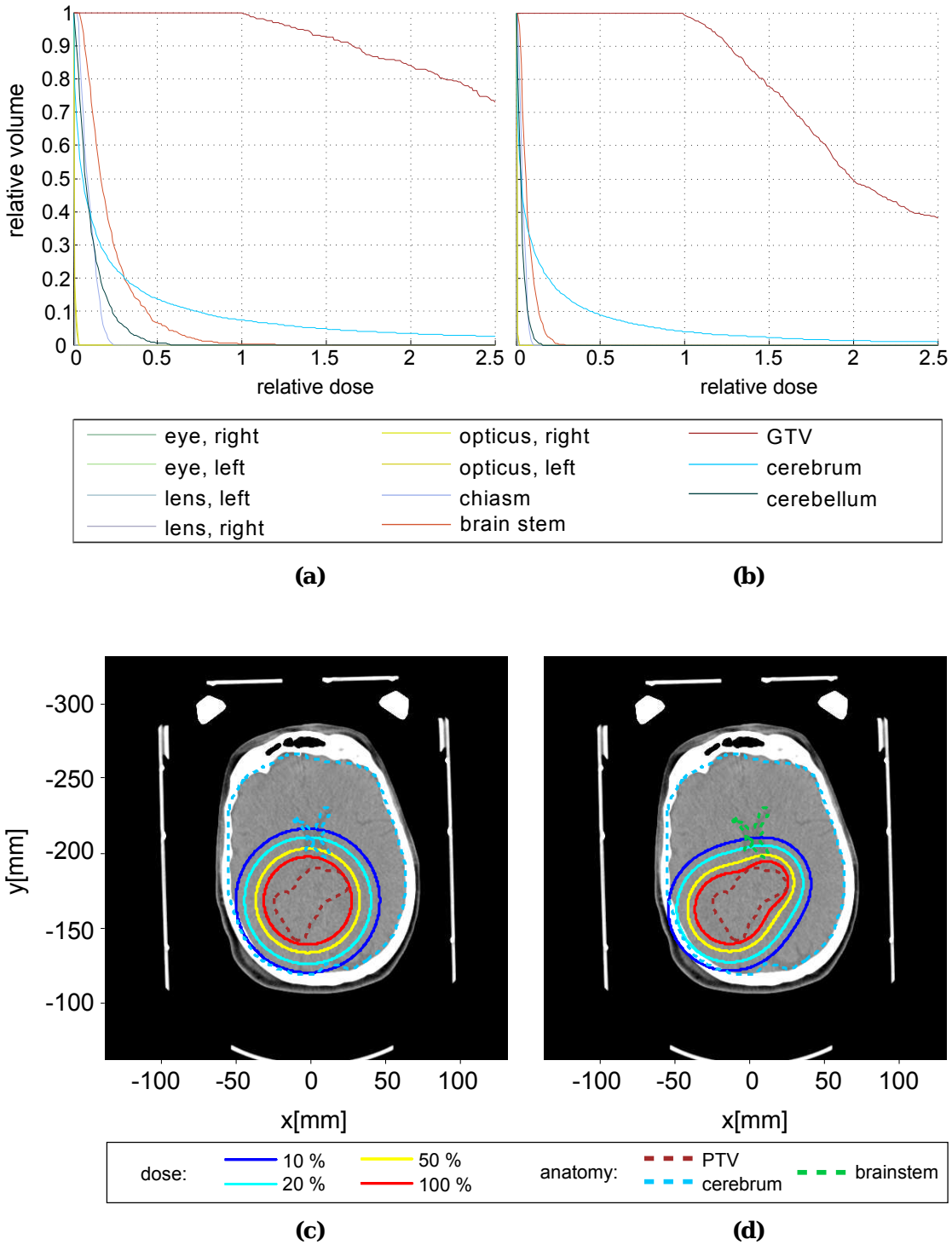

Figure 6.5: Two plans for an intra-operative radiation therapy for an unresectable glioblastoma. The conventional approach (a,c) with source placed in the center of mass of the tumor. In addition, (b,d) shows the novel approach using a stepping source. The DVHs are shown in (a,b) and the isodose lines in (c,d). Due to the high dose of the brain stem only the right plan is clinically acceptable.

[165]. This allows a very precise focusing of the beams and an irradiation of small lesions.
Treatment planning ranges from trial-and-error manual methods to inverse planning based on nonlinear programming, genetic algorithms, SA, LP and formulations as MILP [166, 167]. Due to the large search space, a sparse solution is promoted by manual restrictions of the domain of potential configurations.
Taking the demand of sparsity and a linear objective function into account, the Gamma Knife ITP can be formulated as a problem which is equivalent to that of CS. Thus, the developed optimizers can be used to tackle this problem, too.

7 Summary and Outlook

Brachytherapy has its well established niche in radiation therapy. Especially for prostate carcinoma, diagnosed as a local disease, brachytherapy offers a 90 % chance of relapse-free survival [168]. ITP tools strive to cover the tumor region with at least the prescribed dose while minimizing dose to healthy tissue. However, the state-of-the-art optimizers for the ITP problem are often very slow and abstract thresholds and weights of the used objective functions do not allow an intuitive planning process [31, 29].
Thus, manual forward planning methods such as GrO, where the user gets an feedback intermediately, are preferred in clinical routine. However, this trial-and-error based procedure is known to produce plans which are worse than those generated with ITP optimizers such as IPSA and HIPO.

Consequently, there was a strong need for new optimization strategies that allow real-time planning, whereby the user can interactively tailor the plan to the patient's anatomy. In addition, more realistic objective functions would allow a more intuitive steering of the planning procedure.
The state-of-the-art optimization strategies are based on general class solutions which can be used for a variety of different optimization problems without modification. However, it is often observed that problem specific heuristics which are tailored to the underlying structure can outperform the standard approaches by far.

By analyzing the LDR and HDR ITP problem it was observed that only a small number of all potential seed positions contribute to the final solution. Mathematically speaking, the solution is sparse. Sparsity optimization is addressed by the theory of CS and can be tackled using different strategies. Among these, the greedy inspired pursuit algorithms are in general considered to be one of the fastest. The research question was whether it is possible to reformulate the ITP problem into an optimization problem that is equivalent to that in CS and whether this leads to a comparable gain in performance as observed in CS.
Therefore, the ITP problem using the state-of-the-art objective function was reformulated to mathematically match CS type. This was done for the different treatment modalities LDR and HDR, as well as for the ITP problems with and without needle optimization.
However, the state-of-the-art CS solvers cannot be used to optimize ITP problems

for two reasons. Firstly, there exist restrictions in the domain of all potentials solutions, where the solution vector is binary for LDR and nonnegative for HDR. Secondly, the ITP objective function cannot be handled by the state-of-the-art implementations.
To overcome this limitations multiple solvers to tackle the different ITP problemens in brachytherapy were developed. Each solver has its own advantage either in quality or in runtime.
It is assumed that all objective functions that are of the same structure as the DBOF can be used with the newly developed CS inspired algorithms as well. Based on this assumption two more realistic and more intuitive objective function addressing dosimetric and biological optimization have been developed.

To be able to compare the newly developed methods against each other and against the state-of-the-art methods, a treatment planning system was developed. The system includes a full DICOM interface and incorporates the different optimizers such as IPSA, HIPO, and CPLEX. The dose-calculation is based on the worldwide standard recommended by TG-43. The system can either be used script-based to perform automated comparative tests on a large cohort of patient data or with a GUI. The program has been implemented in Matlab using an object oriented programming strategy and uses MEX files as an interface for C++ subroutines.

The study showed that the developed CS inspired solvers by far outperform the state-of-the-art methods in terms of returned objective function value and runtime.
For LDR without needle optimization, the LSUP algorithm represents an excellent compromise between runtime and quality. In detail, it is up to 330 times faster than state-of-the-art strategies and, at the same time, provides solutions that are equivalent to the estimated global optimum. Considering treatment planning including needle optimization, the algorithms LSUP and LSPA performed comparable. Both showed advantages either in speed or in complexity. Since both did not differ significantly from the estimated lower bound given by MILP, LSUP which has a small advantage in runtime, and is hence recommended for the LDR ITP. The optimization time lies between $0.03\,s$ and $0.24\,s$ and underlines the capability of real time-planning for LDR brachytherapy.

For HDR, the returned solutions from the solvers HSIS and SISA do not differ significantly from the estimated lower bound obtained using MILP. Compared to the state-of-the-art method HIPO, the CS inspired solvers HSIS and SISA were up to 300 and 132 times faster, respectively. The optimization time is abot $1\,s$ for HSIS and $4\,s$ for SISA, which makes both capable of intra-operative treatment planning. Due to its underlying heuristic is SISA able to provide multiple plans

with different numbers of used needles per single execution of the optimizer.
With respect to the state-of-the-art methods, the newly developed CS based optimizers yield a significant improvement of the objective function value. The returned values are near the global optimum for the different approaches. In general IPSA and HIPO can return the global optimum too. However, in clinical routine, a compromise between quality and optimization time is chosen, which explains the observed difference.

The newly introduced dosimetric and biological based objective functions showed the potential to improve the ITP procedure in future. For dosimetric based planning a more realistic objective function and the reduction from 16 to 4 parameters lead to a more intuitive fine-tuning of the plans and thus simplifies the planning procedure. With optimization times of less than $0.55\,s$ for LDR and $5.7\,s$ for HDR including needle optimization, the new objective function outperforms the DBOF in terms of runtime. The BBOF optimization leads to plans with a TCP for LDR of $95.1\,\%$ and HDR of $99.3\,\%$. Especially for LDR, this is a significant increase in the TCP compared to the state-of-the-art methods. While the NTCPs are almost the same for HDR, a significant decrease in the NTCP of the rectum was observed for LDR. However, due to the calculation times of several seconds up to minutes biological planning cannot be used for intra-operative ITP. Nevertheless, ITP with clinically relevant dose models is in reach.

The CS based ITP is a promising approach. As expected, a huge gain in performance was observed. The sparsity strategy allows real-time treatment planning. The different comparative tests showed that LSuP and SISA have the potential to become the gold standard in optimization strategies for LDR and HDR ITP in the near future.
The new strategies simplify the planning procedure and allow interactive ITP. Even unexperienced users are able to generate clinically acceptable plans within less than two minutes. In addition, these plans reduce the number of used needles which shortens the intervention time and decreases the risk of trauma induced side-effects.

Another aspect of real-time planning is that automated intra-operative re-planning is possible. Using high precision tracking devices, a potential misplacement of needles and seeds could be detected and corrected by re-running the optimization. However, this relies on high-precision tracking devices which have to be implemented into the clinical routine. A first prototype was developed in parallel to this thesis and will be presented in future.
Besides the benefits achieved in the planning process, there is still a need for further improvement. The most critical point is the dose calculation based on water-equivalent look-up tables which leads to a known deviation by a factor of

up to ten. Since the sparsity approach gives plans that are proven to reduce seeds and needles an accurate dose calculation is inevitable. A solution might be to use more realistic dose models. Currently, these are computationally too expensive and the system would loose the real-time capability. Thus, there is a strong need for the development of fast and efficient dose calculation routines.
The novel ITP system in combination with the improvement in tracking devices and more realistic dose calculation allow for more individualized brachytherapy treatment with an increase in tumor control and a reduction of side-effects. In addition, this might allow the treatment of the recurrences of rectal carcinoma, spinal metastasis, head and neck tumors, and metastatic sites in patients with oligometastatic disease.
In general, CS inspired solvers have the potential to be used for many different radiation therapy modalities. This requires that a plan is formed using a sparse representation of elements of the dose-dictionary and that the used objective function can be reformulated or approximated using linear or partially linear functions. When analyzing the different modalities, the concept can be applied to intensity modulated radiation therapy, gamma knife stereotactic surgeries, and intra-operative radiation therapy, as well as combinations thereof.

Summing up, sparse solution with optimization strategies inspired by CS is a new paradigm in medical physics. It has the potential to speed-up and improve the planning for the different radiation therapy modalities in future. Both, patients and clinics will benefit from these novel approaches.

A Parameters and Settings

Table A.1: The physical properties of radionuclides used in brachytherapy. The data have been taken from the National Nuclear Data Center [169]. Electrons from β^- decay are absorbed by the core of the capsule [59].

	I-125	PD-103	Ir-192	Cs-137	Co-60
Half-life [d]	59.4	17.0	73.8	30.1	1924.9
Decay	-	-	β^-(95.1 %)	β^-(100 %)	β^-(100 %)
	EC (100 %)	EC (100 %)	EC (4.9 %)	-	-
x-ray energy $[keV]$	28	21	350	613	1253
β^- energy $[keV]$	-	-	181	188	87

Table A.2: Summary of the performed patient study. $V_{Prostate}$ is the volume of the, S_k is the referenced air kerma strength of the used sources $U = 1\,\mu Gy\,m^2/h$ for the different modalities and D_{Rx} is the prescribed dose.

Patient	$V_{Prostate}$ $[cm^3]$	LDR S_k $[U]$	D_{Rx} [Gy]	HDR S_k $[U]$	D_{Rx} [Gy]
1	52.7	0.75	120	4.03×10^4	10.5
2	77.0	0.75	140	4.03×10^4	10.5
3	54.3	0.75	140	4.03×10^4	10.5
4	43.0	0.75	120	4.03×10^4	10.5
5	62.6	0.75	120	4.03×10^4	10.5
6	46.3	0.75	120	4.03×10^4	10.5
7	62.1	0.75	140	4.03×10^4	10.5
8	56.5	0.75	120	4.03×10^4	10.5
9	51.7	0.75	120	4.03×10^4	10.5
10	52.9	0.75	120	4.03×10^4	10.5

Table A.3: Recommended dosimetric criteria for LDR and HDR interstitial brachyhterapy [60, 10]. To distinguish between the dosimetric criteria for urethra and rectum they are labeled with 'U' and 'R', respectively.

Modality	Organ	Criteria	Constraint (%)
LDR	Prostate	V100	>95
		V150	<50
	Urethra	UD10	<150
		UD30	<130
	Rectum	RD0.1cc	<150
		RD2.1cc	<100
HDR	Prostate	V100	>90
		V150	<45
		V200	<20
	Urethra	UD0.1cc	<130
		UD1.0cc	<120
	Rectum	RD0.1cc	<110
		RD02.0cc	<110

Table A.4: Prescribed dose (D_{Rx}) and fraction scheme for the different brachytherapy modalities and used radionuclides [60, 10].

Modality	Radionuclide	permanent	fractions	$D_{Rx}[Gy]$
LDR	I-125	x	-	145.0
	PD-103	x	-	125.0
	CS-131	x	-	131.0
HDR	Ir-192/Co-60	-	3	10.5
	Ir-192/Co-60	-	4	8.5-9.5
	Ir-192/Co-60	-	6	4.0-6.0

Table A.5: Parameters of the DBOF for LDR and HDR treatment planning[29].

Modality	Organ	min Dose (%)	Weight	max Dose (%)	Weight
LDR	PTV (surface)	100	100	150	10
	PTV (surface)	100	100	150	10
	PTV (volume)	100	100	150	5
	Urethra (surface)	-	-	67	5
	Rectum (surface)	-	-	50	5
HDR	PTV (volume)	100	100	200	10
	Urethra (surface)	-	-	125	5
	Rectum (surface)	-	-	83	5

Table A.6: Biological parameters used to calculate TCP and NTCP according to [10, 65, 66]. The complication probabilities of urethra and rectum are labeled with NTCPU and NTCPR.

Probability	Parameters				
TCP	α	β	μ	T_p	N_0
	$0.15\,Gy^{-1}$	$0.05\,Gy^{-2}$	$42\,d$	$0.27\,h$	10^6
NTCPU	δ	γ			
	2.6 ± 0.5	$(6.6 \pm 1.6)\,mGy$			
NTCPR	s	k	D50		
	0.75	10.24	$80\,Gy$		

B Danksagung

Am Ende dieser Arbeit möchte ich die Gelegenheit nutzen mich bei allen zu bedanken, die mich in den letzten drei Jahren unterstützt und zum Gelingen dieser Arbeit beigetragen haben.

Mein besonderer Dank gilt Prof. Dr. Jürgen Hesser für die Bereitstellung dieses interessanten Themas, für die vielen produktiven Diskussionen und Rücksprachen während der gesamten Arbeit. Außerdem auch für die Möglichkeiten, die du mir gibst meine Ziele zu verwirklichen und das Vertrauen, dass du mir entgegenbringst. Ich hoffe auf noch viele gemeinsame Projekte.

Außerdem gilt mein Dank Prof. Dr. Peter Bachert, der sich sofort dazu bereiterklärt hat diese Arbeit zu begutachten.

Den Kollegen aus dem Uniklinikum Mannheim danke ich für die vielen beratenden Gespräche und viele gemeinsame Projekte. Mein besonderer Dank gilt dabei Prof. Dr. Frederik Wenz und Dr. Frank Giordano. Den Kollegen aus dem Uniklinikum Würzburg um Prof. Dr. Otto Sauer danke ich für die Beratung über die klinischen Aspekte der HDR Brachytherapie.

Meinen Kollegen in der Arbeitsgruppe, vor allem Katharina, Leoni, Lisa, Matthias und Romy danke ich für die vielen lustigen Stunden sowohl im Büro als auch in der Freizeit. Ich bin froh, dass wir in einer Arbeitsgruppe sind und ihr niemals meine Paper reviewen werdet.

Abschließend noch ein ganz persönliches Dankeschön an meine Eltern, die mich während meiner Studienzeit immer und in jeglicher Hinsicht unterstützt haben. Auch an Torsten, Anja und Lea, dafür, dass sie mich auch in stressigen Zeiten immer wieder ermuntert haben.

Zum Schluss meiner Freundin Romy, für ihre unendliche Geduld und Unterstützung während meiner Promotionszeit. Vielen Dank auch für die vielen fachlichen Diskussionen, die mir sehr geholfen haben.

Bibliography

[1] M. J. Rivard, J. L. M. Venselaar, and L. Beaulieu. "The evolution of brachytherapy treatment planning." In: *Medical Physics* 36.6 (May 2009), pp. 2136–2153.

[2] J. Dutreix, M. Tubiana, and B. Pierquin. "The hazy dawn of brachytherapy." In: *Radiotherapy and Oncology* 49.3 (1998), pp. 223–232.

[3] J. N. Aronowitz, L. Grimard, and R. Robison. "Precedence for prostate brachytherapy." In: *Brachytherapy* 10.3 (Jan. 2011), pp. 201–207.

[4] R. Walstam. "Remotely-controlled afterloading radiotherapy apparatus. (A preliminary report)." In: *Physics in medicine and biology* 7 (1962), pp. 225–228.

[5] R. Pötter and J.-J. Mazeron. "The GEC ESTRO Handbook of Brachytherapy." In: *Brachytherapy* (2002).

[6] M. M. Center et al. "International variation in prostate cancer incidence and mortality rates." In: *European urology* 61.6 (June 2012), pp. 1079–92.

[7] J. Ferlay et al. "Estimates of worldwide burden of cancer in 2008: GLOBOCAN 2008." In: *International journal of cancer. Journal international du cancer* 127.12 (Dec. 2010), pp. 2893–917.

[8] O. W. Brawley. "Prostate cancer epidemiology in the United States." In: *World journal of urology* 30.2 (Apr. 2012), pp. 195–200.

[9] R. Siegel, J. Ma, Z. Zou, and A. Jemal. "Cancer Statistics , 2014." In: 64.1 (2014), pp. 9–29.

[10] R. Nath et al. *AAPM recommendations on dose prescription and reporting methods for permanent interstitial brachytherapy for prostate cancer: report of Task Group 137.* Vol. 36. 11. Nov. 2009, pp. 5310–5322.

[11] J. Mohler et al. "NCCN clinical practice guidelines in oncology: prostate cancer." In: *Journal of the National Comprehensive Cancer Network : JNCCN* 8.2 (Feb. 2010), pp. 162–200.

[12] M. Stöckle and R. Bussar-Maatz. "Localised prostate cancer: the PREFERE trial." In: *Zeitschrift für Evidenz, Fortbildung und Qualität im Gesundheitswesen* 106.5 (Jan. 2012), pp. 333–335.

[13] P. Grimm et al. “Comparative analysis of prostate-specific antigen free survival outcomes for patients with low, intermediate and high risk prostate cancer treatment by radical therapy. Results from the Prostate Cancer Results Study Group.” In: *BJU international* 109 Suppl (Feb. 2012), pp. 22–29.

[14] M. J. Zelefsky et al. “Five-year biochemical outcome and toxicity with transperineal CT-planned permanent I-125 prostate implantation for patients with localized prostate cancer.” In: *International Journal of Radiation Oncology Biology Physics* 47.5 (2000), pp. 1261–1266.

[15] A. S. Sandhu et al. “Long-term urinary toxicity after 3-dimensional conformal radiotherapy for prostate cancer in patients with prior history of transurethral resection.” In: *International Journal of Radiation Oncology Biology Physics* 48.3 (2000), pp. 643–647.

[16] B. Bauer-Kirpes, V. Sturm, W. Schlegel, and W. J. Lorenz. “Computerized optimization of 125I implants in brain tumors.” In: *International Journal of Radiation Oncology Biology Physics* 14.5 (May 1988), pp. 1013–1023.

[17] J. N. Roy, K. E. Wallner, L. L. Anderson, and C. Ling. “CT-based optimized planning for transperineal prostate implant with customized template.” In: *International Journal of Radiation Oncology Biology Physics* 21.2 (July 1991), pp. 483–489.

[18] J. Pouliot, D. Tremblay, J. Roy, and S. Filice. “Optimization of permanent 125I prostate implants using fast simulated annealing.” In: *International Journal of Radiation Oncology Biology Physics* 36.3 (Oct. 1996), pp. 711–720.

[19] E. Lessard. “Development and clinical introduction of an inverse planning dose optimization by simulated annealing (IPSA) for high dose rate brachytherapy.” en. In: *Medical Physics* 31.10 (Oct. 2004), p. 2935.

[20] A. Karabis, P. Belotti, and D. Baltas. “Optimization of catheter position and dwell time in prostate HDR brachytherapy using HIPO and linear programming.” In: *IFMBE Proceedings* 25.1 (2009), pp. 612–615.

[21] Y. Yu. “A genetic algorithm for the optimization of prostate implants.” en. In: *Medical Physics* 23.12 (Dec. 1996), pp. 2085–2091.

[22] D. L. Donoho and Y. Tsaig. “Fast Solution of l1 -Norm Minimization Problems When the Solution May Be Sparse.” In: *Information Theory, IEEE Transactions on Information Theory - TIT* 54.11 (2008), pp. 4789–4812.

[23] S. Yoo, M. E. Kowalok, B. R. Thomadsen, and D. L. Henderson. “Treatment planning for prostate brachytherapy using region of interest adjoint functions and a greedy heuristic.” In: *Physics in medicine and biology* 48.24 (Dec. 2003), pp. 4077–4090.

[24] R. Alterovitz et al. “Optimization of HDR brachytherapy dose distributions using linear programming with penalty costs.” en. In: *Medical Physics* 33.11 (Oct. 2006), pp. 4012–4019.

[25] S. Yoo, M. E. Kowalok, B. R. Thomadsen, and D. L. Henderson. “A greedy heuristic using adjoint functions for the optimization of seed and needle configurations in prostate seed implant.” In: *Physics in medicine and biology* 52.3 (Feb. 2007), pp. 815–828.

[26] B. L. Gorissen, D. den Hertog, and a. L. Hoffmann. “Mixed integer programming improves comprehensibility and plan quality in inverse optimization of prostate HDR brachytherapy.” In: *Physics in Medicine and Biology* 58 (2013), pp. 1041–1057.

[27] W. D. D’Souza, R. R. Meyer, B. R. Thomadsen, and M. C. Ferris. “An iterative sequential mixed-integer approach to automated prostate brachytherapy treatment plan optimization.” In: *Physics in medicine and biology* 46.2 (Feb. 2001), pp. 297–322.

[28] C. Guthier and J. Hesser. “Comparison of two different MILP optimizers for LDR brachytherapy treatment planning.” In: *Jahreskongress der Deutschen Gesellschaft für Radioonkologie (DEGRO)*. 2014, pp. 67–68.

[29] A. M. Dinkla et al. “A comparison of inverse optimization algorithms for HDR/PDR prostate brachytherapy treatment planning.” In: *Brachytherapy* (Oct. 2014), pp. 1–10.

[30] D. Baltas. *A handbook for the optimization and optimization tools in SWIFT Version 3.0 (Oncentra Prostate)*. 2006, pp. 1–45.

[31] T. Siauw et al. “IPIP: A new approach to inverse planning for HDR brachytherapy by directly optimizing dosimetric indices.” en. In: *Medical Physics* 38.7 (June 2011), pp. 4045–4051.

[32] G. C. Morton, R. Sankreacha, P. Halina, and A. Loblaw. “A comparison of anatomy-based inverse planning with simulated annealing and graphical optimization for high-dose-rate prostate brachytherapy.” In: *Brachytherapy* 7.1 (2008), pp. 12–16.

[33] L. Du et al. “Analysis on greedy reconstruction algorithms based on compressed sensing.” In: *2012 International Conference on Audio, Language and Image Processing* 1 (July 2012), pp. 783–789.

[34] C. Guthier, K. A Aschenbrenner, F. Wenz, and J. Hesser. “Compressed Sensing-Based LDR Brachytherapy Inverse Treatment Planning with Biological.” In: *World Congress on Medical Physics and Biomedical Engineering, June 7-12, 2015, Toronto, Canada*. Ed. by D. A. Jaffray. Toronto: Springer International Publishing, 20015, pp. 421–424.

[35] C. Guthier et al. "A new optimization method using a compressed sensing inspired solver for real-time LDR-brachytherapy treatment planning." In: *Physics in Medicine and Biology* 60.6 (2015), pp. 2179–2194.

[36] C. Guthier and J. Hesser. "Compressed Sensing-Based LDR Brachytherapy Inverse Treatment Planning with Dosimetric Criteria." In: *Strahlentherapie and Onkologie* acc. for. (2015).

[37] S. Nag et al. "American brachytherapy society (ABS) recommendations for transperineal permanent brachytherapy of prostate cancer." In: *International Journal of Radiation Oncology Biology Physics* 44.4 (1999), pp. 789–799.

[38] J. F. Williamson. "Brachytherapy technology and physics practice since 1950: a half-century of progress." In: *Physics in medicine and biology* 51.13 (2006), R303–R325.

[39] G. Wilson and J. R. Dennison. "Approximation of range in materials as a function of incident electron energy." In: *IEEE Transactions on Plasma Science* 40.2 PART 1 (2012), pp. 291–297.

[40] W. Demtröder. *Experimentalphysik 4: Kern-, Teilchen- Und Astrophysik*. de. Gabler Wissenschaftsverlage, Oct. 2009, p. 560.

[41] R. H. Pratt, A. Ron, and H. K. Tseng. "Atomic photoelectric effect above 10 keV." In: *Reviews of Modern Physics* 45.2 (1973), pp. 273–325.

[42] O. Klein and T. Nishina. "Über die Streuung von Strahlung durch freie Elektronen nach der neuen relativistischen Quantendynamik von Dirac." In: *Zeitschrift für Physik* 52.11-12 (1929), pp. 853–868.

[43] R. Evans. *Corpuscles and Radiation in Matter II and Korpuskeln und Strahlung in Materie II*. Springer Berlin Heidelberg5, 1958, pp. 218–298.

[44] J. H. Hubbell. "Electron-positron pair production by photons: A historical overview." In: *Radiation Physics and Chemistry* 75.6 (2006), pp. 614–623.

[45] W. Schlegel and J. Bille. *Medizinische Physik 2*. Ed. by W. Schlegel and J. Billi. Springer Berlin Heidelberg, 2002, p. 548.

[46] E. J. Hall and A. Giaccia. *Radiobiology for the Radiologist*. 5th ed. Lippincott Williams & Wilkins, 2006, p. 564.

[47] D. J. Brenner. "The Linear-Quadratic Model Is an Appropriate Methodology for Determining Isoeffective Doses at Large Doses Per Fraction." In: *Seminars in Radiation Oncology* 18.4 (2008), pp. 234–239.

[48] S. J. Damore, A. M. Syed, A. A. Puthawala, and A. Sharma. "Needle displacement during HDR brachytherapy in the treatment of prostate cancer." In: *International Journal of Radiation Oncology Biology Physics* 46.5 (2000), pp. 1205–1211.

[49] *LDR Prostate Brachytherapy*. Estern Radiation Oncology, 2015.

[50] *HDR Brachytherapy*. Radiation Oncology Victoria, 2015.

[51] *microSelectron ® Digital Brachytherapy is in our DNA*. Elekta, AB, 2015.

[52] *Needles for LDR Brachytherapy*. Eckert & Ziegler BEBIG GmbH, 2015.

[53] A. V. D'Amico et al. "Biochemical outcome after radical prostatectomy, external beam radiation therapy, or interstitial radiation therapy for clinically localized prostate cancer." In: *JAMA : The journal of the American Medical Association* 280.11 (1998), pp. 969–974.

[54] M. Ghilezan. "Role of high dose rate brachytherapy in the treatment of prostate cancer." In: *Cancer/Radiothérapie* 16.5 (2012), pp. 418–422.

[55] L. L. Anderson. "Dosimetry of Interstitial Brachytherapy Sources Dosimetry of Interstitial Brachytherapy Sources." In: *Medical Physics* 43.51 (1995), pp. 209–234.

[56] M. J. Rivard et al. "Update of AAPM Task Group No. 43 Report: A revised AAPM protocol for brachytherapy dose calculations." In: *Medical Physics* 31.3 (2004), pp. 633–674.

[57] M. J. Rivard et al. "Supplement to the 2004 update of the AAPM Task Group No. 43 Report." In: *Medical Physics* 34.6 (2007), pp. 2187–2205.

[58] S. D. Davis et al. "Report of the Task Group 186 on model-based dose calculation methods in brachytherapy beyond the TG-43 formalism: Current status." In: 39.October (2012), pp. 6208–6236.

[59] J. Perez-Calatayud et al. *Dose calculation for photon-emitting brachytherapy sources with average energy higher than 50 keV: Report of the AAPM and ESTRO*. Vol. 39. 5. 2012, pp. 1–136.

[60] G. Kovács et al. "GEC-ESTRO-EAU recommendations on temporary brachytherapy using stepping sources for localised prostate cancer." In: *Radiotherapy and oncology : journal of the European Society for Therapeutic Radiology and Oncology* 74.2 (Feb. 2005), pp. 137–148.

[61] R. Takam, E. Bezak, E. E. Yeoh, and L. Marcu. "Assessment of normal tissue complications following prostate cancer irradiation: Comparison of radiation treatment modalities using NTCP models." In: *Medical Physics* 37.9 (2010), pp. 5126–5137.

[62] C. Salembier et al. "Tumour and target volumes in permanent prostate brachytherapy: A supplement to the ESTRO/EAU/EORTC recommendations on prostate brachytherapy." In: *Radiotherapy and Oncology* 83.1 (2007), pp. 3–10.

[63] D. Baltas et al. “A conformal index (COIN) to evaluate implant quality and dose specification in brachytherapy.” In: *International Journal of Radiation Oncology*Biology*Physics* 37.3 (1997), pp. 731–736.

[64] R. G. Dale. “The application of the linear quadratic dose effect equation to fractionated and protracted radiotherapy.” In: *British Journal of Radiology* 58.August (1985), pp. 515–528.

[65] M. Zaider et al. “Methodology for biologically-based treatment planning for combined low-dose-rate (permanent implant) and high-dose-rate (fractionated) treatment of prostate cancer.” In: *International Journal of Radiation Oncology Biology Physics* 61.3 (2005), pp. 702–713.

[66] R. I. MacKay et al. “Predicting late rectal complications following prostate conformal radiotherapy using biologically effective doses and normalized dose-surface histograms.” In: *The British Journal of Radiology* 70.833 (1997), pp. 516–26.

[67] A. Daşu, I. Toma-Daşu, J. Olofsson, and M. Karlsson. “The use of risk estimation models for the induction of secondary cancers following radiotherapy.” In: *Acta oncologica (Stockholm, Sweden)* 44.4 (2005), pp. 339–347.

[68] E. Candes and M. Wakin. “An Introduction To Compressive Sampling.” In: *IEEE Signal Processing Magazine* 25.2 (Mar. 2008), pp. 21–30.

[69] G. Wallace. “The JPEG still picture compression standard.” In: *IEEE Transactions on Consumer Electronics* 38.1 (1992), pp. 1–17.

[70] C. Christopoulos. “The jpeg2000 still image coding system: an overview.” In: *IEEE Transactions on Consumer Electronics* 46.4 (2000), pp. 1103–1127.

[71] M. Lustig, D. Donoho, and J. M. Pauly. “Sparse MRI: The application of compressed sensing for rapid MR imaging.” In: *Magnetic Resonance in Medicine* 58.6 (2007), pp. 1182–1195.

[72] W. Yin, S. Osher, D. Goldfarb, and J. Darbon. “Bregman Iterative Algorithms for l1-Minimization with Applications to Compressed Sensing.” In: *SIAM Journal on Imaging Sciences* 1.1 (2008), pp. 143–168.

[73] G.-H. Chen, J. Tang, and S. Leng. “Prior image constrained compressed sensing (PICCS): a method to accurately reconstruct dynamic CT images from highly undersampled projection data sets.” In: *Medical physics* 35.2 (2008), pp. 660–663.

[74] T. Goldstein and S. Osher. “The Split Bregman Method for L1-Regularized Problems.” In: *SIAM Journal on Imaging Sciences* 2.2 (2009), pp. 323–343.

[75] M. Elad. *Sparse and Redundant Representations*. Springer, 2010, p. 376.

[76] B. K. Natarajan. "Sparse Approximate Solutions to Linear Systems." In: *SIAM Journal on Computing* 24.2 (1995), pp. 227–234.

[77] G. Davis. "Adaptive Greedy Approximations." In: *Constructive Approximation* 13.1 (1997), pp. 57–98.

[78] J. Tropp. "Greed is Good: Algorithmic Results for Sparse Approximation." In: *IEEE Transactions on Information Theory* 50.10 (2004), pp. 2231–2242.

[79] S. S. Chen, D. L. Donoho, and M. A. Saunders. "Atomic Decomposition by Basis Pursuit." In: *SIAM Journal on Scientific Computing* 20.1 (1998), pp. 33–61.

[80] S. G. Mallat. *IEEE Xplore - Matching pursuits with time-frequency dictionaries*. 1993.

[81] L. K. Jones. "On a Conjecture of Huber Concerning the Convergence of Projection Pursuit Regression." In: *The Annals of Statistics* 15.2 (1987), pp. 880–882.

[82] S. Mallat and Z. Zhang. "Adaptive time-frequency decomposition with matching pursuits." In: *Proceedings of the IEEE-SP International Symposium*. Vol. 2. 1993, pp. 4–7.

[83] D. Needell and J. A. Tropp. "CoSaMP: Iterative signal recovery from incomplete and inaccurate samples." In: *Information Theory and Applications Workshop* (2008).

[84] W. Dai and O. Milenkovic. "Subspace Pursuit for Compressive Sensing Signal Reconstruction." In: (2008), pp. 1–19.

[85] D. L. Donoho, Y. Tsaig, I. Drori, and J. L. Starck. "Sparse solution of underdetermined systems of linear equations by stagewise orthogonal matching pursuit." In: *IEEE Transactions on Information Theory* 58.2 (2012), pp. 1094–1121.

[86] Å. Holm, T. Larsson, and Å. C. Tedgren. "A linear programming model for optimizing HDR brachytherapy dose distributions with respect to mean dose in the DVH-tail." In: *Medical Physics* 40.8 (2013), pp. 1–11.

[87] E. K. Lee et al. "Treatment planning for brachytherapy : an integer programming model , two computational approaches and experiments with permanent prostate implant planning Treatment planning for brachytherapy : an integer programming model , two computational approaches." In: *Physics in Medicine and Biology* 44 (1999), pp. 145–165.

[88] E. Lee and M. Zaider. "Mixed Integer Programming Approaches to Treatment Planning for Brachytherapy – Application to Permanent Prostate Implants." In: *Annals of Operations Research* (2003), pp. 147–163.

[89] I. K. K. Kolkman-Deurloo. "Optimization of interstitial volume implants." In: *Radiotherapy and Oncology* 31.3 (1994), pp. 229–239.

[90] F. T. Lin, C. Y. Kao, and C. C. Hsu. "Applying the genetic approach to simulated annealing in solving some NP-hard problems." In: *IEEE Transactions on Systems, Man and Cybernetics* 23.6 (1993), pp. 1752–1767.

[91] R. R. Meyer. "On the existence of optimal solutions to integer and mixed-integer programming problems." In: *Mathematical Programming* 7.1 (1974), pp. 223–235.

[92] S. Kirkpatrick, C. D. Gelatt, and M. P. Vecchi. "Optimization by simulated annealing." In: *Science (New York, N.Y.)* 220.4598 (1983), pp. 671–680.

[93] S. M. Morrill et al. "Very fast simulated reannealing in radiation therapy treatment plan optimization." In: *International journal of radiation oncology, biology, physics* 31.1 (1995), pp. 179–188.

[94] A. de la Zerda Lerner. "Inverse planning for low-dose-rate prostate brachytherapy by simulated annealing under fuzzy expert control." In: *Medical Physics* 31.4 (2004), p. 950.

[95] J. Clausen. "Branch and bound algorithms-principles and examples." In: (1999), pp. 1–30.

[96] R. J. Gallagher and E. K. Lee. "Mixed integer programming optimization models for brachytherapy treatment planning." In: *Proceedings : a conference of the American Medical Informatics Association / AMIA Annual Fall Symposium* (1997), pp. 278–282.

[97] R. R. Meyer, W. D. D'Souza, and M. C. Ferris. "MIP Models and BB Strategies in Brachytherapy Treatment Optimization." In: *Journal of Global Optimization* 25.1 (2003), pp. 23–42.

[98] N. Milickovic et al. "Multiobjective anatomy-based dose optimization for HDR-brachytherapy with constraint free deterministic algorithms." In: *Physics in medicine and biology* 47.13 (2002), pp. 2263–2280.

[99] K. Miettinen. *Nonlinear Multiobjective Optimization*. 1st ed. Springer US, 1998.

[100] M. Lahanas, D. Baltas, and S. Giannouli. "Global convergence analysis of fast multiobjective gradient-based dose optimization algorithms for high-dose-rate brachytherapy." In: *Physics in medicine and biology* 48.5 (2003), pp. 599–617.

[101] E. Lessard and J. Pouliot. "Inverse planning anatomy-based dose optimization for HDR-brachytherapy of the prostate using fast simulated annealing algorithm and dedicated objective function." In: *Medical Physics* 28.5 (2001), pp. 773–779.

[102] E. Lessard, I.-C. Hsu, and J. Pouliot. "Inverse planning for interstitial gynecologic template brachytherapy: truly anatomy-based planning." In: *International Journal of Radiation Oncology Biology Physics* 54.4 (2002), pp. 1243–1251.

[103] P. Mavroidis et al. "Radiobiological evaluation of the influence of dwell time modulation restriction in HIPO optimized HDR prostate brachytherapy implants." In: *Journal of Contemporary Brachytherapy* 2.3 (2010), pp. 117–128.

[104] D. G. Luenberger and Y. Ye. *Linear and Nonlinear Programming*. 3rd ed. Springer, 2008, p. 550.

[105] W. D. Renner, T. P. O'Connor, and N. M. Bermudez. "An algorithm for generation of implant plans for high-dose-rate irradiators." In: *Medical physics* 17.1 (1989), pp. 35–40.

[106] T. Siauw et al. "NPIP: A skew line needle configuration optimization system for HDR brachytherapy." In: *Medical Physics* 39 (2012), pp. 4339–4346.

[107] E. Chajon et al. "Inverse Planning Approach for 3-D MRI-Based Pulse-Dose Rate Intracavitary Brachytherapy in Cervix Cancer." In: *International Journal of Radiation Oncology Biology Physics* 69.3 (2007), pp. 955–961.

[108] D. Baltas et al. "Influence of Modulation Restriction in Inverse Optimization with HIPO of Prostate Implants on Plan Quality: Analysis using Dosimetric and Radiobiological Indices." In: *IFMBE Proceedings* 25 (2009), pp. 283–286.

[109] A. Holm, T. Larsson, and A. Carlsson Tedgren. "Impact of using linear optimization models in dose planning for HDR brachytherapy." In: *Medical physics* 39.2 (2012), pp. 1021–1028.

[110] D. Giantsoudi et al. "A gEUD-based inverse planning technique for HDR prostate brachytherapy: Feasibility study." In: *Medical Physics* 40.4 (2013), pp. 1–12.

[111] A. M. Dinkla et al. "Novel tools for stepping source brachytherapy treatment planning: Enhanced geometrical optimization and interactive inverse planning." In: *Medical Physics* 42.1 (2015), pp. 348–353.

[112] X. A. Li, J. Z. Wang, R. D. Stewart, and S. J. DiBiase. "Dose escalation in permanent brachytherapy for prostate cancer: dosimetric and biological considerations." In: *Physics in medicine and biology* 48.17 (2003), pp. 2753–65.

[113] T. Bortfeld, J. Bürkelbach, R. Boesecke, and W. Schlegel. "Methods of image reconstruction from projections applied to conformation radiotherapy." In: *Physics in medicine and biology* 35.10 (1990), pp. 1423–1434.

[114] S. Webb. "Optimization by simulated annealing of three-dimensional conformal treatment planning for radiation fields defined by a multileaf collimator." In: *Physics in medicine and biology* 36.9 (1991), pp. 1201–1226.

[115] J. Stein et al. "Number and orientations of beams in intensity-modulated radiation treatments." In: *Medical physics* 24.2 (1997), pp. 149–160.

[116] S. Foucart. "A note on guaranteed sparse recovery via -minimization." In: *Applied and Computational Harmonic Analysis* 29.1 (July 2010), pp. 97–103.

[117] M. Yaghoobi, D. Wu, and M. E. Davies. "Fast Non-Negative Orthogonal Matching Pursuit." In: 22.9 (2015), pp. 1229–1233.

[118] C. C. Ling. "Permanent implants using Au-198, Pd-103 and I-125: radiobiological considerations based on the linear quadratic model." In: *International Journal of Radiation Oncology Biology Physics* 23.1 (1992), pp. 81–7.

[119] C. Ling et al. "Quantifying the effect of dose inhomogeneity in brachytherapy: Application to permanent prostatic implant with 125I seeds." In: *International Journal of Radiation Oncology*Biology*Physics* 28.4 (1994), pp. 971–977.

[120] R. G. Stock, N. N. Stone, J. A. Cesaretti, and B. S. Rosenstein. "Biologically effective dose values for prostate brachytherapy: effects on PSA failure and posttreatment biopsy results." In: *International Journal of Radiation Oncology Biology Physics* 64.2 (2006), pp. 527–533.

[121] M. Zaider and G. N. Minerbo. "Tumour control probability: a formulation applicable to any temporal protocol of dose delivery." In: *Physics in Medicine and Biology* 45.2 (2000), pp. 279–293.

[122] Matlab. *version 8.1.0 (R2013a)*. Math Workds, Natick Ma, USA.

[123] B. Meindl and M. Templ. "Analysis of commercial and free and open source solvers for linear optimization problems." In: *ESSnet on commom tools and harmonised methodology for SDC in the ESS* (2012), pp. 1–14.

[124] M. Lahanas et al. "Generation of Uniformly Distributed Dose Points for Anatomy-Based-Three-Dimensional Dose Optimization in Brachytherapy." In: *Medical physics* 27 (2000), pp. 1034–1046.

[125] J. Claude and P. Belisle. "Convergence Theorems for a Class of Simulated Annealing Algorithms on Rd." In: *Journal of Applied Probability* 29.4 (1992), pp. 885–895.

[126] D. Baltas et al. "Influence of Modulation Restriction in Inverse Optimization with HIPO of Prostate Implants on Plan Quality: Analysis Using Dosimetric and Radiobiological Indices." In: *World Congress on Medical Physics and Biomedical Engineering, September 7 - 12, 2009, Munich, Germany.* 2009, pp. 283–86.

[127] S. Pokharel et al. "Evaluation of hybrid inverse planning and optimization (HIPO) algorithm for optimization in real-time , high-dose-rate (HDR) brachytherapy for prostate." In: *Journal of Applied Clinical Medical Physics* 14.4 (2013), pp. 96–107.

[128] J. Z. Wang and X. A. Li. "Evaluation of external beam radiotherapy and brachytherapy for localized prostate cancer using equivalent uniform dose." In: *Medical physics* 30.1 (2003), pp. 34–40.

[129] J. A. M. Cunha, B. Pickett, and J. Pouliot. *Inverse planning optimization for hybrid prostate permanent-seed implant brachytherapy plans using two source strengths*. 2010.

[130] W. D. D'Souza, H. D. Thames, and D. a. Kuban. "Dose-volume conundrum for response of prostate cancer to brachytherapy: Summary dosimetric measures and their relationship to tumor control probability." In: *International Journal of Radiation Oncology Biology Physics* 58.5 (2004), pp. 1540–1548.

[131] A. Haworth et al. "Assessment of i-125 prostate implants by tumor bioeffect." In: *International Journal of Radiation Oncology Biology Physics* 59.5 (2004), pp. 1405–1413.

[132] A. Haworth et al. "Prostate implant evaluation using tumour control probability–the effect of input parameters." In: *Physics in medicine and biology* 49.16 (2004), pp. 3649–3664.

[133] G. S. Merrick et al. "Prostate Cancer Distribution in Patients Diagnosed by Transperineal Template-Guided Saturation Biopsy." In: *European Urology* 52.3 (2007), pp. 715–724.

[134] N. N. Stone et al. "Prostate gland motion and deformation caused by needle placement during brachytherapy." In: *Brachytherapy* 1.3 (2002), pp. 154–160.

[135] J. S. Eshleman et al. "Radioactive seed migration to the chest after transperineal interstitial prostate brachytherapy: Extraprostatic seed placement correlates with migration." In: *International Journal of Radiation Oncology Biology Physics* 59.2 (2004), pp. 419–425.

[136] A. Tiong et al. "A Small Tolerance for Catheter Displacement in High-Dose Rate Prostate Brachytherapy is Necessary and Feasible." In: *International Journal of Radiation Oncology Biology Physics* 76.4 (2010), pp. 1066–1072.

[137] M. Gao, J. Z. Wang, S. Nag, and N. Gupta. "Effects of seed migration on post-implant dosimetry of prostate brachytherapy." In: *Medical Physics* 34.2 (2007), pp. 471–480.

[138] N. Chng et al. "Prostate brachytherapy postimplant dosimetry: Seed orientation and the impact of dosimetric anisotropy in stranded implants." In: *Medical Physics* 39.2 (2012), pp. 721–731.

[139] N. Kovalchuk, K. M. Furutani, O. K. MacDonald, and T. M. Pisansky. "Dosimetric effect of interfractional needle displacement in prostate high-dose-rate brachytherapy." In: *Brachytherapy* 11.2 (2012), pp. 111–118.

[140] a. S. Meigooni, J. a. Meli, and R. Nath. "Interseed effects on dose for 125I brachytherapy implants." In: *Medical Physics* 19.2 (1992), pp. 385–390.

[141] K. Weeks and M. Dennett. "Dose Calculation and Measurements for a CT Compatible Version of the Flechter Applicator." In: *International Journal of Radiation Oncology Biology Physics* 18 (1990), pp. 1191–1198.

[142] J. F. Williamson. "The sievert integral revisited: Evaluation and extension to 125I, 169YB, and 192IR brachytherapy sources." In: *International Journal of Radiation Oncology Biology Physics* 36.5 (1996), pp. 1239–1250.

[143] S. Mashouf et al. "A simplified analytical dose calculation algorithm accounting for tissue heterogeneity for low-energy brachytherapy sources." In: *Physics in medicine and biology* 58.18 (2013), pp. 6299–6315.

[144] G. Anagnostopoulos et al. "An analytical dosimetry model as a step towards accounting for inhomogeneities and bounded geometries in 192Ir brachytherapy treatment planning." In: *Physics in medicine and biology* 48.11 (2003), pp. 1625–1647.

[145] A. K. Carlsson and A. Ahnesjö. "The collapsed cone superposition algorithm applied to scatter dose calculations in brachytherapy." In: *Medical Physics* 27.10 (2000), pp. 2320–2332.

[146] K. A. Gifford et al. "Comparison of a finite-element multigroup discrete-ordinates code with Monte Carlo for radiotherapy calculations." In: *Physics in medicine and biology* 51.9 (2006), pp. 2253–2265.

[147] S. Hissoiny et al. "Sub-second high dose rate brachytherapy Monte Carlo dose calculations with bGPUMCD." In: *Medical Physics* 39.7 (2012), pp. 4559–4567.

[148] J. J. Wang et al. "CT-guided radioactive seed implantation for recurrent rectal carcinoma after multiple therapy." In: *Medical Oncology* 27.2 (2010), pp. 421–429.

[149] J. Wang et al. "Interstitial 125I seeds implantation to treat spinal metastatic and primary paraspinal malignancies." In: *Medical Oncology* 27.2 (2010), pp. 319–326.

[150] K. J. Chang and A. Irisawa. "EUS 2008 Working Group document: evaluation of EUS-guided injection therapy for tumors." In: *Gastrointestinal Endoscopy* 69.2 (2009), S59–S63.

[151] H. Badakhshi et al. "Oligometastases: The new paradigm and options for radiotherapy: A critical review." In: *Strahlentherapie und Onkologie* 189.5 (2013), pp. 357–363.

[152] A. Brahme, J. E. Roos, and I. Lax. "Solution of an integral equation encountered in rotation therapy." In: *Physics in medicine and biology* 27.10 (1982), pp. 1221–1229.

[153] A. Cormack and R. Cormack. "A problem in rotation therapy with x-rays: Dose distributions with an axis of symmetry." In: *International Journal of Radiation Oncology Biology Physics* 13 (1987), pp. 1921–1925.

[154] M. Langer and J. Leong. "Computer ApplicationsOptimization of beam weights under dose-volume restrictions." In: *International Journal of Radiation Oncology Biology Physics* 13.2 (1987), pp. 1255–1260.

[155] H. E. Romeijn et al. "A novel linear programming approach to fluence map optimization for intensity modulated radiation therapy treatment planning." In: *Physics in medicine and biology* 48.21 (2003), pp. 3521–3542.

[156] S. Webb, D. J. Convery, and P. M. Evans. "Inverse planning with constraints to generate smoothed intensity-modulated beams." In: *Physics in medicine and biology* 43.10 (1998), pp. 2785–2794.

[157] T. Bortfeld. "Optimized planning using physical objectives and constraints." In: *Seminars in radiation oncology* 9.1 (1999), pp. 20–34.

[158] D. M. Shepard et al. "Direct aperture optimization: a turnkey solution for step-and-shoot IMRT." In: *Medical physics* 29.6 (2002), pp. 1007–1018.

[159] A. Mestrovic et al. "Direct aperture optimization for online adaptive radiation therapy." In: *Medical physics* 34.5 (2007), pp. 1631–1646.

[160] H. Kim et al. "Efficient IMRT inverse planning with a new L1-solver: template for first-order conic solver." In: *Physics in Medicine and Biology* 57.13 (2012), pp. 4139–4153.

[161] A. Lomax. "Intensity modulation methods for proton radiotherapy." In: *Physics in Medicine and Biology* 185-205 (1999).

[162] L. Olofsson et al. "Intensity modulated radiation therapy with electrons using algorithm based energy/range selection methods." In: *Radiotherapy and Oncology* 73.2 (2004), pp. 223–231.

[163] T. Bortfeld and S. Webb. "Single-Arc IMRT?" In: *Physics in medicine and biology* 54 (2009), pp. 8–20.

[164] M. A. Myers et al. "Phase I/II trial of single-fraction high-dose-rate brachy therapy-boosted hypofractionated intensity-modulated radiation therapy for localized adenocarcinoma of the prostate." In: *Brachytherapy* 11.4 (2012), pp. 292–298.

[165] L. Ma et al. "Clinical Realization of Sector Beam Intensity Modulation for Gamma Knife Radiosurgery: A Pilot Treatment Planning Study." In: *International Journal of Radiation Oncology Biology Physics* 91.3 (2015), pp. 661–668.

[166] Q. J. Wu et al. "Real-time inverse planning for Gamma Knife radiosurgery." In: *Medical Physics* 30.11 (2003), pp. 2988–2995.

[167] D. M. Shepard, M. C. Ferris, R. Ove, and L. Ma. "Inverse treatment planning for Gamma Knife radiosurgery." In: *Medical Physics* 27.12 (2000), pp. 2748–2756.

[168] R. E. Peschel and J. W. Colberg. "Review Surgery , brachytherapy , and external-beam radiotherapy for early prostate cancer Treatment for early prostate cancer." In: *The Lancet Oncology* 4 (2003), pp. 233–241.

[169] NUDAT2.6. "National Nuclear Data Center." In: *NY: Brookhaven National Laboratory* (2015).

Erklärung:

Ich versichere, dass ich diese Arbeit selbstständig verfasst habe und keine anderen als die angegebenen Quellen und Hilfsmittel benutzt habe.

Heidelberg, den .....